Exploring the factors and mechanisms involved in triggering the Alternative Lengthening of Telomeres Pathway

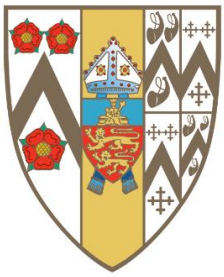

Thomas Kent

Brasenose College

University of Oxford

A thesis submitted for the degree of

DPhil Medical Sciences

Trinity 2021

Acknowledgements

A PhD is a journey, but unlike most journeys it isn't always clear what path we should take. Many find themselves lost more than once in their PhD, and sometimes the way forward is difficult to see. Without many people, I would still be lost on this journey. I'd like to thank, first and foremost, my supervisors Dr David Clynes and Prof Richard Gibbons for their tireless support, encouragement, wisdom, and suggestions on the direction my research has taken.

I'd also like to thank the members of the Gibbons and Clynes lab who have supported my work over the last 4 years. From Julia who welcomed me into the Gibbons lab in October 2016, to members who have joined the Clynes lab along my journey. You have all worked with me during my research, providing ideas, criticism and assistance when the experiments piled up. Some of the data presented in this thesis could not truly be called my own, especially as we went into reduced occupancy in the lab during the coronavirus lockdown. Without you all, much of these experiments simply wouldn't have worked without your cooperation and assistance with things like cell culture and assays. I'd particularly like to thank Sam Shepherd for the work we did in collaboration on ALT assays, Tomas Goncalves for his assistance with C-circle blots and Siobhan Cunniffe for her tireless work in tissue culture maintaining the lab's cell line clones. Details of individual contributions to figures can be found in section 8.

Finally, and most importantly I'd like to thank my friends and family for their support over the last 5 years. Without the continuous support and motivation from Dakshi I certainly wouldn't have made it to Oxford, nevermind submit a PhD thesis.

Contents

Abstract

Maintaining replicative immortality is a crucial step in the development of cancers and is achieved by activating a telomere lengthening mechanism. While the majority of cancers rely on upregulation of telomerase, approximately 10-15% of cancers achieve telomere length maintenance through a telomerase-independent mechanism referred to as the Alternative Lengthening of Telomeres (ALT) pathway. ALT cancers exhibit a number of characteristic markers and recent work has sought to understand the mechanisms that underly the generation of these markers and of ALT telomere maintenance.

Previous work has also highlighted the striking loss of the chromatin remodelling protein ATRX and its histone chaperon partner DAXX in ALT cancers, and the ability of ATRX and DAXX to suppress the ALT pathway. Until now, however, it has remained unclear as to the mechanisms by which ATRX loss drives ALT development given that ATRX loss alone is generally insufficient to generate the ALT phenotype.

In this thesis a novel marker of ALT, the presence of Replication Protein A coincident with telomeric sequences, is shown. This marker is dependent on the presence of the endonuclease Mus81, which is known to cleave stalled replication forks. In conjunction, evidence is presented showing that the telomeric replication stress or lesions on telomeric DNA when combined with loss of ATRX or DAXX are able to trigger ALT pathway induction. This induction can be triggered both through artificial means with genotoxic agents, but also through loss of the histone lysine methyltransferase SETD2, which is responsible for the methylation of Histone H3.3 at lysine 36. Together these observations provide critical understanding of a possible route of ALT development, given the frequent co-occurrence of

112 histone H3.3 G34R/V mutations, which are known to be detrimental to SETD2 activity, and

113 ATRX/DAXX mutations in ALT cancers.

Introduction

2.1 What is ATRX?

Alpha thalassemia mental retardation X-linked, or ATRX, is a protein first discovered when attempting to ascertain the underlying genetic lesion responsible for an X-linked syndrome with characteristic α-thalassemia and mental retardation, which we now know as ATR-X syndrome (Weatherall *et al.*, 1981; Gibbons *et al.*, 1995, 2003). Patients, who present in childhood with distinctive craniofacial features, genital anomalies, microcephaly, developmental delays and intellectual disability also present with mild to moderate α-thalassemia due to reduced globin expression (Stevenson, 2020). Consistent with its X-linked inheritance pattern ATR-X syndrome predominantly affects males, although in very rare cases 46XX heterozygous females have been observed (Badens *et al.*, 2006).

Despite the wide range of phenotypes associated with ATR-X syndrome, to date ATRX remains the only mutation to be known to cause ATR-X syndrome. The severe developmental abnormalities that occur in ATR-X syndrome indicate that ATRX has wide ranging roles throughout development. Despite the wide range of phenotypes associated with ATR-X syndrome, to date ATRX remains the only mutation to be known to cause ATR-X syndrome. In particular, proteins known to interact with ATRX, including its histone chaperone partner death-domain associated protein (DAXX), are not found to be mutated in ATR-X syndrome patients (Gibbons *et al.*, 2008).

ATRX itself is comprised of multiple domains including the two primary domains: an amino-terminal ADD (ATRX-DNMT3-DNMT3L) domain and carboxyl-terminal helicase domain, as well as a number of other domains including a central DAXX interacting domain and an EZH2 interacting domain that harbours a region known to bind to the heterochromatin protein 1

family protein HP1α (Cardoso *et al.*, 1998; Lechner *et al.*, 2005; Argentaro *et al.*, 2007). The amino-terminal ADD domain contains a GATA-like domain, PHD finger (plant homeodomain) and C-terminal alpha-helix which together recognise the histone methylation mark H3K9me3 when the nearby H3K4 is unmethylated on the N-terminal tails of histone H3 (Dhayalan *et al.*, 2011; Eustermann *et al.*, 2011; Iwase *et al.*, 2011). The carboxyl-terminal helicase domain, on the other hand, shows DNA translocase activity via ATP-dependent hydrolysis (Xue *et al.*, 2003; Mitson *et al.*, 2011). Within this carboxyl-terminal domain exist seven helicase subdomains that identify ATRX as a member of the SNF2 family of chromatin associated proteins. Despite the fact that many SNF2 proteins have been shown to remodel, remove, or slide nucleosomes using *in vitro* assays, ATRX is most closely related to a subgroup that includes the proteins RAD54 and ARIP4, and performs poorly in such canonical assays. While they are indeed related, it would therefore appear they have varied chromatin-associated functions (Xue *et al.*, 2003; Law *et al.*, 2010).

Through its ADD domain ATRX has been shown to bind to heterochromatin, particularly that marked by H3K9me3. Additionally, ATRX has been shown to have a preference for binding DNA that is naturally G-rich and thus likely to form secondary DNA structures such as G-quadruplexes (Law *et al.*, 2010). These two factors lead ATRX to frequently localise to highly repetitive regions of the genome including telomeres, nucleoprotein structures at the distal ends of chromosomes that protect the chromosomes from the end-replication problem and ribosomal DNA repeat sequences, which encode ribosomal RNA sequences.

While mutations in ATR-X patients have been shown to occur across the ATRX protein, sequencing of ATR-X syndrome patients has shown clustering of ATRX missense mutations in the two primary domains (Xue *et al.*, 2003; Mitson *et al.*, 2011) and many of these have been

shown to destabilise the protein (Argentaro; Mitson). Mutations in ATRX, however, have also been observed in cancers, where the mutations show reduced clustering around the ADD and helicase domains, with a far more even distribution across the ATRX coding sequence. Due to this distribution, it has been proposed that ATRX mutations in cancer represent loss of function mutations, generally leading to the complete loss of ATRX protein (Heaphy, De Wilde, *et al.*, 2011; Jiao *et al.*, 2011).

2.2 ATRX as a chromatin remodeller

Through its interaction with DAXX, ATRX acts to deposit the histone variant Histone H3.3 into peri-centromeric, ribosomal and telomeric sequences (Drané *et al.*, 2010; Goldberg *et al.*, 2010; Lewis *et al.*, 2010). Although DAXX itself is responsible for the histone chaperon activities of the ATRX/DAXX complex, depositing H3.3-H4 tetramers into naked DNA, the ability of ATRX to localise the complex to H3K9me3 marked regions such as telomeres is essential (Drané *et al.*, 2010; Goldberg *et al.*, 2010; Lewis *et al.*, 2010; Wong, 2010). Previous work has shown the importance of the role of H3.3 in the maintenance of telomere integrity (Wong *et al.*, 2009).

2.3 ATRX and Cancer

Despite mutations in ATRX being identified in a number of cancers including sarcomas and glioblastomas, patients with ATR-X syndrome are generally not reported to have increased risk of cancer. Recent reports, however, of osteosarcoma in two brothers with ATRX syndrome may indicate that the young nature of both ATR-X syndrome patients and the field of ATR-X syndrome research itself may lead to statistical underrepresentation of the effects of ATRX mutations and cancer development (Ji *et al.*, 2017).

Mutations in ATRX have been associated with a number of different cancer types, including in pancreatic neuroendocrine tumours (PanNETs) and glioblastoma multiforme (GBM). The studies in PanNETs identified a number of mutations in key chromatin factors including MEN1, DAXX and ATRX. Strikingly, mutations in ATRX and DAXX were mutually exclusive, but were also found in 43% of all tumours (Jiao *et al.*, 2011). Subsequent studies in GBM uncovered mutations in ATRX and DAXX. Interestingly, these studies also identified mutations that lead to substitutions at residues K27 (K27M) or G34 (G34R/V) of the histone H3.3 tail. Mutations in ATRX, however, are commonly associated with a wider subset of cancers known to use a telomerase independent mechanism of telomere maintenance known as the Alternative Lengthening of Telomeres (ALT) pathway.

2.3.1 The ALT pathway

Achieving replicative immortality is a hallmark of cancer and is essential for cancer proliferation (Hanahan and Weinberg, 2011). Due to the end replication problem, wherein DNA polymerases fail to replicate the distal ends of chromosomes, chromosomal DNA is progressively shortened through each round of division, ultimately threatening genomic stability (Olovnikov, 1973). Humans, like many other species, have evolved protective repetitive sequences called telomeres, nucleoprotein structures that act as buffer sequence to prevent degradation of coding DNA as a result of the end replication problem as well as a barrier to the recognition of DNA ends by DNA repair machinery (De Lange, 2009). These sequences range from 3 to 12 kb in humans and consist of $TTAGGG_n$ repeats bound by a group of telomere proteins called the Shelterin complex (Greider, 1993). The Shelterin complex, consisting of TRF1, TRF2, POT1, TIN1, TPP1 and RAP1, acts primarily to protect and aid in the structuring of telomeres (De Lange, 2005). In this regard, the Shelterin complex works in concert to promote the formation of loop structures named t-loops from the overhanging

206 single-stranded G-rich DNA (ssDNA) that, in turn, prevents the DNA ends from being
207 recognised as a double strand break (DSB) (Griffith *et al.*, 1999).

208 The progressive shortening of telomeres, by approximately 200 bp per cell division, acts as a
209 cellular clock that ensures turnover of cells that have gone through many rounds of division
210 and potentially acquired a large number of mutations. At the end of this process, termed the
211 Hayflick limit, telomeres reach critically short lengths and trigger cellular senescence (Bodnar
212 *et al.*, 1998).

213 Some cells, namely long-lived cells such as stem and early progenitor cells, require
214 maintenance of these telomeric sequences to allow for long term survival. These cells use the
215 telomere elongating enzyme telomerase to maintain telomere length. Telomerase itself is a
216 combination of two principle components, the 1,132 amino acid telomerase reverse
217 transcriptase (TERT) and an associated telomerase RNA molecule (TERC) (Feng *et al.*, 1995;
218 Collins and Mitchell, 2002). Together, telomerase progressively adds telomeric sequence to
219 the end of telomeres (Bodnar *et al.*, 1998). The expression and activity of telomerase is tightly
220 controlled, limiting its use in normal dividing cells (Cong, Wright and Shay, 2002).

221 As many as 85% of cancers are thought to utilise this natural telomere extension mechanism
222 to maintain their own telomeres, allowing them to evade telomere crisis (Heaphy,
223 Subhawong, *et al.*, 2011). A minority of cancers, the so-called ALT cancers, have established
224 telomerase-independent mechanisms of telomere elongation (Bryan *et al.*, 1997). It is
225 proposed that ALT may resemble, or in fact be, the earliest form of telomere maintenance
226 mechanism (TMM), which preceded the evolution of telomerase-dependent telomere
227 maintenance. Indeed, it is additionally plausible that, at very low levels, ALT-like activity

occurs in all cells. Nevertheless, the levels of ALT activity in ALT cancers is significantly higher than that of normal functioning cells (Cesare and Reddel, 2013).

Despite over a decade of work in the field of ALT cancers, to date the exact mechanisms by which the phenotype develops is still largely unknown. One common, and striking feature of ALT cancers is the remarkable prevalence of mutations in the ATRX-DAXX-H3.3 axis. While mutations in ATRX are generally rare in cancers overall, with less than 1% of 84,000 cases in The Cancer Genome Atlas containing an ATRX mutation, rates of ATRX mutations in ALT cancers are comparatively much higher. When assessing panels of ALT cancers, work has previously shown that over 90% of ALT cancers display undetectable levels of ATRX protein and mutations or deletions in the *ATRX* gene (Lovejoy *et al.*, 2012).

2.3.2 Markers of ALT

ALT is characterised by a number of canonical markers. These include: extrachromosomal DNA circles, ALT associated PML bodies (APBs), telomere sister chromatid exchanges (tSCEs), telomere damage induced foci (TIFs), mitotic DNA synthesis (MiDAS), and telomere length heterogeneity (Bryan *et al.*, 1995; Yeager *et al.*, 1999; Henson *et al.*, 2009; Nabetani and Ishikawa, 2009; Chung *et al.*, 2012; Min, Wright and Shay, 2017b). Two markers, APBs and extrachromosomal DNA circles are regarded as the gold standard for ALT detection, being present in the majority of ALT cancers (Lovejoy *et al.*, 2012). More recently, the use of the ALT telomere synthesis at APBs (ATSA) assay, a method for detecting DNA synthesis at APBs in G2 phase of the cell cycle, has been established (J. M. Zhang *et al.*, 2019).

Extrachromosomal DNA circles, or T-circles, describe discontinuous double stranded telomeric DNA circles. They can be subdivided into two categories: C-circles and G-circles. C-circles are DNA circles with a complete telomeric C-strand ($CCCTAA_n$) and a partial

complementary G-strand. G-circles, on the other hand, comprise the opposite, a complete telomeric G-strand ($TTAGGG_n$) and a partial complementary C-strand. When detecting these extrachromosomal DNA circles, a rolling circle amplification technique is used to amplify the partial complementary strand (the G-strand in C-circles and the C-strand in G-circles) which can then be detected through quantitative PCR or with more traditional probe hybridisation techniques. Generally speaking, C-circles are assayed far more frequently, and are present at levels almost 1000-fold higher than in non-ALT fibroblasts (Henson and Reddel, 2010). In contrast, likely due to the tendency for G-circles to generate DNA structures on the exposed, single-stranded, G-rich DNA strand, G-circles are assayed for on a far less frequent basis, possibly due to being more technically challenging to detect as a consequence of structure formation interfering with the rolling circle amplification.

The presence of T-circles suggests an elevated rate of trimming from T-loops. Indeed, evidence in the GM847 ALT positive cell line shows a correlation with the size of T-circles and the size of the loop portion of t-loops as measured by electron microscopy (Cesare and Griffith, 2004). Furthermore, work has deduced that t-loop formation and stability requires TRF2 function, and that expression of the truncated TRF2 protein lacking the basic domain ($TRF2^{\Delta B}$) in cells results in telomere rapid deletions (TRD) and the formation of T-circles (Stansel, De Lange and Griffith, 2001; Wang, Smogorzewska and De Lange, 2004). Further work has shown that T-circle induction by $TRF2^{\Delta B}$ overexpression is dependent on both NBS1 and XRCC3, and that loss of either protein in ALT cells leads to reduced T-circle formation (Compton *et al.*, 2007). Finally, work from the laboratory of Ylli Doksani has shown, using electron microscopy, that the generation of internal telomere damage leads to the formation of internal DNA loops (termed “i-loops”) which in turn are metabolised to form C- and G-

circles. This work additionally cemented the link between the generation of C- and G-circles and telomere erosion (Mazzucco *et al.*, 2020).

ALT associated PML bodies, or APBs, are another canonical marker of ALT that is frequently assayed. APBs are regarded as the active site of telomeric DNA recombination in ALT (Chung *et al.*, 2012). APBs consist of a promyelocytic leukemia nuclear bodies (PML-NB) wherein telomeric sequence has migrated. PML-NBs, also known as nuclear domain-10 (ND10), Kremer (Kr) bodies or PML oncogenic domains (PODs) are nuclear structures comprised of the PML and SP100 proteins. These proteins form distinct sub-compartments within the nucleus which are believed to be mediated through multivalent SUMO-SIM (SUMO-interacting motif) interactions which ultimately leads to liquid-liquid phase separation (LLPS) (Min, Wright and Shay, 2019; Zhang *et al.*, 2020). These sub-compartments, which number from 5 to 30 depending on cell cycle phase, consist of a 50-100nm hollow sphere of PML and SP100 proteins (Lang *et al.*, 2010). To date, a wide array of proteins have been shown to interact with PML bodies in at least a transient manner (Lallemand-Breitenbach and de Thé, 2010). Therefore, PML bodies are considered to be involved in a wide array of nuclear processes.

In normal cells, PML bodies do not contain nucleic acids, with the exception of some evidence of RNA species on the periphery (Boisvert, Hendzel and Bazett-Jones, 2000). In ALT cells, however, multiple telomeres cluster together within large PML bodies (Min and Shay, 2019). Additionally, work to characterise APBs has found a number of DNA repair factors congregate in APBs in ALT. These include RAD51 and RAD52, key proteins required for strand invasion during homology driven DNA repair processes, as well as the endonuclease MUS81, replication protein A (RPA), breast cancer susceptibility protein 1 (BRCA1) or the MRN

296 complex consisting of MRE11, NBS1, and RAD50 (Yeager *et al.*, 1999; Wu *et al.*, 2003; Zeng *et*
297 *al.*, 2009).

298 As previously mentioned, recent work has shed light on the assembly of PML bodies, and the
299 recruitment of telomeric sequence to APBs. In work by Min *et al.,* fusion proteins containing
300 multiple SUMO and SIM motifs were tethered to telomeres in non-ALT cells. The subsequent
301 assembly of poly-SUMO/SIM-induced condensates through LLPS lead to the assembly of
302 pseudo-PML bodies containing telomeric sequence, akin to a classical APB. Strikingly,
303 however, telomere synthesis was absent from these structures, and only when the Bloom
304 syndrome helicase (BLM) was overexpressed in these cells did multiple ALT markers occur.
305 These features, including heterogeneous telomere length and telomere synthesis, therefore
306 clearly rely on BLM and its activity at APBs (Min, Wright and Shay, 2019). This is in agreement
307 with previous literature suggesting that BLM is required for telomere synthesis in ALT
308 (Stavropoulos *et al.*, 2002).

309 Furthermore, work has shown that APB formation is linked to the damage of telomeres or
310 replication stress when replicating through telomeric DNA. Indeed, loss of proteins known to
311 suppress replication stress including FANCM, FANCD2, and SMARCAL1 has been shown to
312 increase APB formation (Cox, Maréchal and Flynn, 2016; Root *et al.*, 2016; Lu *et al.*, 2019; Silva
313 *et al.*, 2019). Additionally, it has been suggested that replication stress at telomeres may lead
314 to MMS21-mediated SUMOylation of Shelterin and other telomere-binding proteins which as
315 discussed may have a role to play in the LLPS process of PML body formation (Potts and Yu,
316 2007). Finally, recent work has suggested that SUMOylation of TRF2 mediates a feed-forward
317 loop of BIR-driven ALT perpetuation. This would suggest that SUMOylation of TRF2 is an
318 essential step in ALT activation, and indeed loss of the SUMO E3-ligase protein PIAS4 leads to

reduced recruitment of repair factors to telomeres, and by extension an ablation of the ALT phenotype (Zhang *et al.*, 2021).

More recently, the presence of mitotic DNA synthesis, or MiDAS, has been observed in ALT (Min, Wright and Shay, 2017b). Like much of the human genome, telomeres are replicated throughout S-phase (Ten Hagen *et al.*, 1990; Wright *et al.*, 1999). This is in contrast to some yeast species, wherein telomere replication only occurs late in S-phase (McCarroll and Fangman, 1988). However, only recently has it been observed that ALT cells engage in unscheduled DNA synthesis in both G2 phase and mitosis. This phenomenon was observed in a number of ALT cells and is absent from cells that rely on telomerase for telomere maintenance (Dilley *et al.*, 2016). Interestingly, and in line with current hypotheses on ALT telomere elongation, MiDAS signals were primarily observed on a single chromatid, and as such are believed to be a consequence of break induced replication (Min, Wright and Shay, 2017a).

Interestingly, overexpression of BLM and RAD52 has been shown to promote telomere clustering, APB formation and MiDAS at telomeres. On the contrary, overexpression of SLX4 has been shown to instead reduce APB formation and leads to reduced telomere extension (Sobinoff *et al.*, 2017; Min, Wright and Shay, 2019). Furthermore, recent work has identified a role for SLX4IP - a protein that has been shown to interact with SLX4 – in the antagonisation of telomere-associated BLM, and subsequent modulation of the ALT phenotype (Panier *et al.*, 2019). This work suggests that ALT processes can be both positively and negatively influenced by factors such as BLM/RAD52 and SLX4, and that mechanisms and the resulting markers of ALT should be considered to be detached from one another. What was previously thought to be a single process is now understood to be a concert of aligned processes.

2.3.3 Break Induced Replication underlies ALT telomere elongation

Understanding the mechanism by which telomeres are maintained in ALT has been the topic of much study in recent work. Naturally, understanding the mechanism of telomere elongation would allow for targeted therapies of ALT cancers.

The ALT pathway was initially described in mutant budding yeast lacking telomerase, wherein there were two surviving populations, described as “types” (McEachern and Haber, 2006). Type I survivors display characteristic duplication of subtelomeric regions, named Y’ elements, but little elongation of telomeric sequences. In contrast, type II survivors stabilise telomere ends by elongation of telomeric sequences (Lundblad and Blackburn, 1993; Le *et al.*, 1999; Teng and Zakian, 1999; Teng *et al.*, 2000; Chen, Ijpma and Greider, 2001). Historically, type I survivors were thought to be both Rad51- and Rad52-dependent and, conversely, type II survivors were thought to be Rad52-dependent but Rad51-independent (Le *et al.*, 1999). Recently published work, however, has shown that the majority of ALT-like survival in yeast instead relies on a unified pathway consisting of RAD51-mediated ALT-precursor generation, followed by a RAD52-dependent telomere elongation phase in type II survivors (Kockler, Comeron and Malkova, 2021). In yeast, Rad51 acts as the primary homologous recombination (HR) recombinase, whereas Rad52 acts to bind Rad51 to single-stranded DNA and has some ability to anneal complementary ssDNA (Mortensen *et al.*, 1996; New *et al.*, 1998; Krogh and Symington, 2004).

Work by Dilley *et al.* in 2016 brought significant understanding of the underlying mechanisms of ALT telomere elongation in their work investigating the RFC-PCNA-Polδ axis and its involvement in ALT (Dilley *et al.*, 2016). In this work, it was shown that ALT telomere elongation exists as a form of aberrant break induced replication (BIR). BIR is a repair pathway

that is uniquely able to repair one ended DSBs. Mammalian telomeres present a unique substrate for BIR, where replication fork stalling can lead to one-ended breaks due to an absence of converging replication forks from the relatively replication-origin-devoid telomeres (Falaschi *et al.*, 2007; Sfeir *et al.*, 2009; Higa, Fujita and Yoshida, 2017). In contrast, replication fork stalling occurring in other regions can be rescued by converging forks, allowing for the opportunity to undertake more typical homologous recombination.

This work also highlighted a striking independence from the key homology search and strand invasion protein RAD51, which is a key player in other homology driven processes. Nevertheless, work has suggested that the RAD51 associated meiotic factors Hop2-Mnd1 are required for telomere movement and clustering, and that loss of these factors reduces telomeric recombination in ALT (Cho *et al.*, 2014). Work by others additionally showed that ALT is a bifurcated pathway, with RAD52-dependent and RAD52-independent pathways (J. M. Zhang *et al.*, 2019). Here, it was shown that RAD52 directly promotes telomeric D-loop formation and is required for the maintenance of telomeres in ALT-positive cells. Strikingly, however, RAD52 is dispensable for C-circle formation, with RAD52 knockout cells showing robust C-circle generation that increased as telomere length shortened. These activities were instead dependent on BLM and the BIR proteins POLD3 and POLD4. Other features, such as G2 DNA synthesis measured by ATSA are largely reported to have RAD51-dependent and RAD51-independent aspects. When considering the literature it is clear that there is significant importance on when in the cell cycle DNA synthesis occurs, with MiDAS primarily relying on RAD52, but other telomeric DNA synthesis being less reliant on RAD52 itself.

2.3.4 The role of replication stress in ALT

ALT cells display, along with previously discussed phenotypic markers, increased levels of the long non-coding RNA transcript TERRA (telomere repeat containing RNA), a G-rich RNA species transcribed from telomeres (Flynn *et al.*, 2015). Given their sequence homology to telomeric DNA, TERRA transcripts have been shown to form DNA:RNA hybrid structures at telomeres named R-loops (Arora *et al.*, 2014). These R-loops are proposed to act as barriers to replication through telomeres, inducing replicative stress, which may be important for the generation of the ALT phenotype (Pan *et al.*, 2019). Indeed, literature evidence suggests that proteins involved in the response to replication stress may play a role in ALT suppression.

One such protein is SMARCAL1, an ATP-dependent DNA helicase that is proposed to counter replication stress through the promotion of replication fork reversal at stalled forks (Bétous *et al.*, 2012). Indeed, SMARCAL1 has been shown to localise to ALT telomeres and suppress the ALT phenotype, with loss of SMARCAL1 in ALT increasing telomere clustering events, telomere damage, and telomere heterogeneity (Poole *et al.*, 2015; Cox, Maréchal and Flynn, 2016). Furthermore, two ALT positive cell lines, NY and CAL78, have recently been shown to harbour mutations in or display loss of expression of the *SMARCAL1* gene (Diplas *et al.*, 2018; Mason-Osann *et al.*, 2018).

In addition to SMARCAL1, proteins in the Fanconi Anaemia (FA) pathway have also been shown to have roles in the suppression of ALT. Recent work has demonstrated that FANCD2 suppresses BLM-dependent telomere extension in ALT cells, and that loss of FANCM results in ALT cells with enhanced ALT phenotypes including APBs, C-circles, telomere clustering, and unscheduled DNA synthesis (Root *et al.*, 2016; Pan *et al.*, 2017; Lu *et al.*, 2019; Silva *et al.*, 2019). In addition, loss of FANCM disproportionately affects viability in ALT positive cells,

where its presence was found to be critical, compared to ALT negative cells (Lu *et al.*, 2019; Silva *et al.*, 2019). Finally, FANCM is proposed to restrict TERRA levels and suppress R-loop formation at ALT telomeres, which results in reduced replication stress during telomeric DNA replication (Silva *et al.*, 2019).

2.3.5 The role of ATRX in ALT

Following from the discovery of the ALT pathway and the striking loss of ATRX in ALT cancers, significant work has been undertaken to understand the role of ATRX in ALT. Indeed, work from our lab has previously shown the ability for ATRX to suppress some of the hallmark features of ALT, namely ALT associated PML bodies (APBs) and extrachromosomal DNA circles (C- and G-circles) (Clynes *et al.*, 2015). In this work, ATRX was re-expressed in the ALT-positive U2OS cells under a doxycycline inducible promoter. Strikingly, levels of C-circles decreased by 90% within 5 days of ATRX induction and recovered after doxycycline was removed. Similarly, levels of APBs reduced by 66% under ATRX expression, and other features of ALT such as telomere damage induced foci (TIFs), telomere length and telomere crossover events reduced with ATRX expression. Additionally, the work also demonstrated that loss of DAXX prevents the depletion of ALT markers by ATRX (Clynes *et al.*, 2015). This work, therefore, implicates ATRX, in cooperation with DAXX, in the prevention of the ALT phenotype.

Given the prevalence of ATRX mutations in ALT, and its ability to suppress the ALT phenotype, one might expect that ATRX loss is uniquely responsible for ALT development. However, previous work has shown that, in fact, loss of ATRX is generally insufficient to trigger ALT in most cells. Indeed, loss of ATRX has been shown to enrich for ALT survivors in cells grown into crisis, and some recent work has shown that loss of ATRX alone is sufficient to induce ALT markers (Brosnan-Cashman *et al.*, 2018). However, these are isolated cases, and the case of

ATRX loss alone triggering ALT in recent work is likely due to other mutations that are, as of yet, unidentified. In conclusion, while ATRX loss appears to be an important step in the development of ALT, additional research is needed to understand exactly what the role of ATRX is in preventing ALT.

Beyond ATR-X syndrome and ALT cancer suppression ATRX has a number of described roles. Although one of ATRX's primary roles is in the ATRX-DAXX-H3.3 histone deposition pathway, wherein ATRX promotes the deposition of histone variant H3.3 into telomeres, ATRX has also been found to be a potent regulator of histone variant macroH2A incorporation into chromatin (Ratnakumar *et al.*, 2012). It has recently been shown that the interaction between ATRX and macroH2A1.2 additionally acts in a protective capacity to maintain fork stability during acute replication stress (Kim *et al.*, 2018). In ALT cells lacking ATRX, despite telomeric macroH2A1.2 being generally enriched, macroH2A1.2 is transiently lost during replication stress, leading to increased fork collapse, a potential driver of the ALT pathway (Kim *et al.*, 2019). In concert with this, loss of ATRX additionally permits the binding of the alternative macroH2A isoform, macroH2A1.1, to the poly(ADP-ribose) polymerase tankyrase 1 in a DNA damage response dependent manner, preventing its localisation to telomeres and resolution of cohesion. The result of this persistent telomere cohesion is an increase in tSCEs and a simultaneous suppression of excessive non-sister telomeric recombination that is detrimental to ALT cell growth (Ramamoorthy and Smith, 2015).

Many of the proteins mutated in ALT cancers are related, in part, to replication stress or DNA break repair deficiency. ATRX has previously been shown to be involved in both of these processes, with loss of ATRX being associated with increases in replicative stress, fork stalling, and reduction in fork restart, and fork protection (Leung *et al.*, 2013; Clynes *et al.*, 2014; Huh

et al., 2016). A recent analysis of proteins recruited to common fragile sites (CFS) identified ATRX as a pivotal player in CFS stability upon induction of replicative stress, with ATRX being recruited to a subset of CFS with DAXX in a FANCD2 dependent manner (Pladevall-Morera *et al.*, 2019). The notion of functional interactions between the ATRX/DAXX complex and FANCD2 is further evidenced in recent work showing that ATRX and FANCD2 localise to stalled forks and recruit the resection factor CtIP and promote MRE11 exonuclease-dependent fork restart. Furthermore, this mechanism was dependent on the deposition of H3.3 through ATRX/DAXX, demonstrating that coordinated deposition is a critical event in reinitiation of replicative DNA synthesis (Raghunandan *et al.*, 2020).

Additionally, evidence exists for a role of ATRX downstream of fork collapse in DNA double strand break repair. Work in human glioblastomas has indicated that ATRX loss leads to a reduction in non-homologous end joining (NHEJ), and renders cells lacking ATRX sensitive to a number of DSB inducing agents and ionizing radiation (IR) (Koschmann *et al.*, 2016). In contrast, Juhász et al. demonstrated no reduction in NHEJ efficiency in response to the loss of ATRX, and instead implicated ATRX in long tract DNA repair by homologous recombination (Juhász *et al.*, 2018).

Roles in replication stress and DNA repair could explain the involvement of ATRX in ALT, wherein DNA double strand breaks (DSBs) at telomeres are required for the initiation of BIR. However, until recently it was unclear as to how telomeric DSBs repaired by aberrant BIR would lead to telomere lengthening. Generally speaking, homology driven DSB repair processes are carefully orchestrated to ensure that strand invasion mediated by RAD51 (or RAD52 in the case of BIR) remains “in-register” (wherein sister chromatids remain aligned due to cohesin and lead to strand invasion in the reciprocal region of a sister chromatid). Recent

work, however, has highlighted an additional role for ATRX in the maintenance of telomere cohesion. Specifically, that loss of ATRX results in a telomere-specific loss of cohesion of sister chromatids (Lovejoy *et al.*, 2020). This observation is significant, in that it may explain why "out of register" BIR occurs so frequently in ALT cancers, but not in non-ALT cells. This "out of register" BIR is proposed to lead to invasion of ssDNA ends into distal sites on the sister chromatid, leading to an effective lengthening or shortening of telomeric DNA, depending on the invasion site.

A wealth of evidence now exists to demonstrate that ATRX is a critical factor in the suppression of ATRX and the mechanisms that underly many of the canonical markers of ALT have been the subject of a significant portion of research to date. However, many questions still remain as to how ALT arises *in vivo*, with loss of ATRX alone being generally insufficient to trigger the ALT pathway.

2.4 Aims

Given the current gaps in understanding of how ALT develops *in vivo*, in this thesis we aim to elucidate novel mechanisms of ALT cancer initiation~~,~~ through the use of model cell lines~~,~~ DNA damaging agents, and targeted gene knockouts. Based on previously published literature regarding the roles for ATRX in the protection of replication forks, and the proposed role for replicative stress in ALT induction, we test our principle hypothesis: that the induction of DNA damage and replicative stress in ATRX deficient cancers will induce an ALT-like response.

In addition, we hope that understanding of ALT development will lead to ALT-specific therapies in the future, and aid in the diagnosis and prevention of ALT development. To further this aim, in this thesis we also discuss the discovery of a potential novel marker of ALT and its possibilities for use in the clinical diagnosis of ALT cancer.

Results Chapter 1: RPA at telomeres as a marker of the ALT pathway

3.1 ALT cells display single stranded telomeric sequence as a marker

Finding new canonical markers for cells that use the ALT pathway of telomere maintenance is critical to improving diagnosis of ALT cancers, especially in the era of personalised medicine. Thus, we first set out to determine if we could identify a novel marker of ALT cells. The first candidate marker was that of the long non-coding telomeric RNA species TERRA. Previous work has shown an increase in TERRA in ALT cells, with previous detection methods including RNA FISH and Northern blotting (Flynn *et al.*, 2015).

To first verify previous findings, RNA fluorescence *in-situ* hybridisation (RNA-FISH) was performed on a panel of ALT cells using a telomeric C-strand $[CCCTAA]_3$ probe as described in Section 7.10.5, taking particular care to avoid RNase contamination.

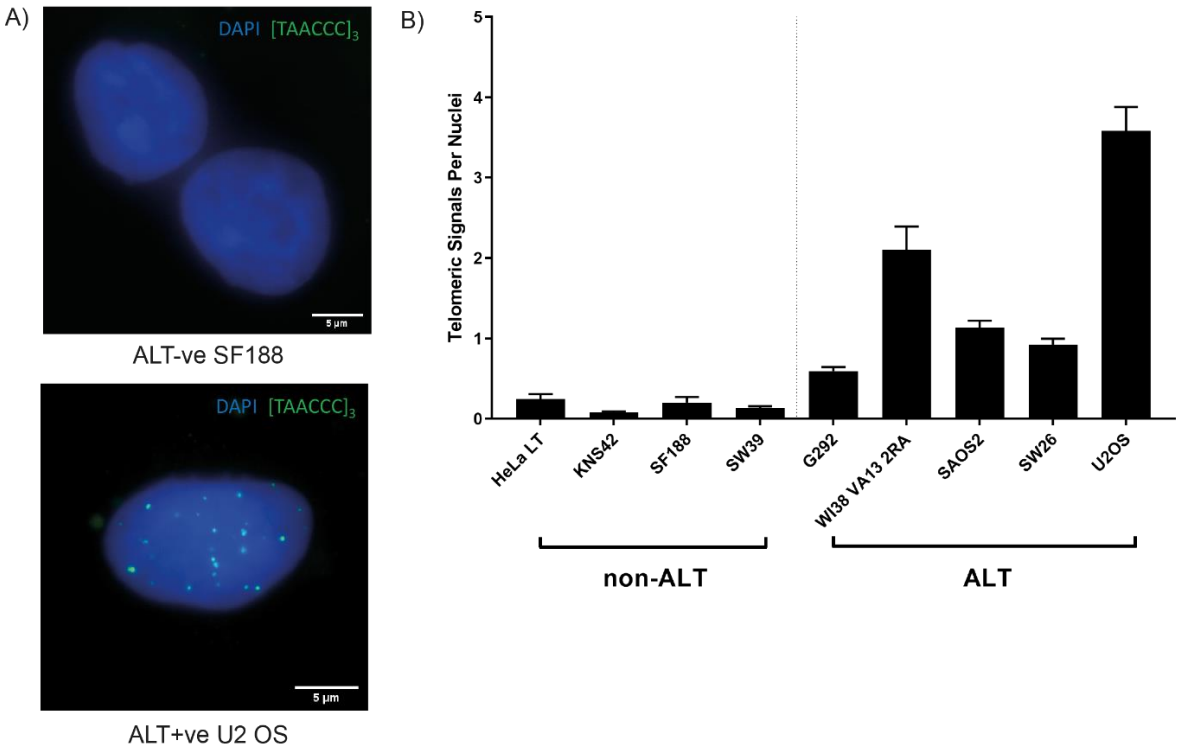

Figure 1: Telomere signals in a panel of ALT and non-ALT cells following RNA-FISH. A) Representative images from the non-ALT SF188 cell line (top) and ALT cell line U2OS (bottom), showing telomere signal foci. B) Quantification of telomere signals across a panel of non-ALT and ALT cells.

As expected, and in agreement with previous studies, significant telomere signals were only observed in ALT cell lines, and not in non-ALT cells (Figure 1~~Figure 1~~). Although variability was seen between ALT cell lines, all tested ALT cell lines displayed significantly higher levels of telomere signals than non-ALT cells. In order to confirm these signals represented telomeric RNA species, such as TERRA, the RNA-FISH process was repeated with the addition of RNase A, an RNase capable of depleting both single and double-stranded RNA species, with the expectation that this step would eliminate telomeric signals in ALT cells. In addition, cells were also treated with RNase H, an RNase capable of depleting three stranded DNA:RNA hybrid structures referred to as R-loops (Cerritelli and Crouch, 2009).

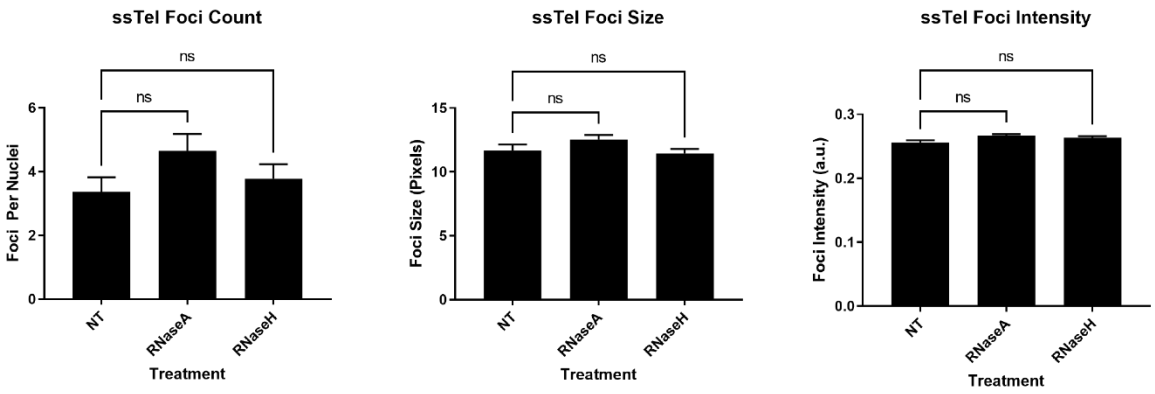

Figure 2: RNase A controls for telomere signals in WI38 VA13 2RA showing telomere foci count, foci intensity, and foci size. Foci count, size, and intensity were determined using automated quantification of at least 200 nuclei per condition across 3 biological repeats. One way ANOVA, Welch correction.

Strikingly, however, RNase treatment was unable to deplete telomeric signals across multiple RNase A/RNase H lots and biological repeats (Figure 2~~Figure 2~~), with no reduction in telomere foci number, size or intensity. Previous literature has discussed the use of RNase A in the depletion of TERRA signals by RNA-FISH, contradicting the findings here (Flynn *et al.*, 2015; Chu *et al.*, 2017). Therefore, although it was possible to conclude that ALT cells display telomere signals following a non-denaturing FISH protocol, it was not possible to confirm that these represent the long non-coding RNA TERRA. Nevertheless, due to the non-denaturing nature of the RNA-FISH it was possible to deduce that these signals did not represent single stranded telomeric DNA that arose as a consequence of the denaturation of telomeres.

3.2 Telomere signals in ALT cells bind Replication Protein A

In order to try to ascertain the origin of telomere signals in ALT cells, the RNA-FISH protocol was adapted to an Immuno-FISH protocol by combining immunofluorescent staining with a sequential DNA FISH probing step to determine if the telomeric sequences in ALT cells colocalised with the single stranded DNA binding protein RPA.

Indeed, ALT cells showed significant colocalisation between RPA32, a 32 kDa subunit of the heterotrimeric protein RPA, and $[CCCTAA]_3$ telomere signals (Figure 3~~Figure 3~~). This indicated that a significant proportion of telomere signals were likely to be single stranded DNA and not RNA as has previously been suggested in the literature. These findings are not the first reported instance of RPA at telomeres, with previous publications drawing associations between telomeres and RPA (Flynn *et al.*, 2015; Loe *et al.*, 2020).

Notably, in both yeast and humans, RPA has been shown to associate with telomeres during S phase of the cell cycle (Verdun and Karlseder, 2006; Moser *et al.*, 2009; McGee *et al.*, 2010). Furthermore, work by Flynn *et al*., in 2015 sought to understand the role of TERRA and the heterogeneous nuclear ribonucleoprotein A1 (hnRNPA1) in orchestrating the switch from RPA coating ssDNA overhands at the ends of telomeres to coating with the shelterin component POT1 (Flynn *et al.*, 2011). The enrichment of RPA at telomeres in ALT cells, however, is an interesting avenue of study in the development of novel ALT detection methodolgies.

To confirm the specificity of RPA bound at telomeric ssDNA, which we now refer to as RPA+ssTel, as a marker for ALT, we compared RPA+ssTel levels in a panel of ALT cells to the levels of C-circles in the same cells (Figure 4~~Figure 4~~). By normalising the C-circle and RPA+ssTel levels to that of the ALT positive U2OS cell line, it is possible to determine whether RPA+ssTel levels are reflective of the level of ALT in a cell line, as measured by C-circles.

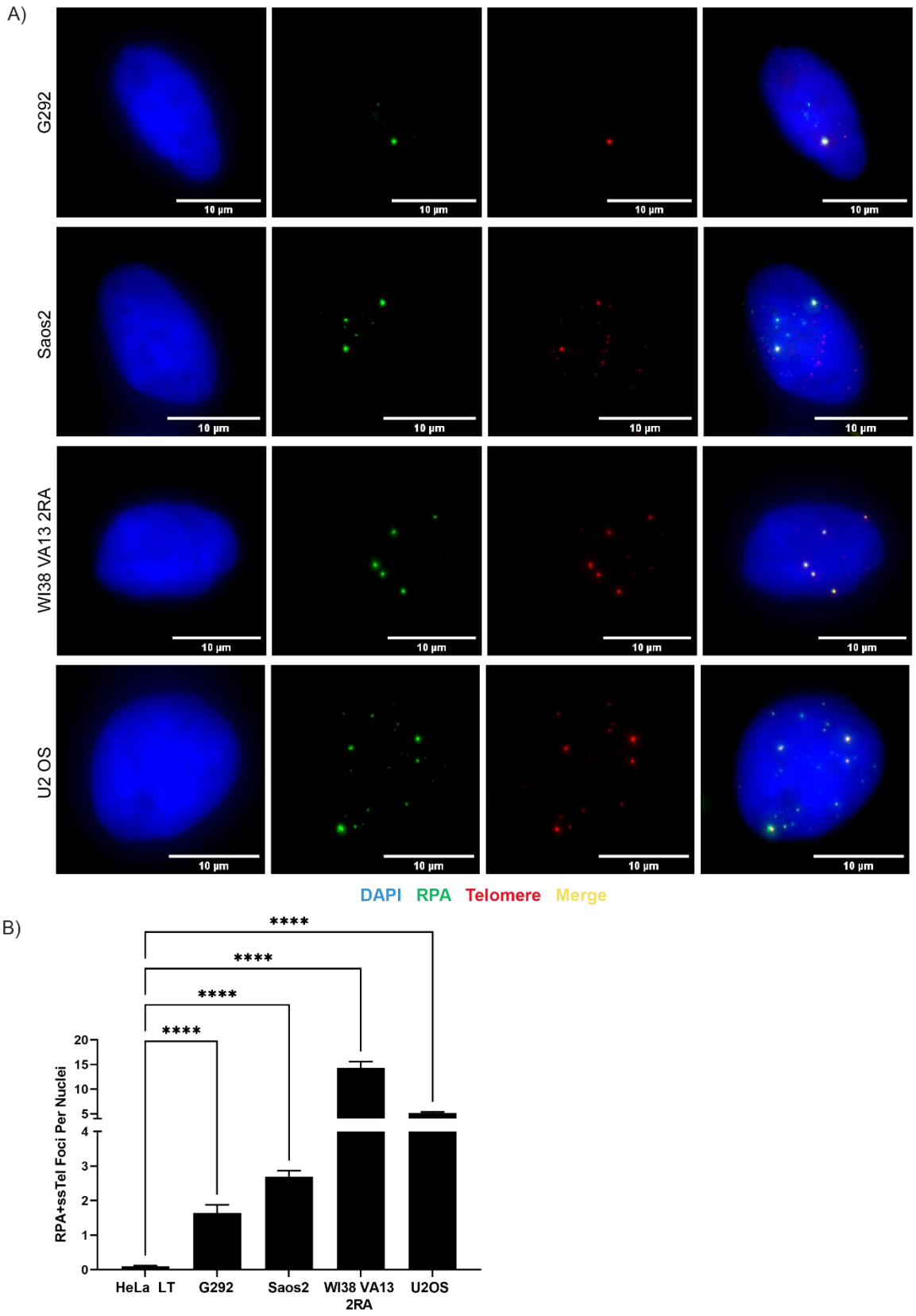

561

562 **Figure 3: RPA colocalises with telomeric signals in ALT cells**. A) Representative images of RPA (red) and telomere signals
563 (green) in a panel of ALT cell lines. B) Quantification of RPA positive telomere foci in ALT cells. 3 biological replicates, >50
564 nuclei per replicate. One Way Anova, **** $P < 0.00005$.

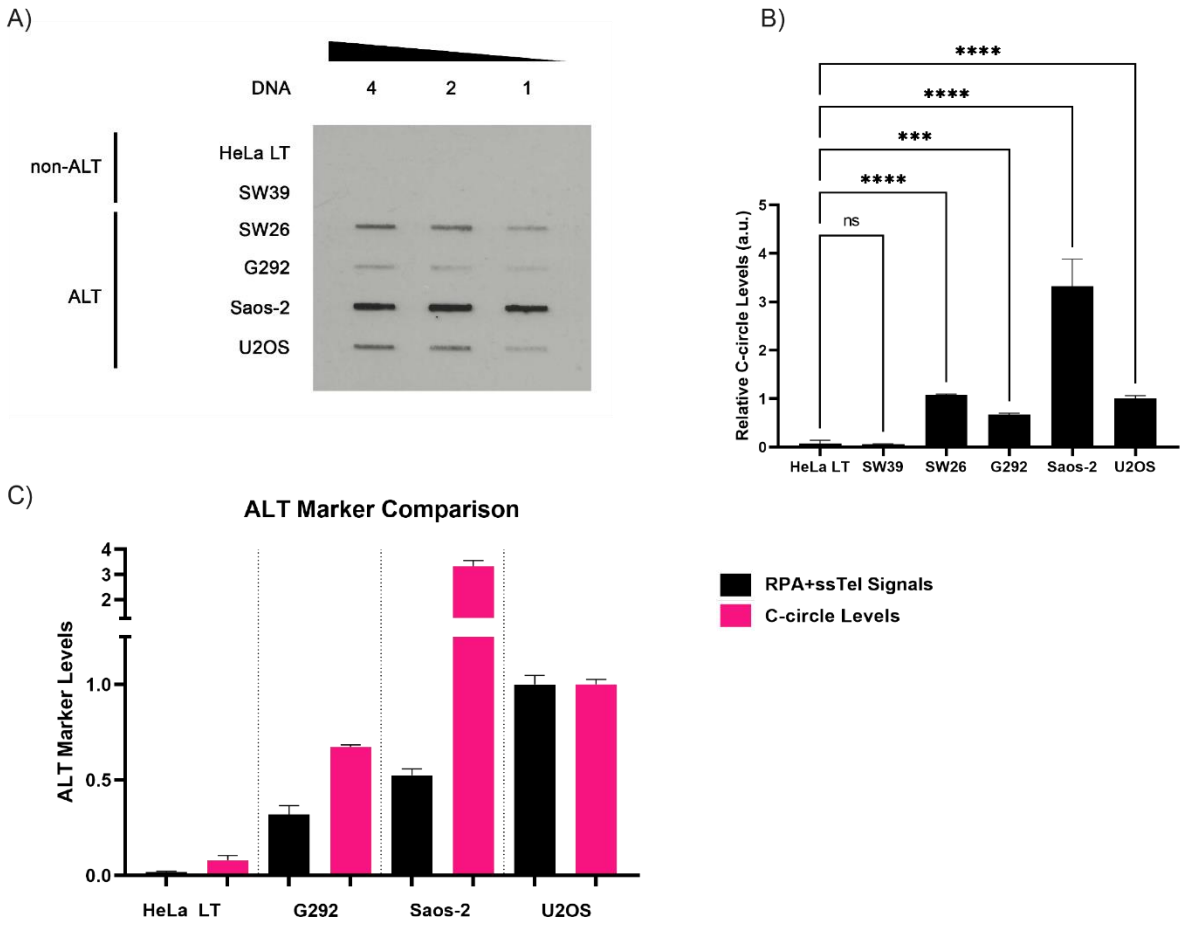

Figure 4: Levels of C-circles in a subset of ALT cells. A) Representative C-circle blot. B) Quantification of C-circles across the ALT cell panel (2 replicates). C) Relative comparison of RPA+ssTel levels and C-circle levels, normalised to the ALT positive U2OS cell line. One way ANOVA, Welch correction. ***, **** $P < 0.0005, 0.00005$.

Strikingly, whilst both C-circle levels and RPA+ssTel levels were elevated in ALT cells compared to non-ALT cells, there was almost no direct correlation between the two. For example, the ALT cell line Saos-2 is described in the literature to have C-circle levels 5-fold higher than U2OS (Lovejoy *et al.*, 2012). In our data whilst we see C-circle levels 3-fold higher than that of U2OS, RPA+ssTel levels across 3 independent replicates are, on average, half of that seen in U2OS. This highlights that whilst RPA+ssTel is generally increased in ALT-positive cell lines when compared to non-ALT cells, this increase is not directly proportional to the level of C-circles.

3.3 ATRX expression suppresses RPA at telomeres

Given that our laboratory has previously shown that ectopic expression of ATRX is sufficient to suppress multiple canonical markers of the ALT pathway we next asked whether the ectopic expression of ATRX in an ALT cell line could likewise suppress the formation of RPA+ssTel (Clynes *et al.*, 2015). To this end, through the use of a doxycycline-inducible ATRX cDNA in the canonical ALT cell line U2OS it was possible to express ATRX in an ALT context with fine control, referred to as U2OS^{ATRX}.

After confirming the expression of ATRX by western blotting, RPA+ssTel levels were measured in the presence and absence of ATRX (Figure 5~~Figure 5~~**A**). Expression of ATRX in an ALT context significantly depleted RPA at telomeric signals to level similar to that of wild type HeLa, confirming the ability of ATRX to suppress RPA+ssTel and providing more evidence that RPA at telomeres is a canonical marker of ALT (Figure 5~~Figure 5~~**B**).

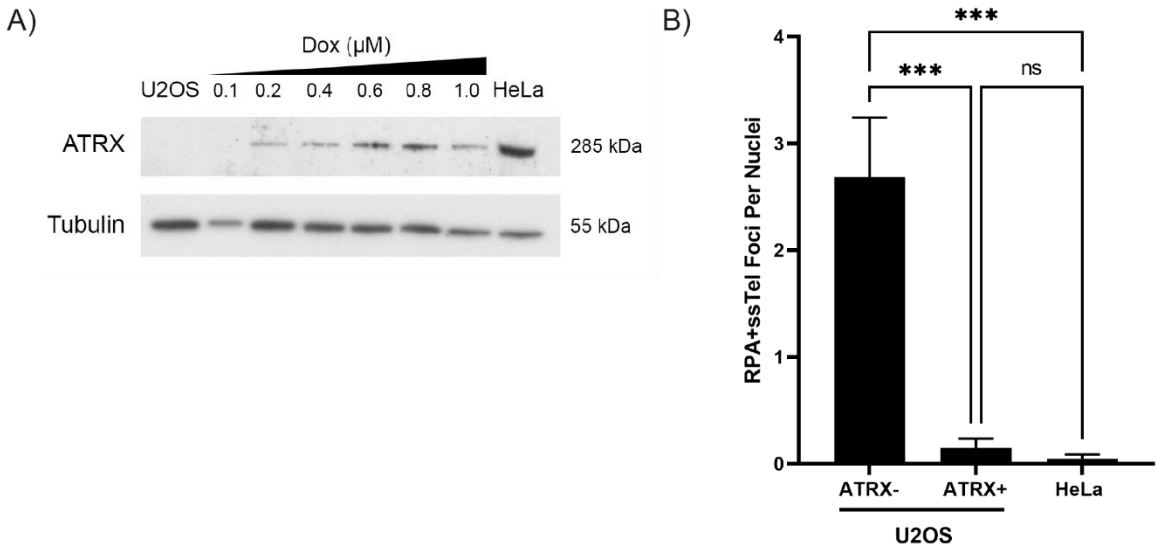

Figure 5: ATRX expression in the ALT cell line U2OS supresses RPA at telomeric signals. A) Western blot showing doxycycline-inducible ATRX expression after 4 days of doxycycline treatment. B) Quantification of RPA at telomeric signals in the presence or absence of ATRX. One way ANOVA, Welch correction. *** $P < 0.0005$. Western blot by Sam Shepherd.

3.4 RPA colocalisation with telomeres is not induced by ATRX loss

Due to the findings of Flynn *et al.*, wherein ATRX loss is associated with a persistence of RPA at telomeres in a TERRA dependent manner, and our observation that ATRX expression in ALT cells is sufficient to deplete the phenotype, we next sought to generate a model system to investigate whether ATRX loss alone in non-ALT cells is sufficient to lead to accumulation of RPA at telomeres (Flynn *et al.*, 2011).

Previous work from both our laboratory and others has shown that ATRX is a crucial factor in the suppression of ALT, however, its precise role in the suppression of the ALT pathway to date remains unclear. Indeed, the question of whether ATRX loss alone can trigger the ALT pathway has been asked by several groups before, with ATRX loss generally found to be insufficient to induce markers of the ALT pathway (Lovejoy *et al.*, 2012; Clynes *et al.*, 2014; Eid *et al.*, 2015; Napier *et al.*, 2015).

Of note, recent work has shown that CRISPR-Cas9 mediated depletion of ATRX induces canonical markers of ALT in two specific glioma cell lines (U-251 and UW479) and a prostate cancer cell line (LAPC-4) (Brosnan-Cashman *et al.*, 2018; Graham *et al.*, 2019). Given that this induction was specific to these cell lines, it is likely that additional genetic or epigenetic events occur alongside ATRX loss to facilitate induction of ALT in human cancer.

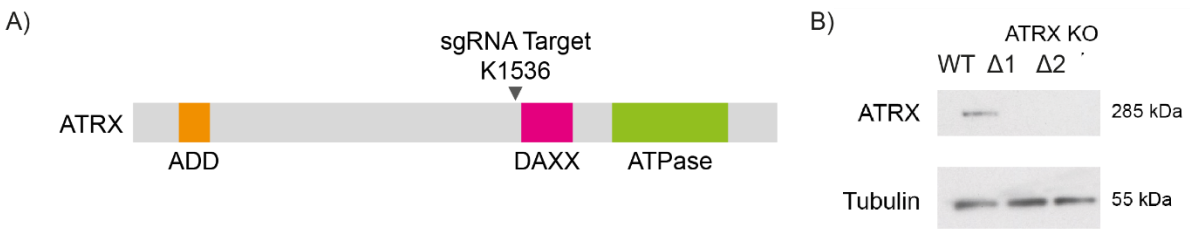

Figure 6: ATRX knockout model system in the non-ALT cell line HeLa LT. A) Schematic of CRISPR Cas9 guide RNA location (Lysine 1536, Exon 16). B) Western blot showing ATRX knockout in two independent clones. Western blot (6B) by Siobhan Cunniffe.

To explore this further CRISPR Cas9 mediated knockouts of ATRX were generated by Sam Shepherd (Clynes Lab) in a subclone of HeLa cells (1.2.11), chosen for their long telomeres, henceforth referred to as HeLa LT ("Long Telomere"). The reasons for choosing this cell line were twofold. Firstly, ALT markers had previously been generated in this cell line through the knockout of ASF1, highlighting this cell line as one that is amenable to manipulation in a way that may generate an ALT-like phenotype (O'Sullivan *et al.*, 2014). Secondly, we hypothesised that should the phenotype represent, or in some way require, telomeric damage to form, a cell line with particularly long telomeres may contain the perfect substrate for ALT generation.

Multiple independent knockout clones were generated (Figure 6~~Figure 6~~). The CRISPR guide chosen targeted exon 16 of ATRX, affecting only the full length ATRX isoform, and not the truncated ATRX isoform (frequently referred to as tATRX). The truncated isoform, however, is not known to be functional, so was not expected to have any effects on this work.

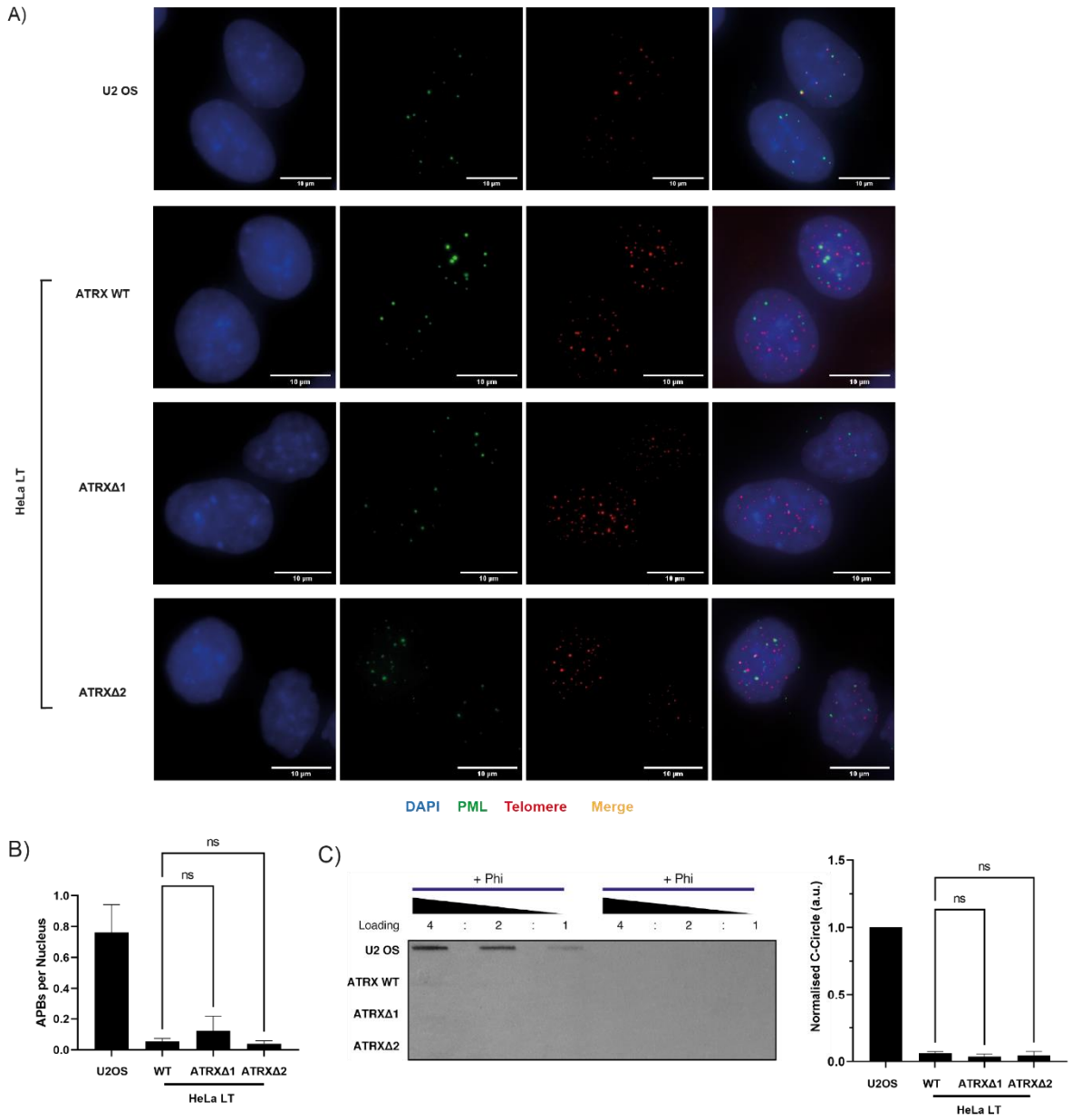

626

627 **Figure 7: Measurement of ALT markers in HeLa LT ATRX Wild Type and Knockout cells**. A) Representative images of APBs
628 in the ALT-positive U2OS and ALT negative HeLa LT, both in the presence and absence of ATRX. B) Quantification of APBs in
629 A. C) Representative C-circle blot as measured by rolling circle amplification and dot-blotting and quantification. N=3,
630 Immuno-FISH experiments >50 nuclei per replicate. One Way ANOVA, ns = not significant. APB (A & B) experiments
631 performed by Sam Shepherd, C-circle experiments (C) performed by Tomas Goncalves.

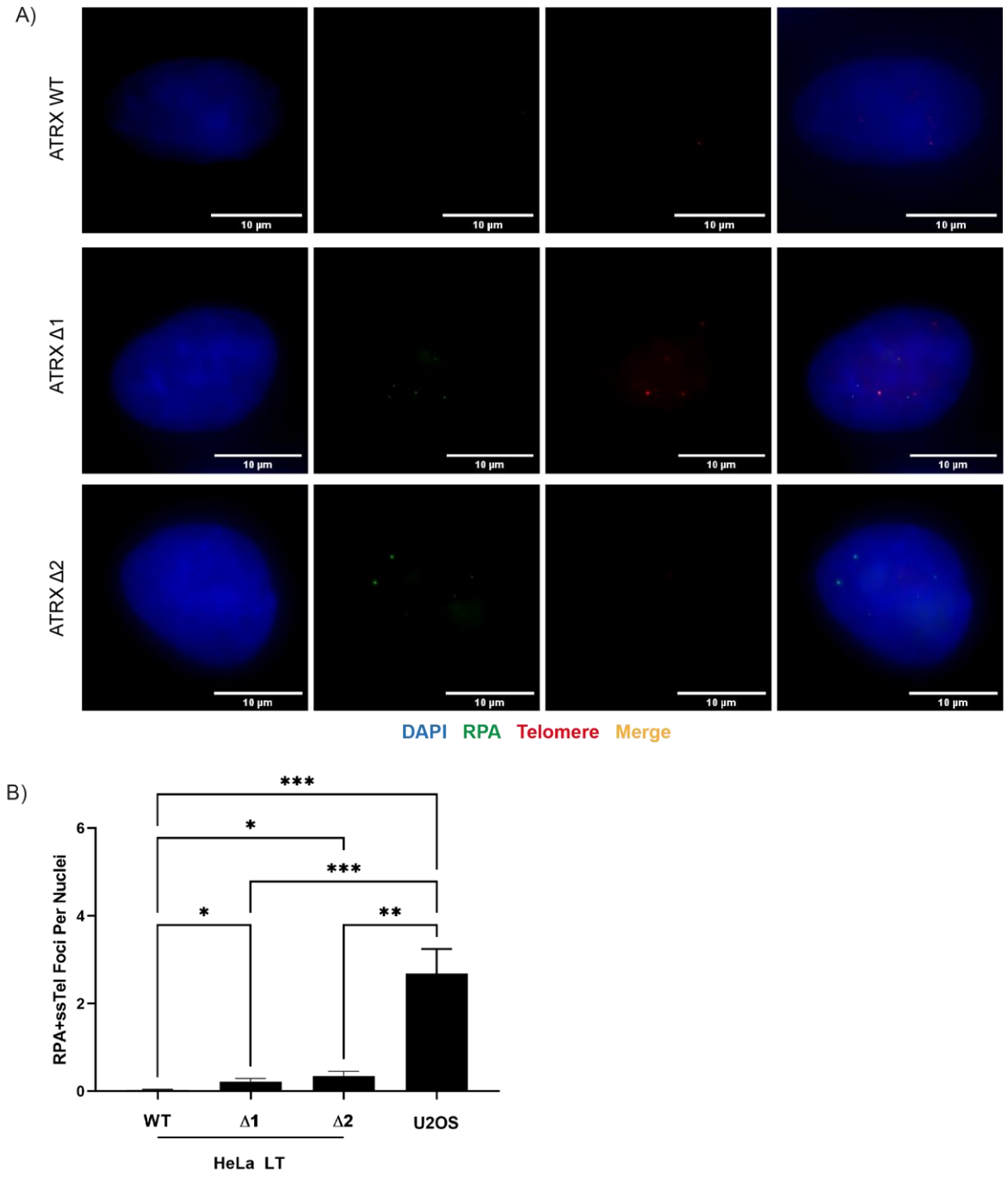

632

633 **Figure 8: RPA at telomeres does not form after knockout of ATRX in a non-ALT cell line.** A) Representative images of RPA
634 positive telomere signals in ATRX wild type (WT) HeLa LT and two independent ATRX knockouts (1 and 2). B) Quantification
635 of RPA positive telomeric signals in A compared with the ALT cell line U2OS. N=2, >50 nuclei per replicate. One Way ANOVA,
636 Welch correction. *,**,*** $P < 0.05, 0.005, 0.0005$.

637 We first sought to determine whether, in this model system, loss of ATRX alone was sufficient

638 to trigger the ALT pathway. In line with the general notion that ATRX loss alone is generally

insufficient to trigger the ALT pathway, assessment of ALT markers including APBs and C-circles in HeLa LT ATRX knockout cells, failed to trigger measurable levels of either marker (Figure 7~~Figure 7~~). Immuno-FISH was then performed on this model system, as previously described, to measure RPA foci at telomeres. This experiment demonstrated that knockout of ATRX alone was insufficient to generate RPA foci at telomeric sites, to the level of that of the ALT positive U2OS control (Figure 8~~Figure 8~~). Nevertheless, there was a minimal induction of RPA+ssTel foci in ATRX knockout cells. Together these data suggest that indeed, in this model system, loss of ATRX alone is not sufficient to trigger the ALT pathway, however, loss of ATRX does induce RPA+ssTel to a small degree.

Naturally, this raises the question of what additional factors alongside ATRX loss are required to trigger the RPA+ssTel phenotype, and by extension trigger ALT itself. Additionally, given the disparity between ALT markers in ALT cells such as C-circles and RPA+ssTel, and the minimal induction of RPA+ssTel alone in ATRX knockout HeLa LT cells, important questions remain as to the underlying mechanism of RPA+ssTel generation.

Results Chapter 2: The role of ATRX in protecting telomeres upon replicative stress

4.1 Stabilisation of G Quadruplexes induces ATRX localisation

Given that ATRX loss alone was unable to stimulate the recruitment of RPA to telomeric sequences in non-ALT cells we next sought to address what else may be required in an *in vivo* system alongside ATRX loss to generate ALT. To date, with the exception of mutations in other genes such as DAXX and SMARCAL1 that usually occur in a mutually exclusive manner to ATRX mutations, and mutations that permeate a large proportion of certain cancer types, such as IDH1 mutant in glioblastoma, or the commonly mutated tumour suppressor p53, no other mutation has been highly correlated with ATRX loss in ALT cells, and particularly none have been shown to exist across a wide range of ALT tumour types. Indeed, when analysing 2212 paediatric tumours from the Pediatric Cancer (PeCan) dataset (**Figure 9**~~**Figure 9**~~) in both brain and solid tumours, ATRX mutations are found in 100 such tumours. When analysing common mutations that cooccur with ATRX mutations, the only common mutations are those of the tumour suppressor TP53 and the histone H3.3 encoding gene H3F3A. Mutations in these genes are discussed in studies within the literature and are particularly common in paediatric glioblastoma (Schwartzentruber *et al.*, 2012). When looking at solid tumours, however, such as the frequently ALT positive osteosarcoma, only around 20% of ATRX mutant solid cancers also harbour mutations in TP53, and no ATRX mutant solid tumours in the PeCan dataset have cooccurring H3F3A mutations. In these tumours, mutations in RB1 are instead more prevalent. Nevertheless, even when combining TP53 and RB1 mutations, the majority of ATRX mutant solid tumours display no other commonly mutated gene.

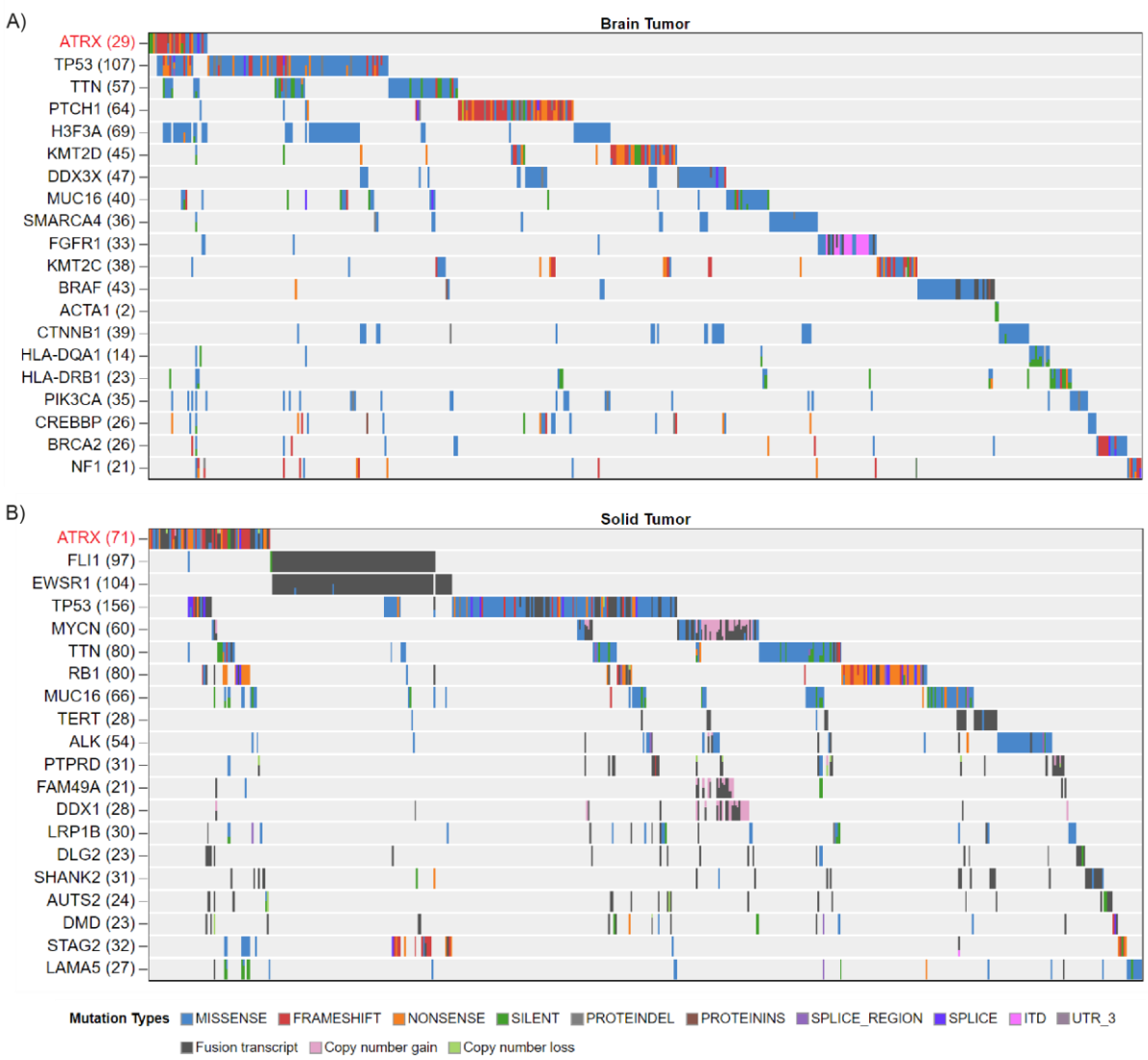

Figure 9: Analysis of mutations in brain and solid tumours from the PeCan analysis of paediatric cancers. A) Analysis of brain tumour mutations in 994 individuals. B) Analysis of solid tumour mutations in 1216 individuals.

Therefore, if it is not a common mutation that occurs with ATRX loss, we hypothesised that it was perhaps an environmental change within cells that predisposed cells that lose ATRX to ALT transformation. To address this, we first considered what role ATRX may be crucial for that, when lost, leaves cells vulnerable to developing ALT.

When considering the sites ATRX is known to bind to through its chromatin binding PHD domain, in many cases, such as at telomeres, these sites are guanine rich and are predicted to form secondary structures such as G-quadruplexes. Additionally, work from our lab and

others has shown that ATRX loss leads to both an increase in the three-stranded RNA:DNA hybrid structures called R-loops, and G4 structures (Nguyen *et al.*, 2017; Wang *et al.*, 2019). It is hypothesised that R-loops and G-quadruplexes occur in tandem, especially where the displaced DNA strand is guanine rich. It therefore stands to reason that ATRX could itself have important roles in response to G-quadruplexes, and perhaps in the prevention or suppression of R-loops.

Therefore, we aimed to determine whether artificial stabilisation of G-quadruplex structures altered the localisation of ATRX. To do this, cells were treated with 5 µM of the G-quadruplex stabiliser pyridostatin (PDS), and the localisation of ATRX was observed by immunofluorescence.

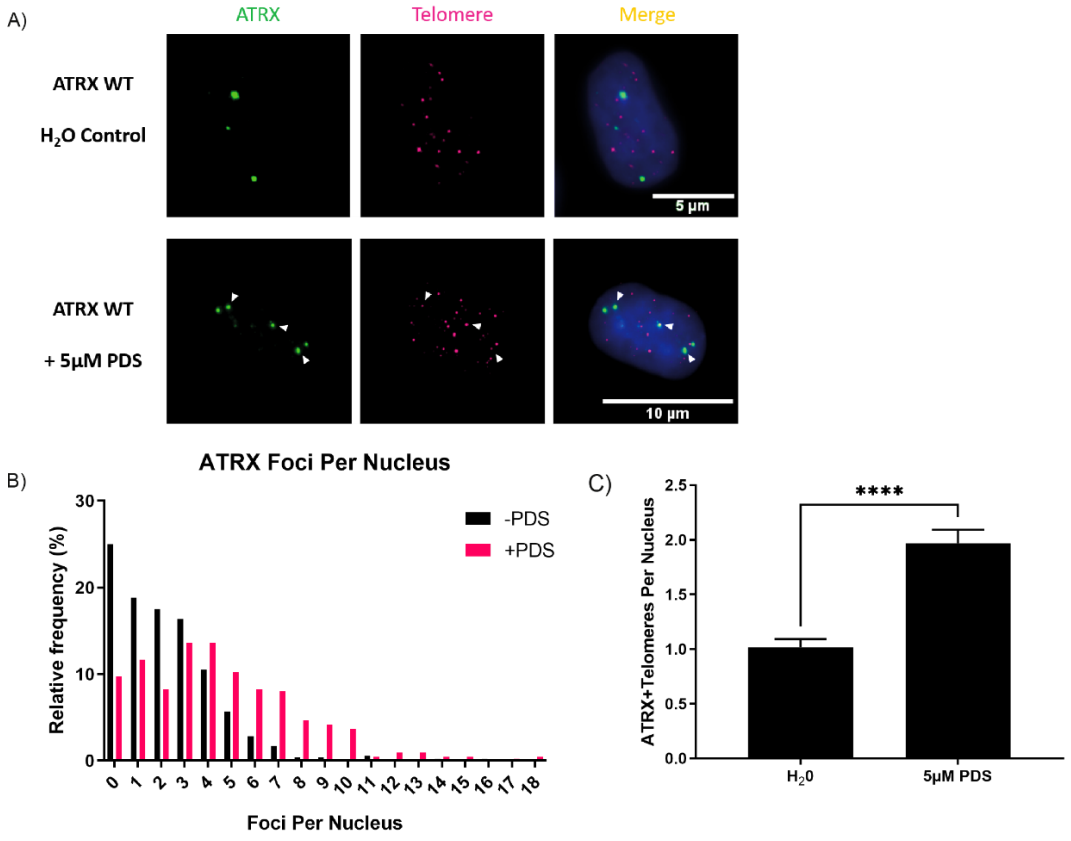

Figure 10: ATRX foci form upon treatment with PDS. A) Representative images showing ATRX foci formation (green). B) B) Histogram of ATRX foci per nucleus. C) Quantification of telomere positive ATRX foci. N=3 biological repeats, minimum 50 nuclei per replicate. Unpaired T-test, Mann-Whitney correction. **** P < 0.00005

Upon treatment with PDS, HeLa LT WT cells showed a significant increase in ATRX foci formation (Figure 10~~Figure 10~~). In the analysis in Figure 10~~Figure 10~~**B** the number of ATRX foci per nucleus is shown in histogram form. These data show a rightward shift in PDS treated cells, indicating that nuclei display greater numbers of ATRX foci than in untreated cells. Similarly, when analysing ATRX foci colocalisation with telomeres through denaturing FISH, colocalisations increased 1.5-fold in PDS treated cells, indicating that the stabilisation of G-quadruplexes leads to an increase in recruitment of ATRX.

In order to determine whether ATRX foci are recruited to sites of G4 we next planned to investigate whether the sites in which ATRX foci form are active sites of G4 structure formation. Unfortunately, despite G4 structures being readily studied in *in-vitro* environments, to date very little literature evidence exists of a reliable method of detecting G-quadruplexes *in-vivo*. The majority of studies attempt to show G4 formation through immunofluorescent detection with antibodies raised to G4 structures (Wang *et al.*, 2019). However, many of these studies have proven to be difficult to replicate. One of the most probable reasons for this is that, unlike protein antigens, DNA structure antigens are often very fluid, and do not necessarily conform to a single shape. Although we attempted to perform G4 immunofluorescence on a number of occasions, we were ultimately unable to ascertain whether ATRX directly colocalised to G4 sites.

4.2 G-Quadruplex stabilisation in ATRX deficient cells induces RPA+ssTel and ALT

Due to the formation of ATRX foci upon PDS treatment, it is plausible that ATRX itself plays some role in the response to G4 stabilisation, or in the very least in the response to PDS treatment. Therefore, we sought to address whether PDS treatment in the absence of ATRX caused any deleterious effects when compared to treatment in the presence of ATRX. As

previous literature evidence has suggested the need for damage at telomeres in the induction of the ALT pathway, it stands to reason that structures like G4 could present the perfect barrier to replication machinery and precipitate this damage. Similarly, as ATRX has been shown to localise readily to telomeric sequences, it is also plausible that one of ATRX's roles at telomeres is the prevention of structures such as G4 that ultimately lead to double strand break formation.

To address this question, we first sought to determine whether PDS induces markers of DNA damage in cells, and whether this DNA damage differs between ATRX wild type and ATRX KO cells. Cells were treated for 24 hours with PDS then fixed to coverslips. Immuno-FISH was then performed, staining for the ataxia-telangiectasia mutated (ATM) serine 1981 phosphorylation (pATMs1981). pATMs1981 is a common marker used to determine activation of the ATM pathway, a key kinase pathway involved in the early stages of DSB repair coordination. By looking for colocalisation between pATMs1981 foci and telomeric foci, it is possible to quantify an approximate level of DNA damage at telomeres.

Following treatment with PDS, both ATRX wild type and ATRX knockout cells saw increased levels of telomeric pATMs1981 signals (**Figure 11**~~**Figure 11**~~). However, in ATRXΔ1 HeLa LT cells, pATMs1981/telomere colocalisations were significantly more frequent, indicative that ATRX null cells, at least in some clones, were far less able to tolerate PDS treatment. ATRXΔ2 cells saw fewer colocalisations and display a much more modest response indicating some degree of clonal variance.

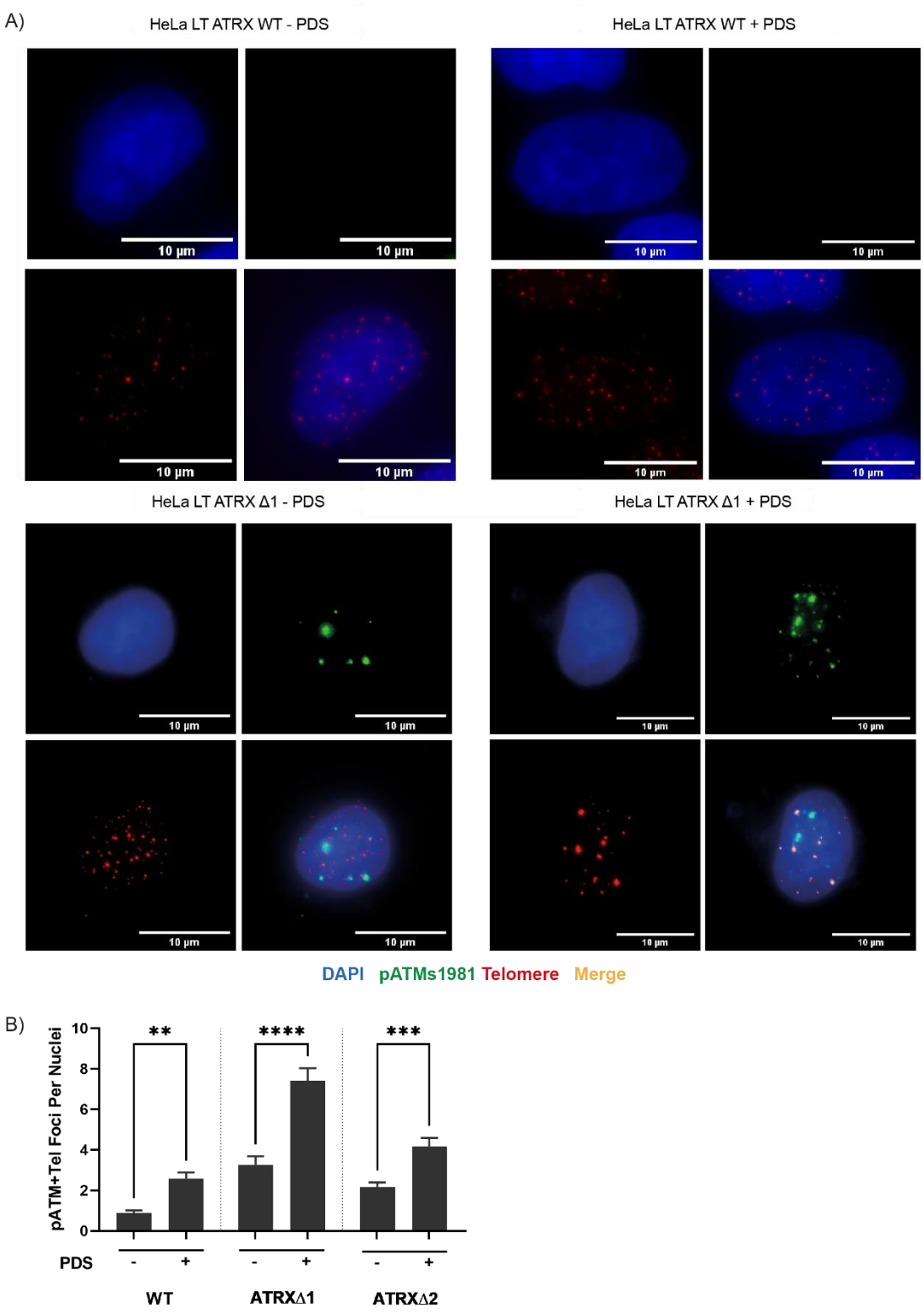

742

743 **Figure 11: PDS induced pATMs1981 colocalisation to telomeres in ATRX deficient cells**. A) Representative images of
744 pATMs1981 (green) at telomeres (red) in HeLa LT ATRX WT and 2 ATRX knockout clones. B) Quantification of
745 pATMs1981+Telomere foci from A. N=3, >50 nuclei per replicate. One way ANOVA **, ***, **** P=0.005, 0.0005, 0.0005

In order to address the hypothesis that ATRX acts to ameliorate damage induced by PDS at telomeres, and thus inhibit ALT, the HeLa LT ATRX knockout cells used previously were treated with 5μM PDS for 24 hours, and markers of ALT were assayed.

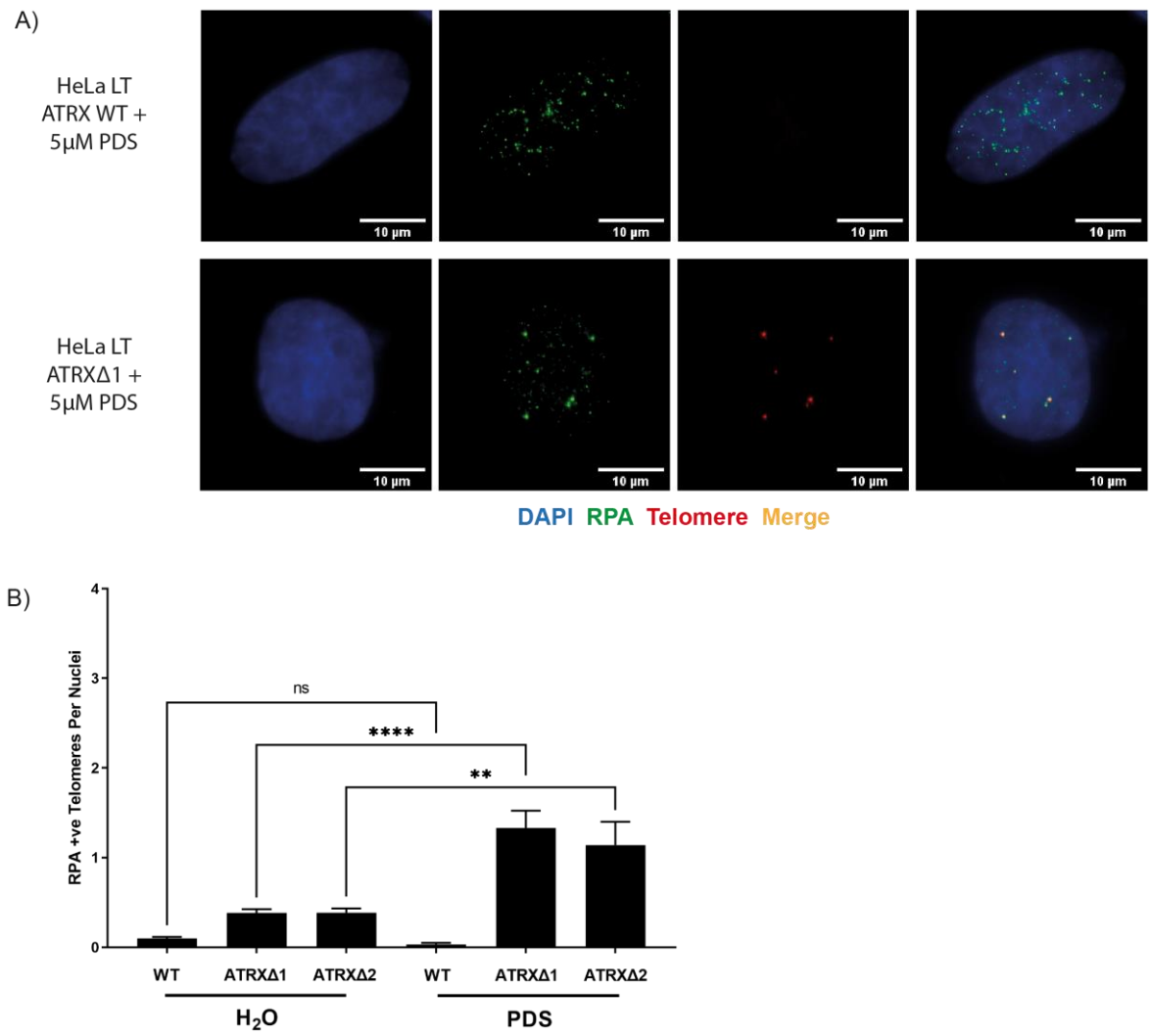

Figure 12: PDS treatment of ATRX knockout cells induces RPA foci formation at telomeres. A) Representative images of RPA foci formation at telomeres. B) Quantification of A. N = 3. >50 nuclei scored per replicate. One way ANOVA. **, **** P < 0.005, 0.00005.

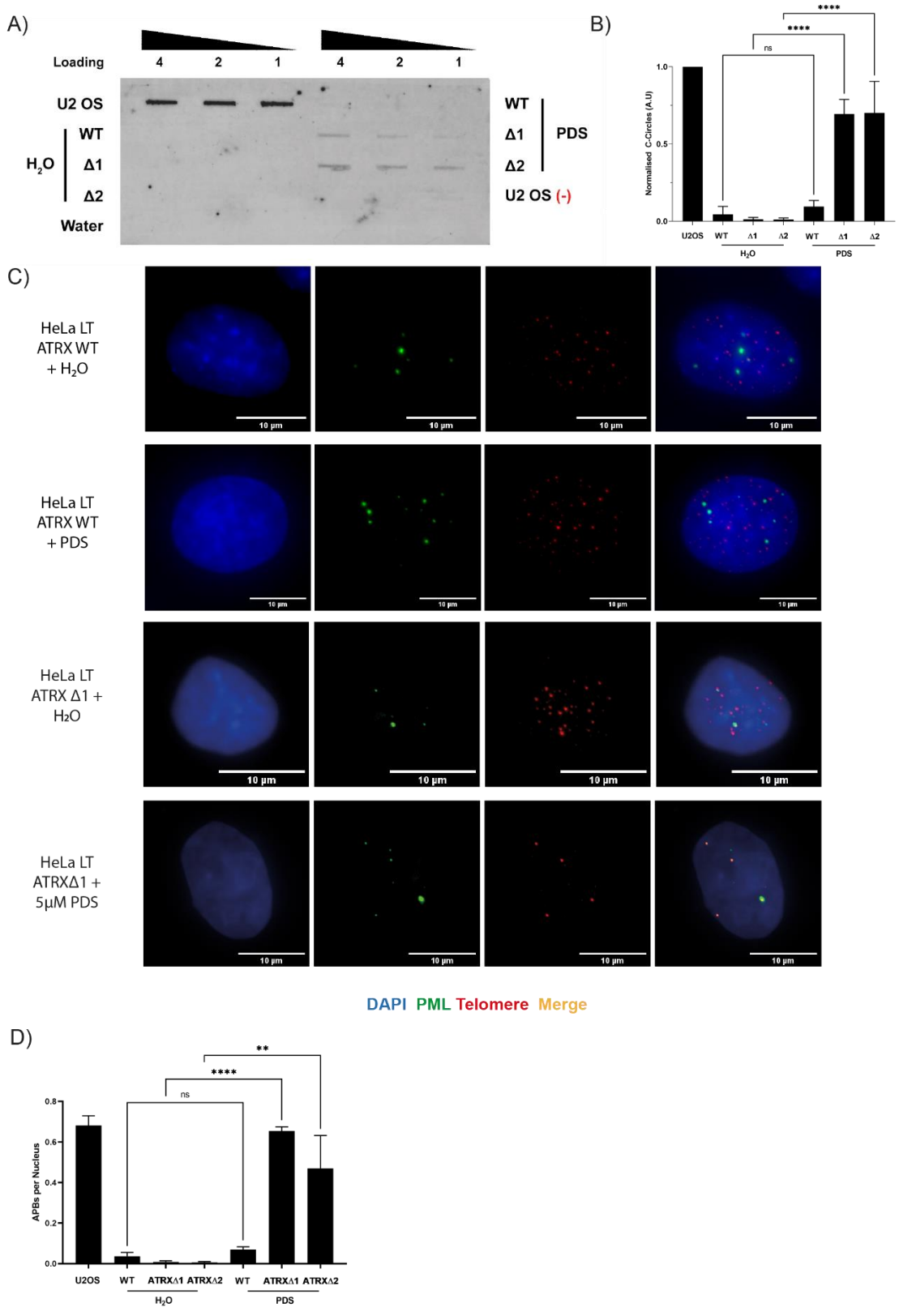

753

754 **Figure 13: In ATRX knockout cells, PDS induces a canonical ALT response.** A) Representative C-circle blot. B) Quantification
755 of A. C) Representative APB images showing PML (green) and telomeres (red) in HeLa LT ATRX KO1. D) Quantification of C. n
756 = 3, minimum of 100 nuclei per replicate. One way ANOVA. **, **** P < 0.005, 0.00005. C-circle experiments (A & B)
757 performed by Tomas Goncalves, APB experiments (C & D) performed by Sam Shepherd.

In agreement with this hypothesis, after treatment of cells on coverslips with 5μM PDS, we assayed for both RPA and telomeric sequence in a non-denaturing environment. In these conditions we observed a striking induction of RPA+ssTel signal in ATRX knockout cells, which was absent from ATRX wild type cells (Figure 12~~Figure 12~~).

Similarly, when observing other canonical markers of ALT, such as C-circle generation and APB formation, ATRX knockout cells saw a clear and significant increase in these respective markers compared to the ATRX wild type cells (Figure 13~~Figure 13~~). C-circle levels, for example, are 60-fold higher in ATRX knockout cells treated with PDS than untreated cells. By contrast, ATRX wild type cells only show a modest increase in C-circle levels to a degree that does not meet statistical significance. Similarly, when measuring APBs, ATRX knockout cells display significant increases in APB levels after treatment with PDS when compared with ATRX wild type cells. Unlike with C-circles, where levels are largely similar for the two ATRX knockout clones, APB levels vary between the two clones. Finally, when assaying telomere length by southern blotting (Figure 14~~Figure 14~~), PDS induces significant increases in telomere length heterogeneity, but only in the absence of ATRX, characteristic of the induction of an ALT like phenotype.

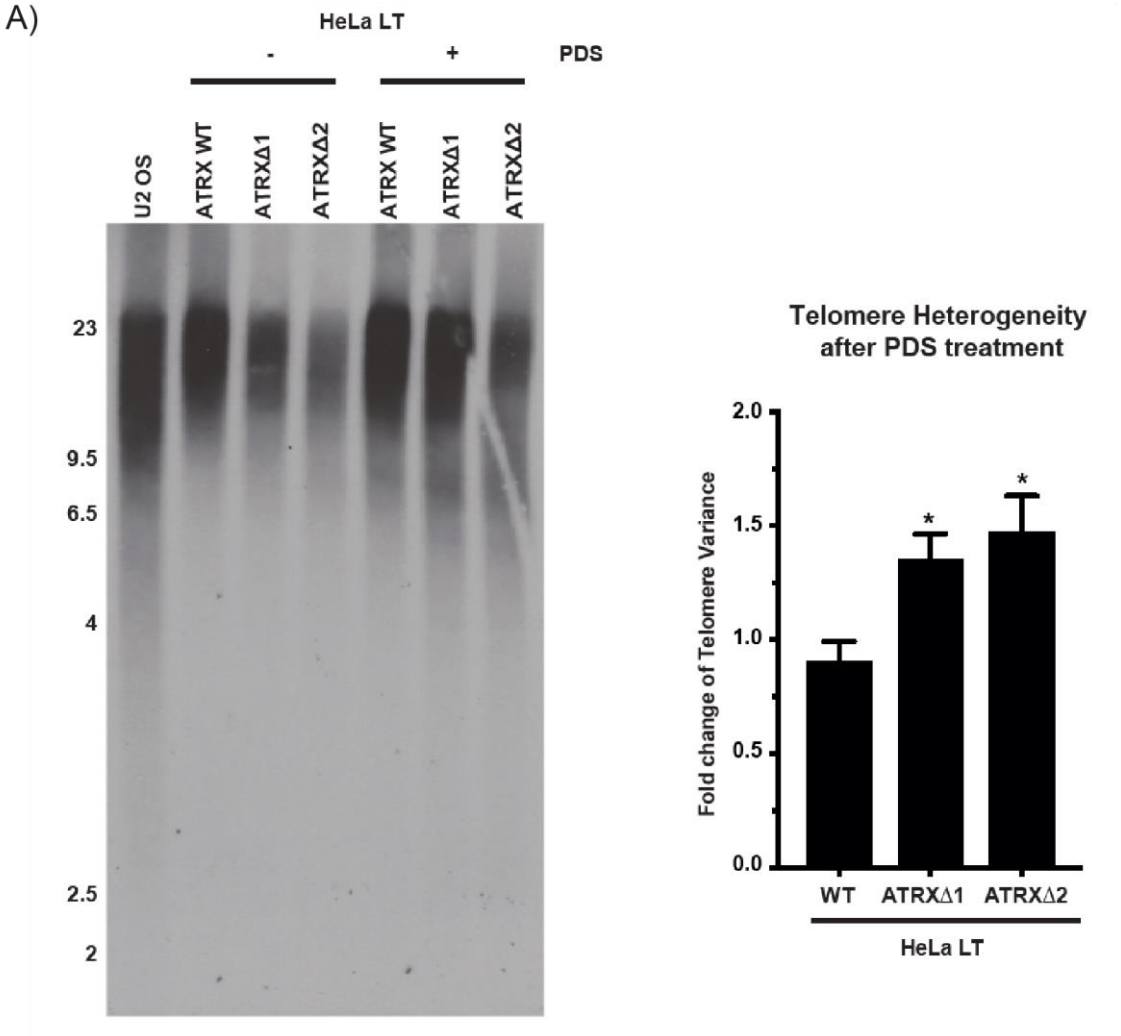

774

775 **Figure 14: PDS treatment leads to increases in telomere length heterogeneity in the absence of ATRX.** Measured as a fold
776 change of telomere length heterogeneity compared to untreated cells. Telomere length heterogeneity determined using
777 Telometric software (Grant *et al.*, 2001). Experiment performed in triplicate by Tomas Goncalves.

778 To rule out these effects being exclusive to HeLa LT cells, we next tested whether PDS was
779 able to induce the RPA+ssTel phenotype in a cell line other than HeLa LT. To do this, we
780 utilised a cell line previously used in the lab to monitor H3.3 deposition. This cell line, which
781 contains a SNAP tagged H3.3 construct, is based upon a wild type HeLa cell line. In this cell
782 line, we observed robust induction of RPA+ssTel (Figure 15~~Figure 15~~) in the shATRX condition.
783 Whilst shScramble (shScr) cells containing a non-targetting shRNA did display a small
784 induction of RPA+ssTel, the loss of ATRX greatly exacerbated this phenotype.

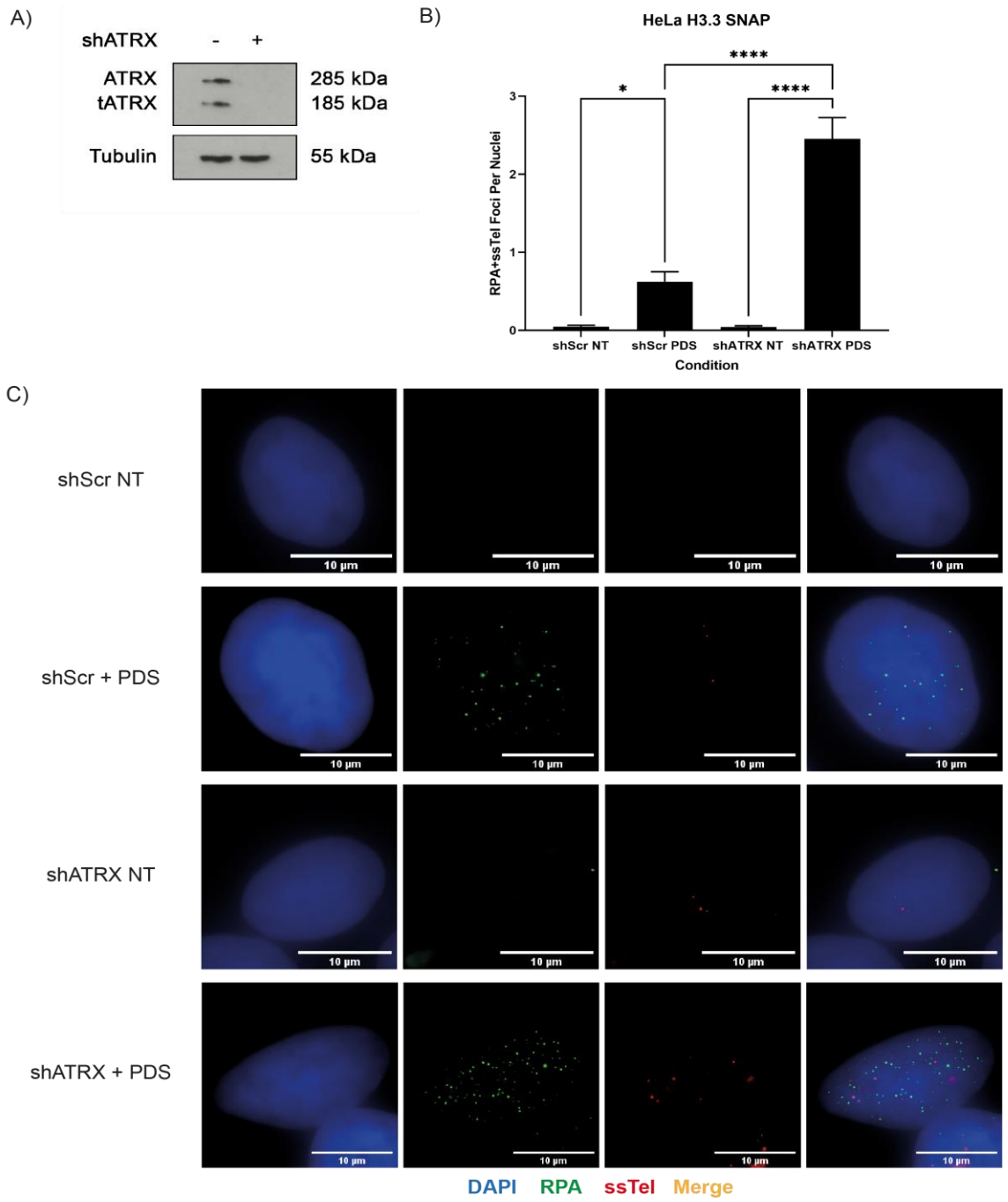

785

786 **Figure 15: PDS induces RPA+ssTel in HeLa H3.3 SNAP tagged cells**. A) Western blot showing ATRX shRNA knockdown. B)
787 Quantification of RPA+ssTel in HeLa H3.3 SNAP cells. C) Representative images of RPA+ssTel foci in HeLa H3.3 SNAP cells.
788 N=3, >50 nuclei per replicate scored. One Way ANOVA. *, **** $P < 0.05, 0.00005$.

789 It is clear, therefore, that ATRX plays an important role in the prevention of both the
790 RPA+ssTel phenotype and a canonical ALT response, both of which are induced strongly by
791 PDS treatment.

One possible explanation for the differences between ATRX wild type and ATRX KO cells is that the absence of ATRX changes cell cycle profiles upon treatment of ATRX when compared with ATRX wild type cells. Previous evidence has suggested that ATRX loss can alter cell cycle progression in certain cell types, resulting in longer S-phase progression (Huh *et al.*, 2012; Clynes *et al.*, 2014). Previous work has suggested that APB formation is enriched in G2/M phase of the cell cycle, raising the possibility that loss of ATRX could specifically cause cell cycle defects that are not present in ATRX wild type cells (Grobelny, Godwin and Broccoli, 2000; Wu, Lee and Chen, 2000).

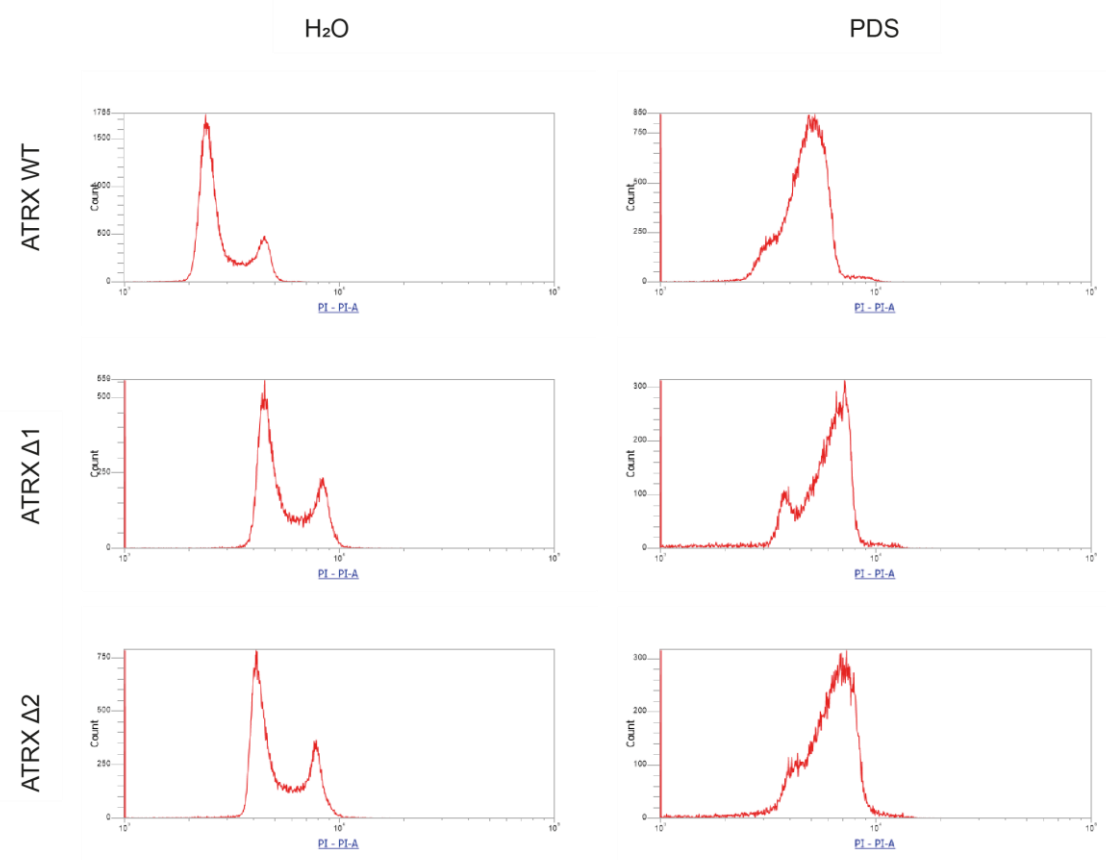

Figure 16: PDS induces consistent G2/M arrest across ATRX wild type and ATRX knockout cells as assessed by propidium iodide staining.

As such, we assessed cell cycle progression following PDS treatment using propidium iodide staining and flow cytometry to confirm that any cell cycle changes observed after PDS

treatment were consistent between ATRX wild type and ATRX knockout clones (Figure 16~~Figure 16~~). Indeed, in H_2O treated cells, both wild type and ATRX knockout clones displayed a characteristic double peak, with a majority of cells containing 1N of DNA, and a small minority (10-25%) containing 2N of DNA, indicative of G2/M phase of the cell cycle. In contrast, following treatment with PDS both wild type and ATRX knockout cells displayed a significant G2/M phase arrest.

These data are consistent with reports in the literature, where PDS treatment induces significant G2/M phase cell cycle arrest (Rodriguez *et al.*, 2012). However, this arrest is consistent across wild type and ATRX knockout cells, indicating that any observed RPA+ssTelomere phenotype is not a consequence of any specific cell cycle difference between the two conditions, and instead is likely to be dependent on ATRX status itself. Propidium iodide staining is generally insufficient to determine late S phase arrest, due to difficulties in separating late-S/G2/M phase populations.

4.3 ATRX cooperates with DAXX to prevent PDS induced ALT markers

ATRX forms a complex with the histone chaperone protein DAXX and this interaction is associated with many of ATRX's roles in the cell. Previous work has established that DAXX and ATRX cooperate in the suppression of ALT markers in the ALT cell line U2OS, where DAXX deficiency inhibits the ability of ATRX to suppress a number of canonical ALT markers (Clynes *et al.*, 2015). Based on this, we next sought to address whether the loss of DAXX also predisposes cells to ALT marker generation upon treatment with PDS.

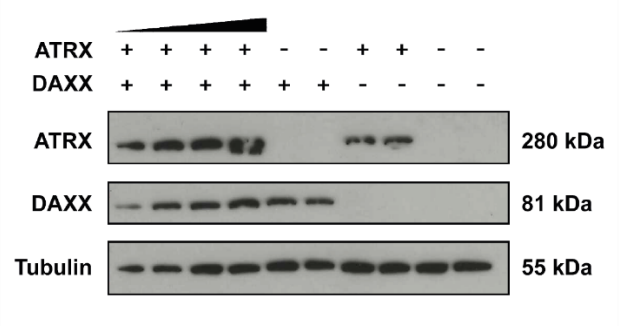

Figure 17: Verification of DAXX KO in HeLa LT WT and HeLa LT ATRX KO cells. Western blot showing ATRX knockout, DAXX knockout, and ATRX/DAXX double knockout clones. ATRX wild type (lanes 1 to 4) in increasing loading volumes. Western blot performed by Sam Shepherd.

To this end, DAXX KO and ATRX/DAXX double KO HeLa LT lines were generated (Figure 17~~Figure 17~~), allowing investigation of the effects of PDS on single ATRX or DAXX KO cells, or loss of both proteins for epistasis experiments. DAXX knockout was achieved using a commercially available DAXX CRISPR Cas9 plasmid (Santa Cruz, #sc-400686-NIC) by Sam Shepherd (Clynes Lab). Two clones for each condition were selected and compared alongside the two previously described ATRX KO clones. Cells were again exposed to 5 µM PDS for 24 hours, before assaying ALT markers.

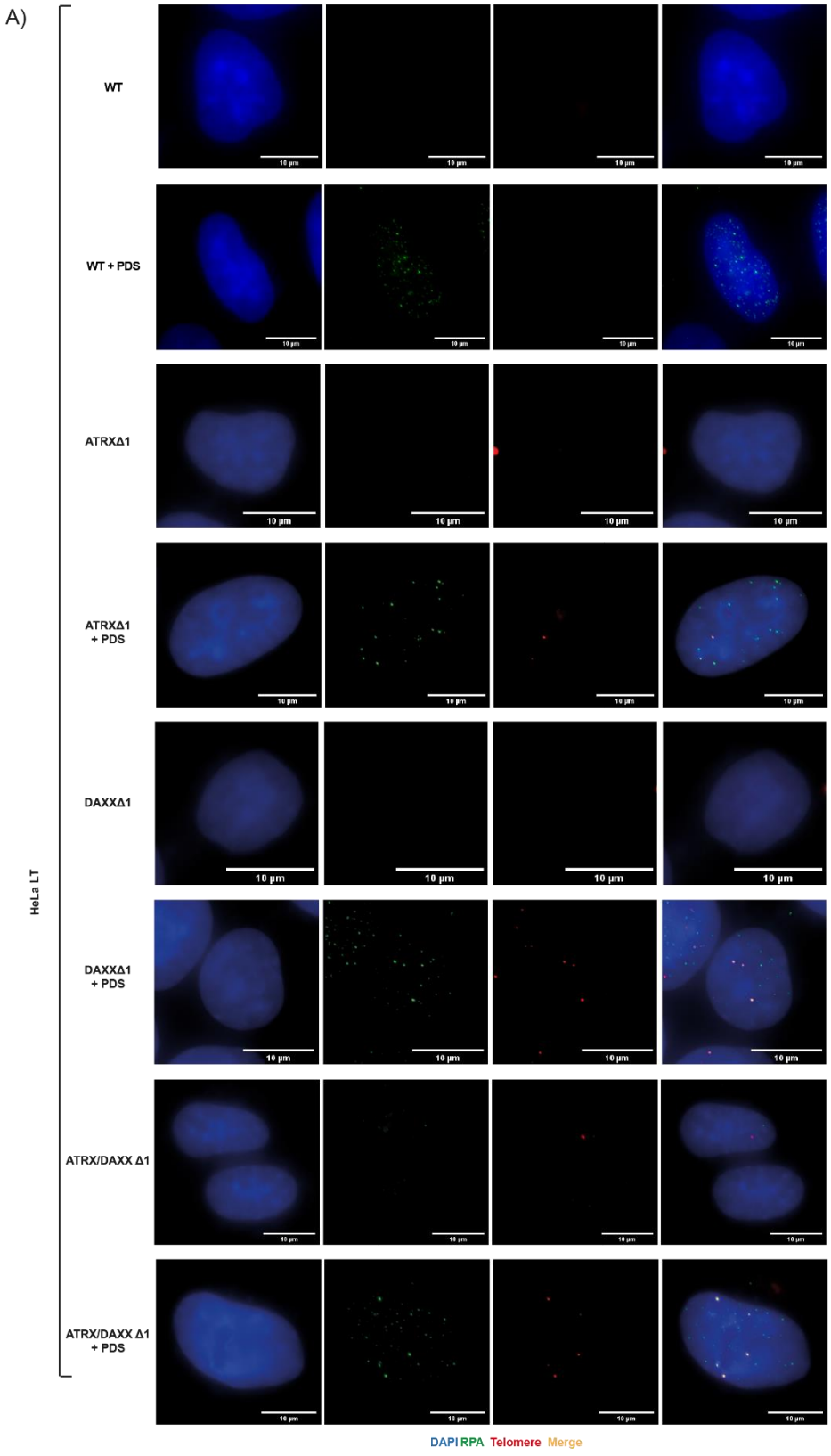
A)
HeLa LT
WT
WT + PDS
ATRXΔ1
ATRXΔ1 + PDS
DAXXΔ1
DAXXΔ1 + PDS
ATRX/DAXX Δ1
ATRX/DAXX Δ1 + PDS
10 µm
DAPI RPA Telomere Merge

836

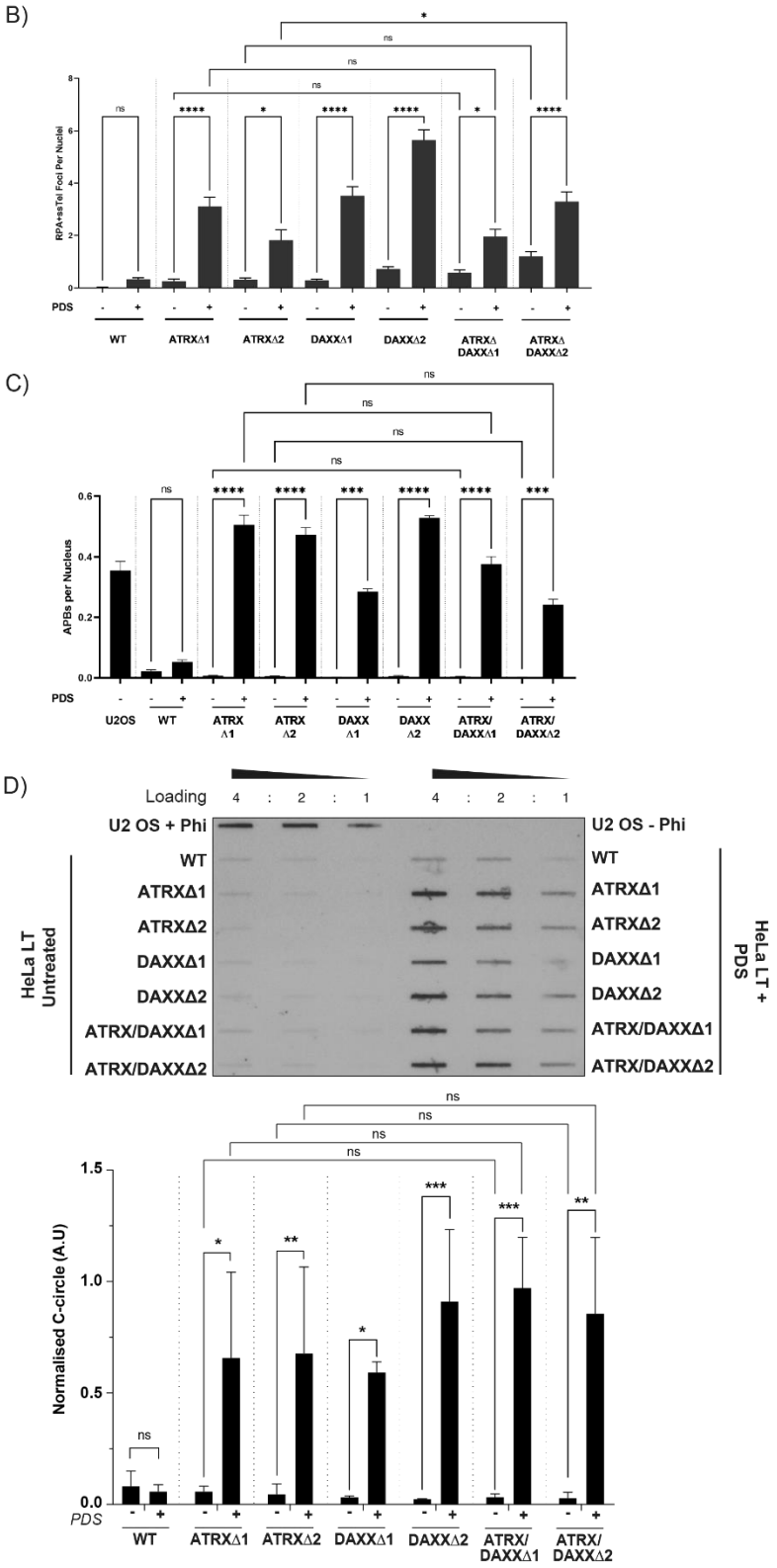

Figure 18: ALT markers were generated upon PDS treatment for both ATRX and DAXX deficient cells. A) Representative images showing RPA+ssTel foci formation in both DAXX KO and ATRX/DAXX double KO cells. B) Quantification of A. C) Quantification of APB formation in ATRX/DAXX knockouts. D) C-circle blot and quantification. N=3 on all experiments, >50 nuclei analysed. One way ANOVA. *, **, ***, **** $P < 0.05, 0.005, 0.0005, 0.0005$. APB experiments (C) performed by Sam Shepherd, C-circles (D) performed by Tomas Goncalves.

As predicted, the cooperative nature of ATRX and DAXX translates to their ability to prevent ALT marker formation upon PDS treatment (Figure 18~~Figure 18~~). Indeed, loss of ATRX or DAXX alone induces ALT markers including RPA+ssTel, APBs and C-circles when treated with PDS. Interestingly, while levels of both RPA+ssTel and APBs are variable, likely due to clonal effects, both double ATRX/DAXX knockout clones displayed reduced or equal levels of ALT markers when compared to single knockouts alone. These data suggest that both ATRX and DAXX act within the same pathway, and that there is no additive effect of loss of both proteins together.

4.4 PDS induced ALT markers require Mus81

PDS has been shown to have a number of effects on a cell. Whilst the principal described mechanism of action of PDS is that it stabilises G4 structures, additional evidence suggests that PDS can trap topoisomerase II (TOP2) on DNA (Olivieri *et al.*, 2020). Both trapped TOP2 and G4 structures present barriers to DNA replication, wherein an approaching replication fork cannot easily replicate over such regions. Certain DNA polymerases, such as the Y-family DNA polymerases have evolved to allow replication machinery to bypass certain DNA lesions. Indeed, evidence in the literature suggests that certain Y-family polymerases are able to bypass structures such as G4 (Betous *et al.*, 2009; Eddy *et al.*, 2016; Yang *et al.*, 2018). However, if a replication fork meets a barrier such as a G quadruplex, and does not recruit such a polymerase, this will instead induce replication fork stalling and replication stress. When a replication fork stalls the replication machinery has, generally speaking, two choices: restart the replication fork or collapse the fork and attempt homology directed repair.

In the case of ALT induction, the latter option creates the perfect environment for the break induced repair that is required for the characteristic HDR mediated telomere elongation seen

in ALT. Therefore, when treating cells lacking ATRX with PDS, and observing the ALT marker induction that results, one prediction is that this process may require replication fork collapse.

Literature evidence supports this hypothesis, in fact, with a key endonuclease, Mus81, being required for ALT survival (Zeng *et al.*, 2009). Additionally, Mus81 is an essential endonuclease for the cleavage step of replication fork collapse, which, in a model for ALT, is essential to generate the required one-ended DSB (Pepe and West, 2014a). Therefore, we next sought to determine whether PDS induced ALT markers required Mus81 activity.

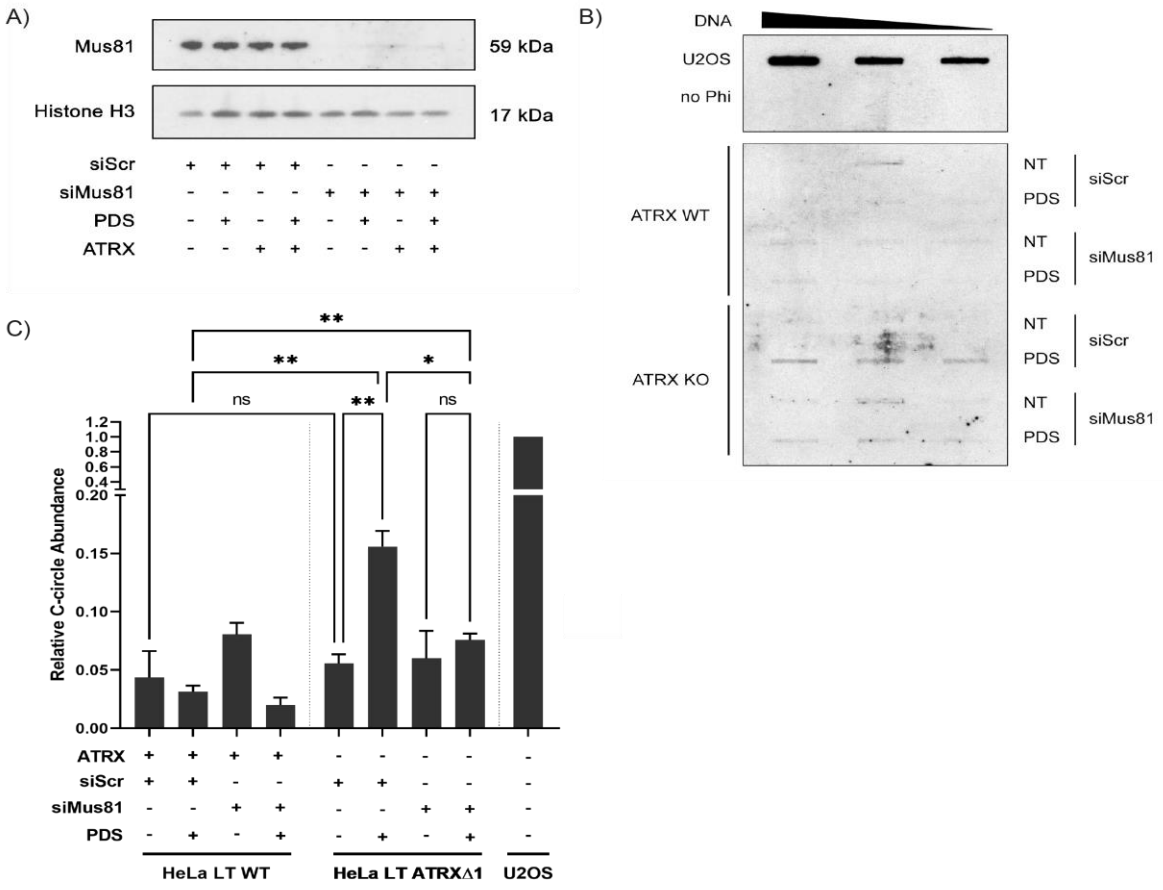

Figure 19: Knockdown of Mus81 by siRNA abrogates PDS induced ALT markers. A) Western blot showing siRNA knockdown of Mus81 in ATRX WT (+) and ATRX Δ1 (-) cells. B) C-circle blot showing induction of C-circles. C) Quantification of C-circles over 3 biological repeats. T-test, Mann-Whitney. *, ** $P < 0.05, 0.005$.

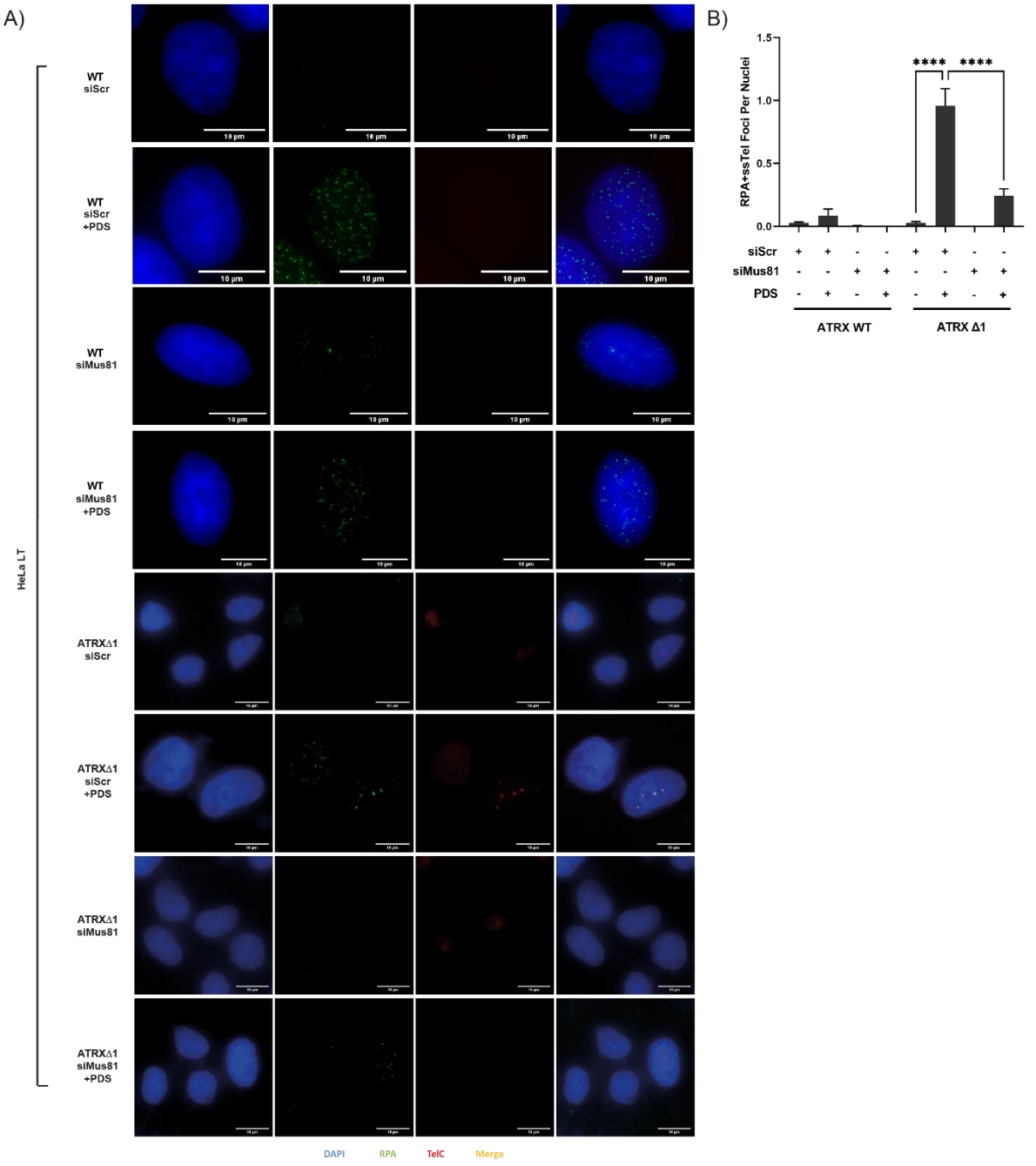

876

877 **Figure 20: Knockdown of Mus81 by siRNA abrogates PDS induced ALT markers (continued).** A) Representative images of
878 RPA+ssTel in HeLa LT ATRX Δ1. B) Quantification of RPA+ssTel following siMus81 knockdown. N=3, >100 nuclei per replicate.
879 T-test, Mann-Whitney. **** $P < 0.00005$.

880 To achieve this, Mus81 was knocked down in cells using siRNA mediated knockdown and
881 assayed by Western blotting. As seen in Figure 19~~Figure 19~~, following effective knockdown of
882 Mus81 with siRNAs, the ability for PDS to induce C-circles in HeLa LT ATRX KO1 was severely

diminished when compared to siScramble transfected cells. Similarly, when assaying for RPA+ssTel foci in ATRX KO1 cells treated with siMus81 showed a significant depletion in RPA+ssTel foci levels (Figure 20~~Figure 20~~). Together these experiments suggest that Mus81 is required for ALT formation following PDS treatment of ATRX KO cells. Additionally, from a mechanistic point of view, it places the RPA+ssTel phenotype downstream of fork collapse.

4.5 Genotoxic agents induce markers of ALT in the absence of ATRX

With the reliance on fork collapse established, we next wanted to determine whether ATRX's role was specifically in response to G4 structure formation, or whether it was a more generic role in response to replication stress events. To address this question a variety of genotoxic agents were investigated for their effects both in the presence and absence of ATRX. These genotoxic agents included the topoisomerase I (TOP1) inhibitor Camptothecin (henceforth referred to as CPT), the topoisomerase II (TOP2) inhibitor Etoposide, the oxidative stress inducing agent Hydrogen Peroxide (H_2O_2), and the DNA polymerase inhibitor Aphidicolin.

We first investigated the topoisomerase inhibitors Camptothecin and Etoposide. Despite being grouped into a generic category of "topoisomerase inhibitors", CPT and Etoposide in fact target very different proteins, and have differing effects. CPT targets human TOP1, a nuclease that is required to relieve torsional stress during transcription by cleaving a single DNA strand before allowing it to unwind and then re-ligating the strand. CPT's mechanism of action is understood to be through the inhibition of the TOP1 cleavage complex (TOP1cc) that forms transiently as a covalent bond between TOP1 and DNA at the 3' end of the cleaved ssDNA section. CPT inhibits TOP1, preventing the release of the TOP1-DNA complex, thus trapping the TOP1 protein. In contrast, Etoposide targets human TOP2, a nuclease that instead cleaves both strands of DNA and allows the DNA to naturally uncoil. TOP2 religates

both strands back once the DNA has reached an uncoiled state. TOP2 is primarily important during replication, where torsional stress in the form of positive supercoiling accumulates ahead of the replication fork. In instances where positive supercoiling ahead of the fork cannot be relieved by TOP2, such as in regions that are inaccessible to TOP2, this torsional stress can be transferred behind the fork through rotation of the fork, generating negatively supercoiled sister chromatids. Nevertheless, this negative supercoiling must be resolved by topoisomerases such as TOP2 to allow for faithful chromatid separation (Keszthelyi, Minchell and Baxter, 2016). Etoposide, as a potent inhibitor of TOP2, causes persistent DNA damage by preventing re-ligation of DNA strands after cleavage, resulting in unresolved DSBs. To investigate the effects of inhibition of both TOP1 and TOP2, we used sublethal doses of CPT and Etoposide that have been shown to have fork-reversal generating effects, but also not cause fork collapse (Zellweger *et al.*, 2015).

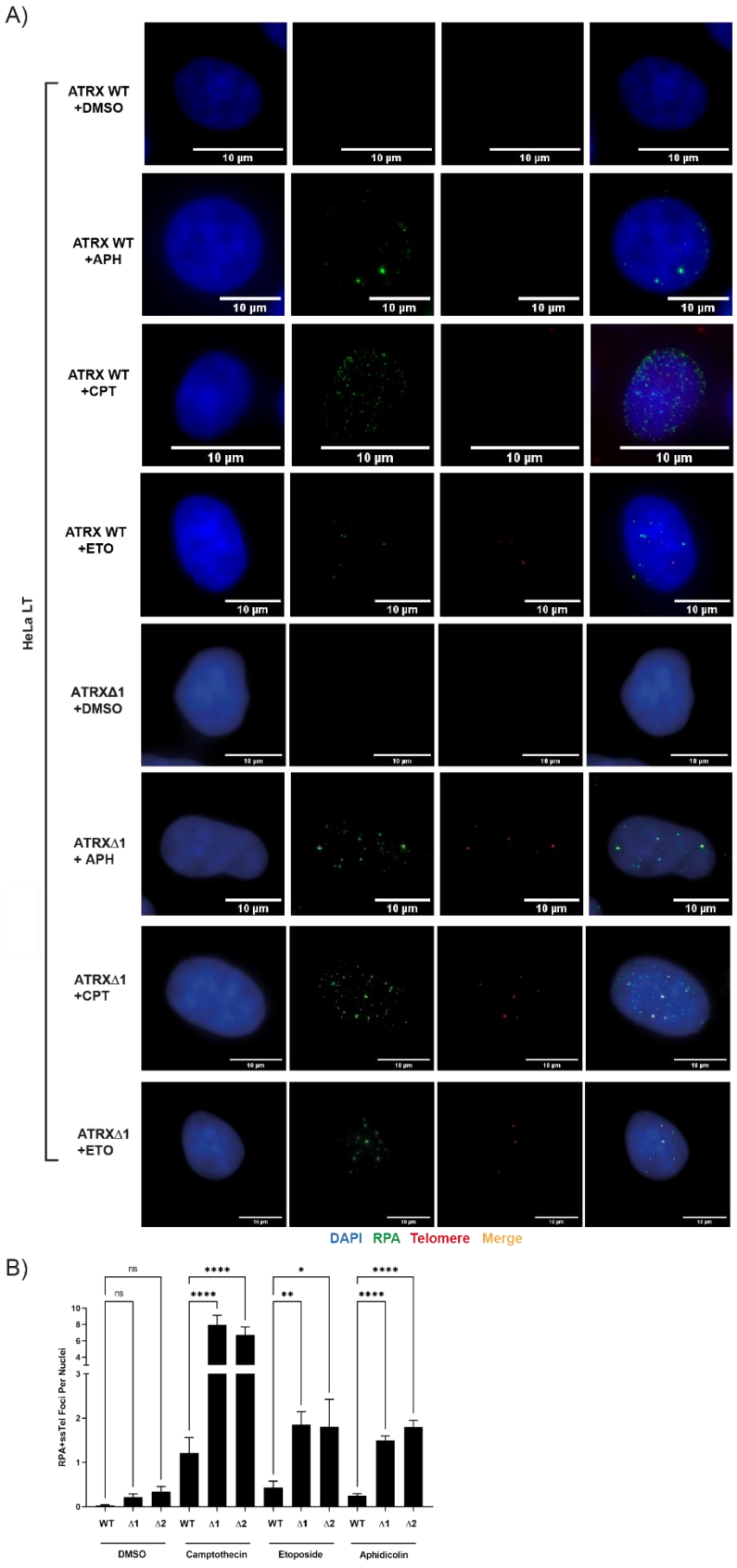

Figure 21: CPT, Etoposide, and APH induce RPA+ssTel. A) Representative images of RPA+ssTel foci upon treatment with APH, CPT or ETO. B) Quantification of A. n=3, >50 nuclei per condition per replicate. One way ANOVA. *, **, ***, **** P < 0.05, 0.005, 0.0005, 0.00005.

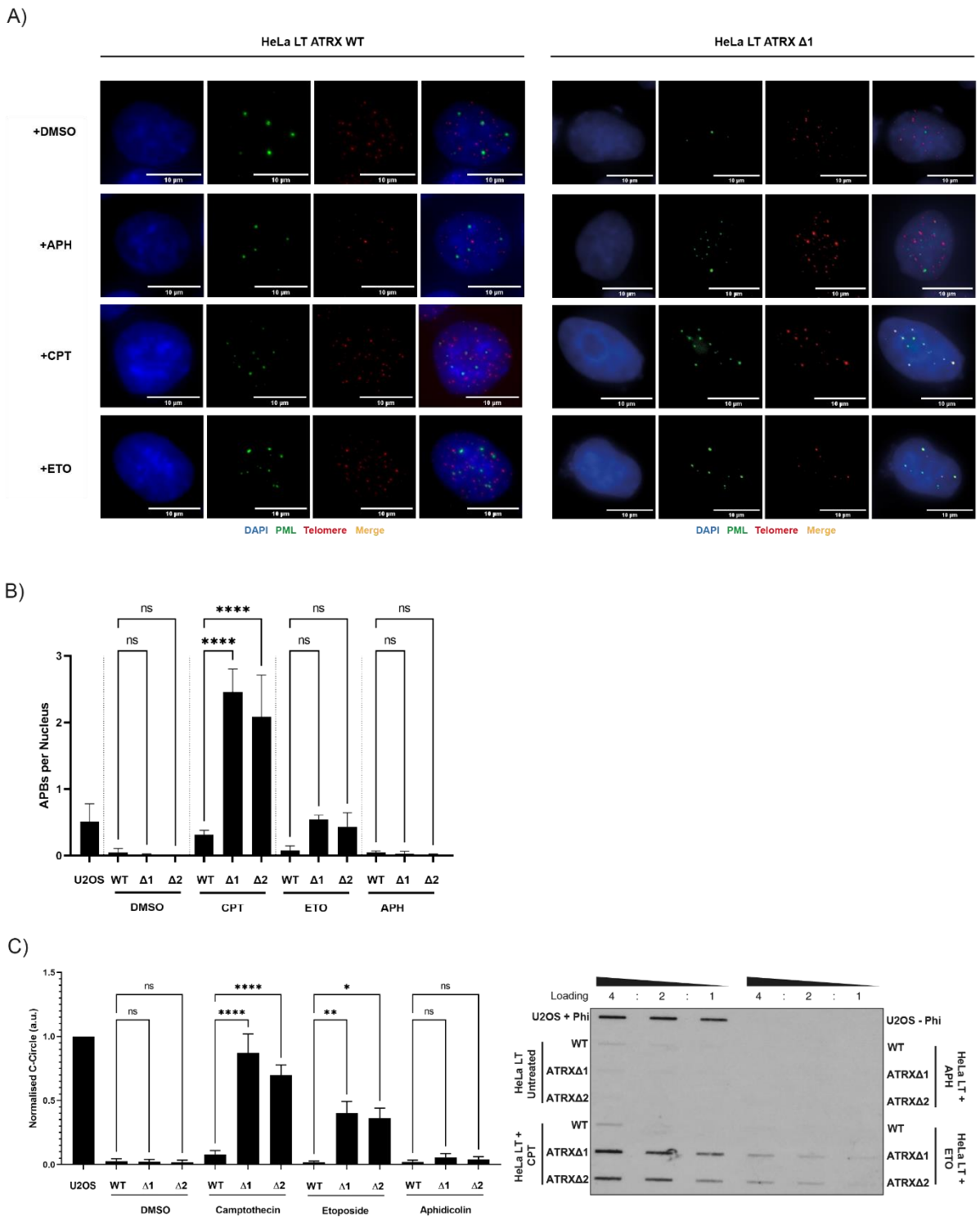

Figure 22: Other ALT markers are induced by DNA genotoxic agents. A) Representative images showing APBs in HeLa LT ATRX KO1 treated with APH, CPT and ETO. B) Quantification of A. C) Quantification and representative image showing C-circle blot in two HeLa LT ATRX KO clones. N=3 for all experiments. Minimum 50 nuclei per replicate for APB analysis. ANOVA with multiple comparisons. *,**,***,**** P < 0.05/0.005/0.0005/0.00005. APB experiments (A & B) performed by Sam Shepherd, C-circles (C) performed by Tomas Goncalves.

Both CPT and Etoposide induce ALT markers including C-circles, APBs and RPA+ssTel (Figure 21~~Figure 21~~ and Figure 22~~Figure 22~~). Interestingly CPT induced a more potent ALT response in terms of C-circles, APBs and RPA+ssTel than in Etoposide. While it is not immediately clear as to why this is the case, it is possible that this is simply a dosing issue. Alternatively, fundamental differences between the mechanisms of action of etoposide and CPT may explain the disparity. During DNA replication, DNA is replicated only once, limiting the number of potential replication forks, and thus the amount of supercoiled DNA. In contrast, telomeres and subtelomeric regions are transcribed to form the long non-coding RNA TERRA (telomere repeat containing RNA). This persistent transcription may indeed generate significantly more supercoiled DNA substrate for TOP1 inhibition to deleteriously affect.

One disadvantage of the use of etoposide and camptothecin is that these agents are largely unspecific, generating excessive torsional stress throughout the genome. While regions such as telomeres may be more susceptible to such stresses, due to their unidirectional replication forks and thus a reduced capacity to rescue stalled forks with a converging fork, topoisomerase inhibitors have wide reaching effects on the genome. Recent literature evidence has suggested that, by comparison, low doses of the DNA polymerase inhibitor Aphidicolin (0.1 - 0.2 µM) (APH) can induce replication stress at common fragile sites including telomeres (Sfeir *et al.*, 2009). This tool allows for far more precise localisation of DNA damage, and as such allows for greater understanding of the events that precipitate ALT markers. Consequently, HeLa LT ATRX wild type and ATRX KO cells were treated with low dose Aphidicolin (0.1 µM) for 24 hours prior to analysis of ALT markers.

Surprisingly, while cells lacking ATRX exposed to low dose Aphidicolin generated a similar level of RPA+ssTel signal induction as was observed in etoposide treated ATRX KO cells, low dose

Aphidicolin failed to induce both APBs and C-circles. Therefore, contrary to previously used DNA damaging agents, low dose Aphidicolin generated a separation of phenotypes, suggesting that RPA+ssTel and other canonical ALT markers represent distinct aspects of the ALT pathway. Indeed, recent literature evidence has suggested that in fact C-circles and APBs represent distinct features of the ALT pathway and are not directly linked in their production.

Because cell cycle progression is necessary for the generation of C-circles, and due to the inability of APH treated cells to induce C-circles or APBs, we sought to determine whether loss of ATRX impacted cellular proliferation following treatment. To do this, we performed CellTiter® Glo assays on cells in the presence or absence of ATRX with increasing concentrations of each agent. We observed reductions in proliferation (**Figure 23**~~**Figure 23**~~) in conditions upon increasing the agent concentration. At lower concentrations, cell populations continued to proliferate, indicating that the cell cycle was progressing. Interestingly, in all agents (PDS, APH, CPT, and ETO), ATRX deficient cells showed reductions in cellular proliferation, suggesting that ATRX deficient cells were disproportionately affected by the adducts or damage created by these agents.

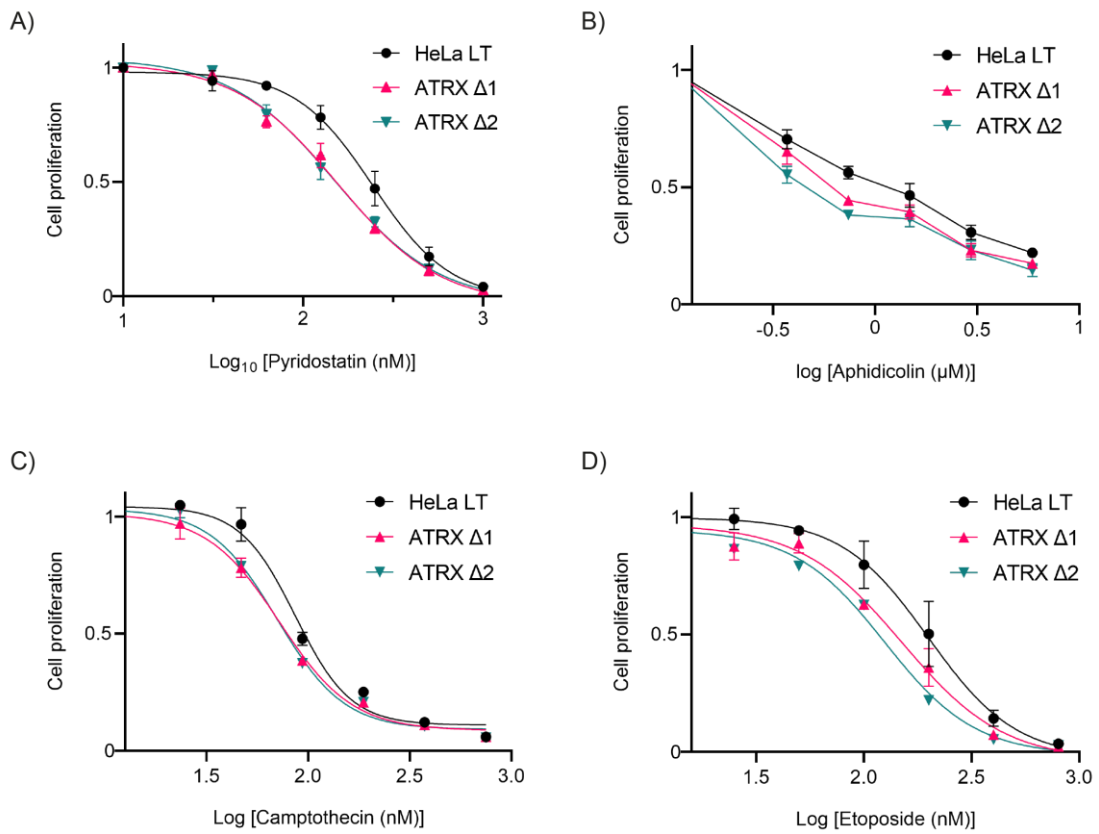

966

967 **Figure 23: Cell Titer Glo assays showing reduced proliferation in ATRX deficient cells following treatment with genotoxic**
968 **agents.** A) Proliferation of cells over 7 days in the presence of pyridostatin. B) Proliferation of cells over 72 hours in the
969 presence of aphidicolin. C) Proliferation of cells over 72 hours in the presence of camptothecin. D) Proliferation of cells over
970 7 days in the presence of etoposide. Experiments performed by Sangwoo Kim in triplicate biological replicates with technical
971 triplicate within each biological replicate.

972 As low dose Aphidicolin is described as generating replicative stress, and ultimately fork
973 stalling and, as previously demonstrated, due to the fact that the RPA+ssTel phenotype
974 requires the activity of Mus81, it presents an interesting question as to exactly what the
975 RPA+ssTel phenotype represents. The requirement for Mus81 places the phenotype
976 downstream of fork collapse and cleavage, implying that RPA+ssTel does not represent RPA
977 binding within stalled or reversed replication forks. The next logical conclusion is that,
978 following DSB formation, telomere ends are resected to allow for strand invasion and break
979 induced replication.

The investigation of the impact of resection factors represents an excellent future avenue of study for this project.

4.6 DNA adducts induce ALT markers in the absence of ATRX

While G4 structures or supercoiled DNA represent a blockage to replication fork machinery, we next sought to determine whether other forms of DNA damage that generate adducts on DNA induced ALT markers. To achieve this, two different forms of damage were chosen. The first, oxidative damage, which primarily leads to the generation of 8-hydroxy-2'-deoxyguanosine (8-OHdG) adducts, was mediated through the use of hydrogen peroxide. Titration of hydrogen peroxide in culture is notoriously difficult, mostly due to its very short half-life both in culture media and within the cell. In order to determine a concentration of hydrogen peroxide that dealt sufficient damage to the HeLa LT ATRX WT and ATRX KO cells, clonogenic survival assays were performed with increasing concentrations of hydrogen peroxide.

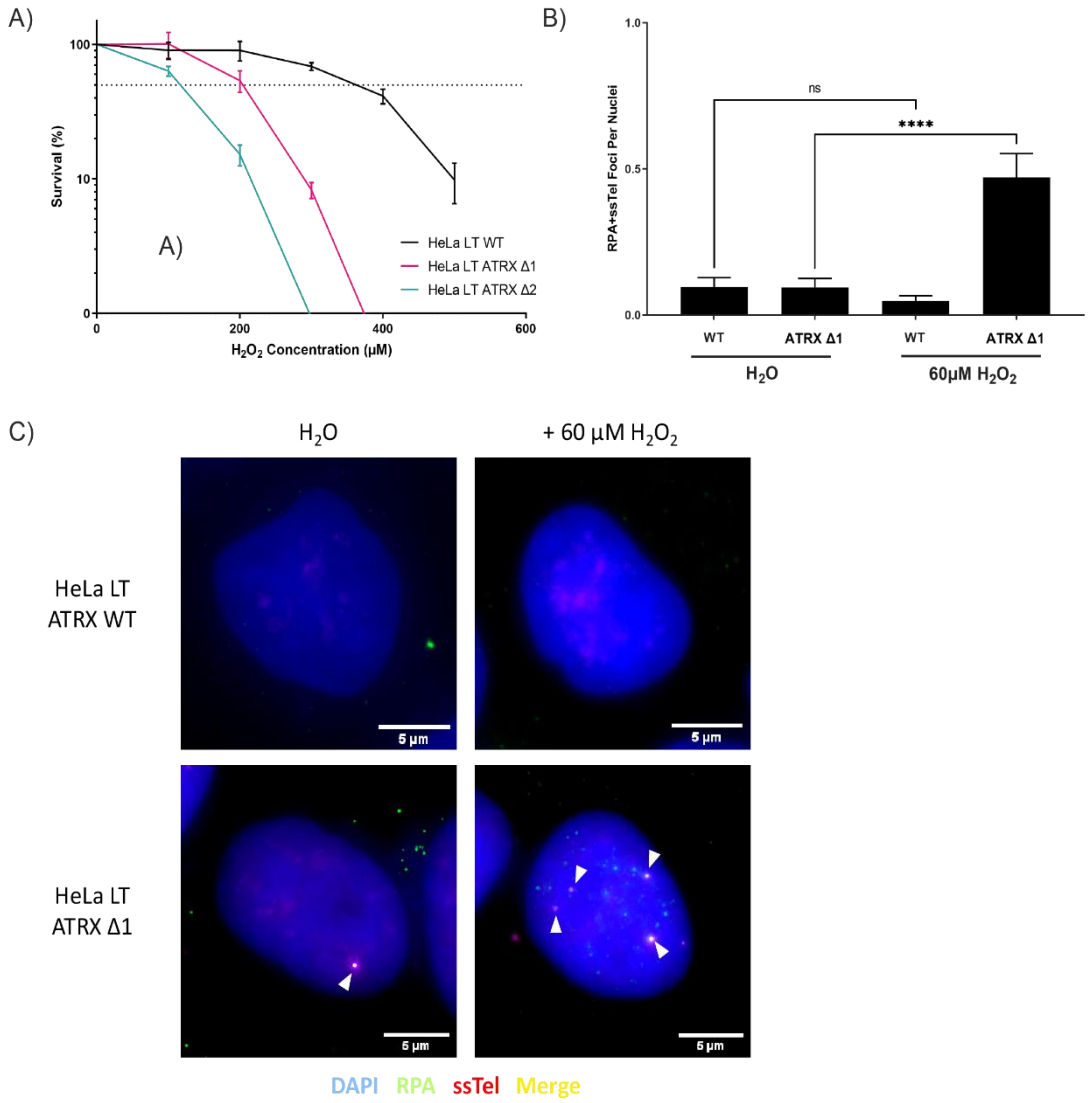

993

994 **Figure 24: HeLa LT ATRX knockout cells are strikingly sensitive to H_2O_2 compared to wild type cells and in these cells**
995 **RPA+ssTel is generated.** A) Clonogenic survival curve showing two ATRX knockout clones with increasing doses of H_2O_2. B)
996 Quantification of RPA+ssTel foci in one knockout clone. C) Representative images showing RPA+ssTel foci formation in HeLa
997 LT ATRX HeLa LT ATRX Δ1.

998 As seen in Figure 24~~Figure 24~~, HeLa LT ATRX knockout cells display striking sensitivity to H_2O_2
999 even at relatively low concentrations. This sensitivity indicated that ATRX is vital for cell
1000 survival in the presence of H_2O_2. To date, there has been no indication in the literature of the
1001 sensitivity of human ATRX knockout cells to H_2O_2. It is known, however, that in drosophila,
1002 DAXX plays a critical role in oxidative stress mediated apoptotic responses, and that upon

exposure to H_2O_2, DAXX expression levels increase. This apoptotic response is mediated through the c-Jun N-terminal kinase (JNK) pathway (Yang *et al.*, 1997).

Following the observation of sensitivity of ATRX KO cells to H_2O_2, cells were treated with 60µM H_2O_2 and ALT markers were assessed. 60 µM was chosen, despite the low cell death in the clonogenic survival assay, in order to minimise apoptosis while generating oxidative stress. While attempting this assay at higher concentrations, apoptosis caused too much cell loss to quantify RPA+ssTel foci. Despite the relatively low concentration, H_2O_2 did indeed trigger a low level of RPA+ssTel signal (**Figure 24**~~**Figure 24**~~), indicating that the presence of low levels of persistent oxidative stress could indeed precipitate an ALT phenotype in the absence of ATRX.

While the levels of RPA+ssTel generated were not as high as in drugs such as camptothecin and PDS, the generation of RPA+ssTel in response to H_2O_2 treatment indicates that, at the very least, oxidative damage induces similar stresses at telomeres that allow for replication fork collapse.

In addition to investigating oxidative damage through the use of H_2O_2, other forms of adducts were investigated through the use of UVC radiation. Unlike the longer wavelength UVA radiation (315-400nm), a common cause of skin cancer and DNA damage in humans, UVC radiation has a much shorter, and thus higher energy, wavelength of below 280nm. Generally, most UVC is absorbed by the ozone layer, preventing the majority from reaching the Earth's surface. Ultimately, this permits life on Earth, as the short wavelength high energy light has the ability to generate a number of lesions directly on the DNA. Unlike UVA, which primarily causes damage through the generation of free oxygen radicals and thus oxidative damage, UVC directly causes alterations to DNA bases. Such damage includes the generation of

cyclobutane pyrimidine dimers (CPDs) and pyrimidine (6-4) pyrimidone photoproducts (6-4PPs). These lesions present a barrier to DNA replication, and as such life has developed a number of mechanisms for bypassing or repairing such damage.

The principle mechanism of repair for UVC induced adducts is nucleotide excision repair (NER) which is a multistep process, involving some twenty different genes. Among these genes, ERCC1 and the seven XP-* genes, XPA to XPG, play critical roles in damage recognition, demarcation, and strand-incision around the damage site. A 24–32 nucleotide incised strand containing the DNA lesion is removed and the resulting gap is subsequently filled by dNTPs, DNA polymerase, and DNA ligase using the complementary strand as template (Spivak, 2015). Alternatively, photoadducts can be bypassed entirely during replication by a pathway known as Translesion Synthesis (TLS) (Quinet *et al.*, 2016). TLS mediates bypass of UV photoadducts through the use of specialised Y family polymerases (Andersen *et al.*, 2011). Interestingly, work has shown that Y family polymerases such as Polκ are also involved in the late stages of NER (Ogi and Lehmann, 2006; Sertic *et al.*, 2018).

Given the literature reports of accumulations of the TLS polymerase Polη in ALT cancers, and previous reports of UV sensitivity in ATRX null cells, we decided to investigate the effects of UVC radiation on ATRX knockout cells (Conte *et al.*, 2012; Garcia-Exposito *et al.*, 2016). We hypothesised that in mammalian cells ATRX's roles in protecting cells from replicative stress and ALT suppression would leave cells vulnerable to UVC radiation, and that in its absence, increased levels of damage at telomeres would lead to ALT activation. However, we also hypothesised that, as with oxidative damage, too much damage at regions such as telomeres would lead to eventual apoptosis.

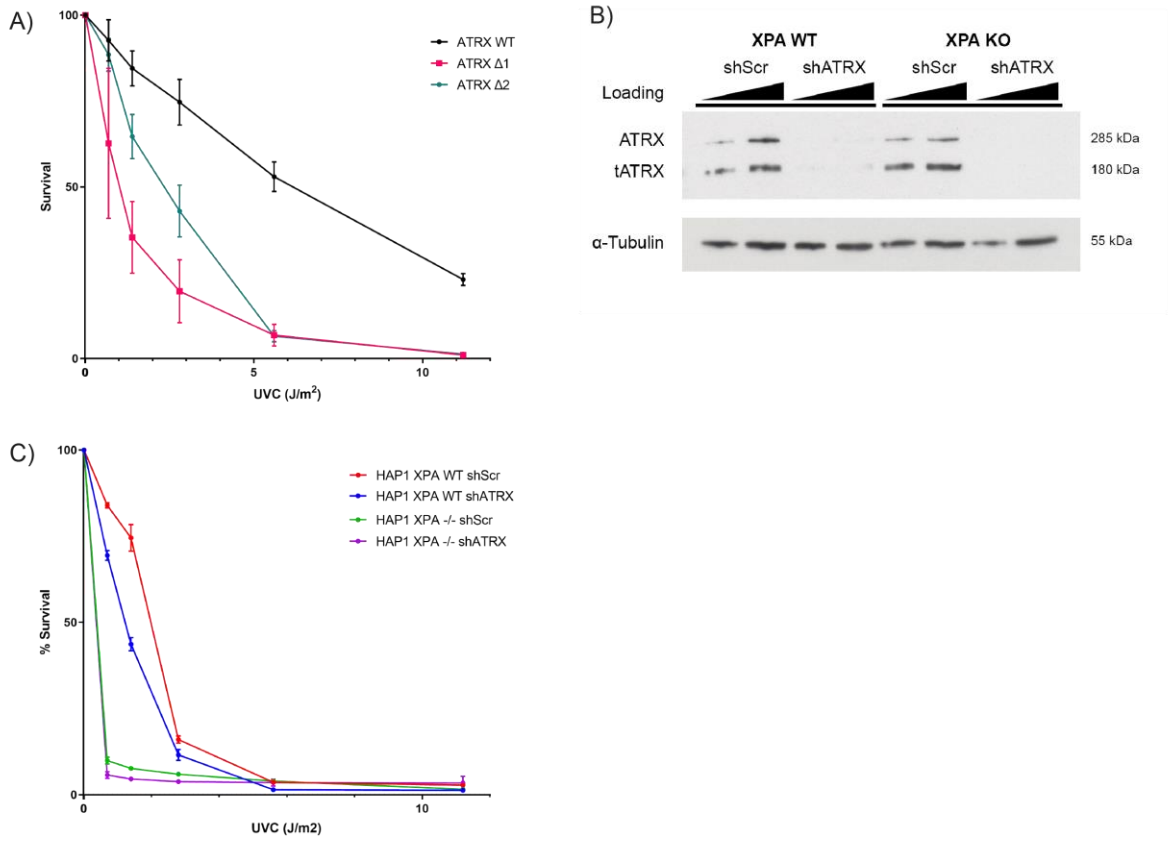

Figure 25: ATRX loss sensitises cells to UVC radiation. A) Clonogenic survival assay showing striking sensitivity in ATRX KO cells to UVC. B) Clonogenic survival assay incorporating HAP1 KO cells for comparison. Clonogenic survival assays represent 3 biological repeats.

As with oxidative damage induced with H_2O_2, we first assayed for overall survival of cells with wild type ATRX and ATRX knockout, to determine whether ATRX KO cells displayed sensitivity (Figure 25~~Figure 25~~). ATRX KO cells displayed striking sensitivity to UVC radiation when compared with ATRX wild type cells. As a control HAP1 cells with both XPA wild type and XPA knockout were transduced with shATRX and shScramble shRNA lentiviruses. When assaying for UVC survival in the HAP1 XPA knockouts loss of XPA, as described in the literature, induced significant cell death. However, interestingly shATRX had both no additive effect, and no significant loss of survival in XPA WT HAP1 cells. The lack of additive effect in XPA KO cells initially appeared to imply that ATRX and XPA act epistatically in the same pathway. However,

due to the essential nature of XPA in NER, it is possible that ATRX was simply unable to measurably reduce survival in comparison. Furthermore, another possible explanation for the negligible effect of ATRX loss is telomere length. Whilst HAP1 cells have a median telomere length of around 8.5kb, HeLa LT have a median telomere length of over 20kb. Should ATRX have a role in response to UVC, and given ATRX's predisposition to favour sites such as telomeres, the increased length of telomeres in HeLa LT may exacerbate sensitivities due to ATRX loss.

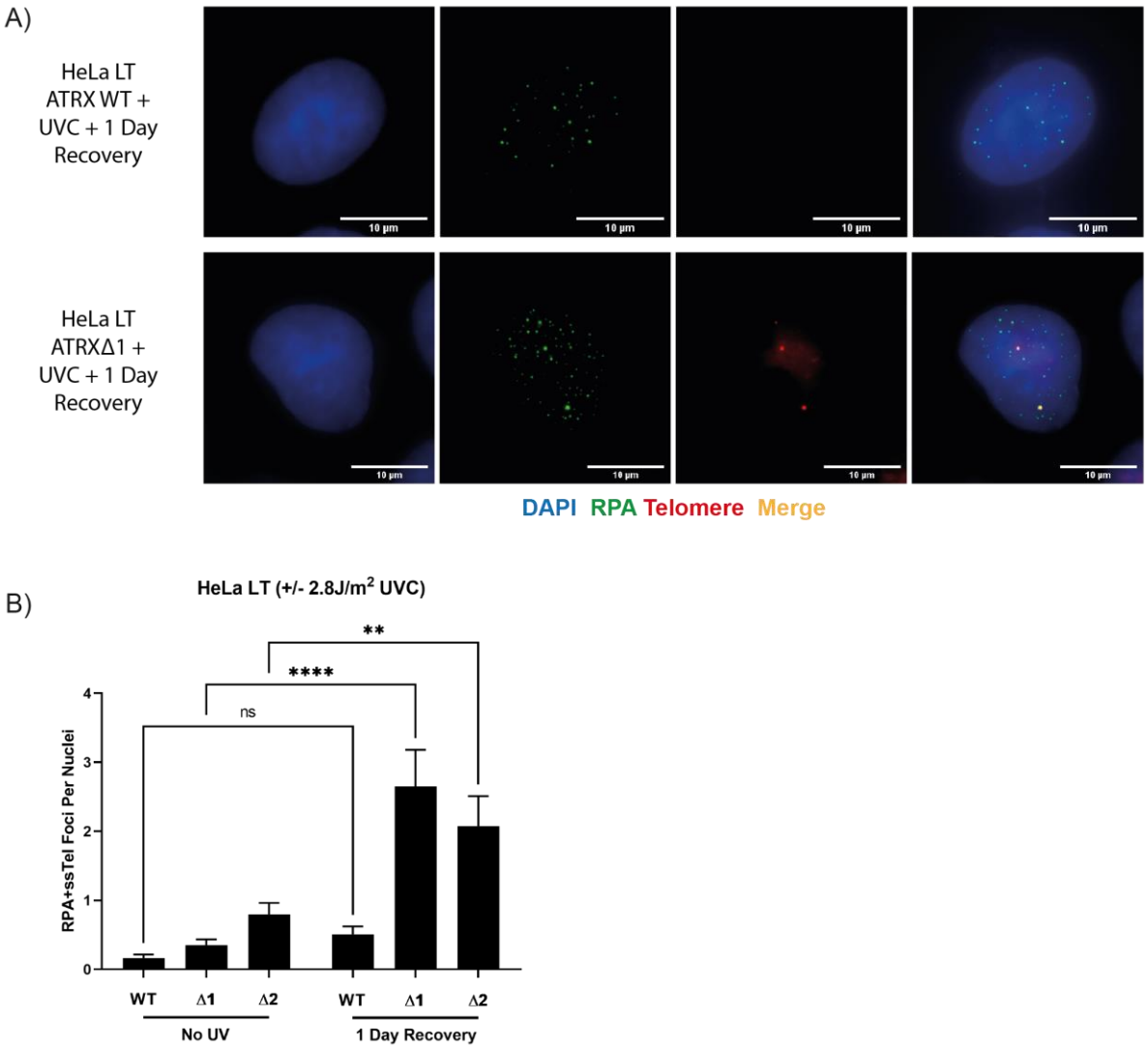

Figure 26: ATRX loss induces RPA+ssTel following UVC exposure. A) Representative images showing RPA+ssTel Immuno-FISH performed 24 hours after exposure to 2.8J/m^2 UVC. B) Quantification of A.

We next sought to determine whether UVC exposure induced RPA+ssTel in ATRX knockout HeLa LT cells. To do this, we exposed HeLa LT ATRX wild type and ATRX KO cells to 2.8 J/m^2 of UVC. As with H_2O_2, this value was chosen based on the clonogenic survival assay insofar as to avoid excessive cell death but allow for the build-up of possible adducts to cause replicative stress. Cells were treated then allowed to recover for 24 hours to allow for the initiation of repair events, or replication through damaged regions. As seen in Figure 26~~Figure 26~~, loss of ATRX facilitates the induction of RPA+ssTel, and unlike H_2O_2 treatment the levels of RPA+ssTel are comparable to that of camptothecin and PDS at approximately 2 foci per nucleus.

The induction of RPA+ssTel in HeLa LT following UVC and H_2O_2 exposure raise important questions as to the role of ATRX in response to oxidative and photo-adducts. Work from the O'Sullivan group using the BioID system showed an accumulation of the TLS polymerase Polη at ALT telomeres, suggesting either activation of the TLS pathway in U2OS ALT cells, or perhaps a failure to complete TLS (Garcia-Exposito *et al.*, 2016). This, combined with the severe sensitivity of ATRX deficient cells, raises the possibility that ATRX has a role in TLS, perhaps particularly at difficult to replicate or highly heterochromatic regions. This development raises exciting possibilities for further study.

4.7 SETD2 loss induces ALT in the absence of ATRX

Whilst the use of genotoxic agents that induce telomeric damage provide a simple and effective way of inducing ALT in ATRX deficient cells, it is important to consider physiologically relevant sources of such stress when attempting to unravel the natural development of ALT *in vivo*. As such, we sought to determine whether natural sources of replication stress or other genotoxic stress could induce an ALT phenotype in the absence of ATRX, in a similar way to that of camptothecin or pyridostatin.

When looking at the mutational landscape of ALT tumours, particularly in ALT cancers of the central nervous system, some of the most frequent mutations found are those in the H3F3A gene, one of two genes responsible for encoding the histone variant H3.3. Mutations in H3F3A are commonly found to affect two residues in high grade gliomas: Lysine 27 (H3.3 K27M) and Glycine 34 (H3.3 G34R/V). Mutations in H3F3B, which also encodes H3.3, are also found at Lysine 36 (H3.3 K36M), although these mutations preferentially affect cancers of the bone.

These three mutations, K27M, G34R/V, and K36M have wide reaching impacts on a cell. For example, K27M mutations lead to significant global reductions in H3K27me3 marks, which are indicative of facultative heterochromatin (Bender *et al.*, 2013; Lewis *et al.*, 2013; Venneti *et al.*, 2013). Loss of H3K27me3 lead to increases in gene expression and could drive the increases in TERRA transcription from subtelomeres (Chu *et al.*, 2017). Similarly, K36M mutations lead to a global reduction in H3K36 methylation through inhibition of mono- and di-methylation of H3K36 by NSD2/MMSET, and subsequently inhibition of the catalysation of di- to tri-methylation of H3K36 by SETD2 (Dong Fang *et al.*, 2016; Lu *et al.*, 2016). Although H3G34 is not typically the target of any histone post-translational modifications, due to its close proximity to H3K36, mutations such as G34R/V have been shown to inhibit H3K36 trimethylation by SETD2 through steric inhibition (Fang *et al.*, 2018). Analyses of tumour samples has shown that mutations such as G34R/V and mutations in SETD2 itself are mutually exclusive, indicating perhaps that either mutation leads to loss of K36 methylation (Fontebasso *et al.*, 2013). Co-mutation rates between ATRX and G34R/V or K27M, particularly in gliomas, is high, with ATRX and G34R/V co-mutation rates varying from 75-100%, and ATRX and K27M co-mutation rates as high as 75% in thalamic gliomas (Schwartzentruber *et al.*, 2012; Pathak *et al.*, 2015; Solomon *et al.*, 2016). Indeed, when analysing ATRX mutant brain tumours in the PeCan dataset, 60% of these tumours have mutations in H3F3A, and of these

mutations 48% are G34R and 50% are K27M mutations (Figure 9~~Figure 9~~**A**). To date, however, no study has performed large scale co-mutation analysis on specifically ALT positive tumours.

Mutations in SETD2 that cooccur with ATRX mutations are also found in the Cancer Genome Atlas (TCGA). When investigating all cancer types that harboured deleterious mutations in ATRX (as designated by SIFT, an algorithm that determines likelihood of amino-acid substitutions having functional effects on proteins), 59 of 229 (25.7%) cases also contained a deleterious mutation in SETD2. Similarly, in the same dataset, 9 of 229 cases (3.9%) harboured H3F3A mutations consistent with SETD2 activity reduction (G34R/V, K27M, K36M).

Recent work has shown that SETD2 loss can have profound effects on replication, with loss of SETD2 leading to a significant reduction in RRM2, a subunit of ribonucleotide reductase. This loss of SETD2, and the subsequent loss of H3K36me3 led to disruption in RRM2 expression, and ultimately dNTP starvation (Pfister *et al.*, 2015).

Consequently, we sought to determine whether SETD2 loss would induce ALT through the generation of replicative stress as a consequence of dNTP shortage, in the absence of ATRX. To this end Sam Shepherd (Clynes Lab) generated a SETD2 CRISPR knockout clone, and two ATRX/SETD2 double knockout clones (Figure 27~~Figure 27~~). As with PDS, pATMs1981 was assessed, with ATRX/SETD2 double knockouts displaying a significant increase in pATMs1981 over ATRX KO alone. Similarly, loss of SETD2 alone led to increased pATMs1981, indicating that loss of SETD2 creates an environment rich in DNA DSBs.

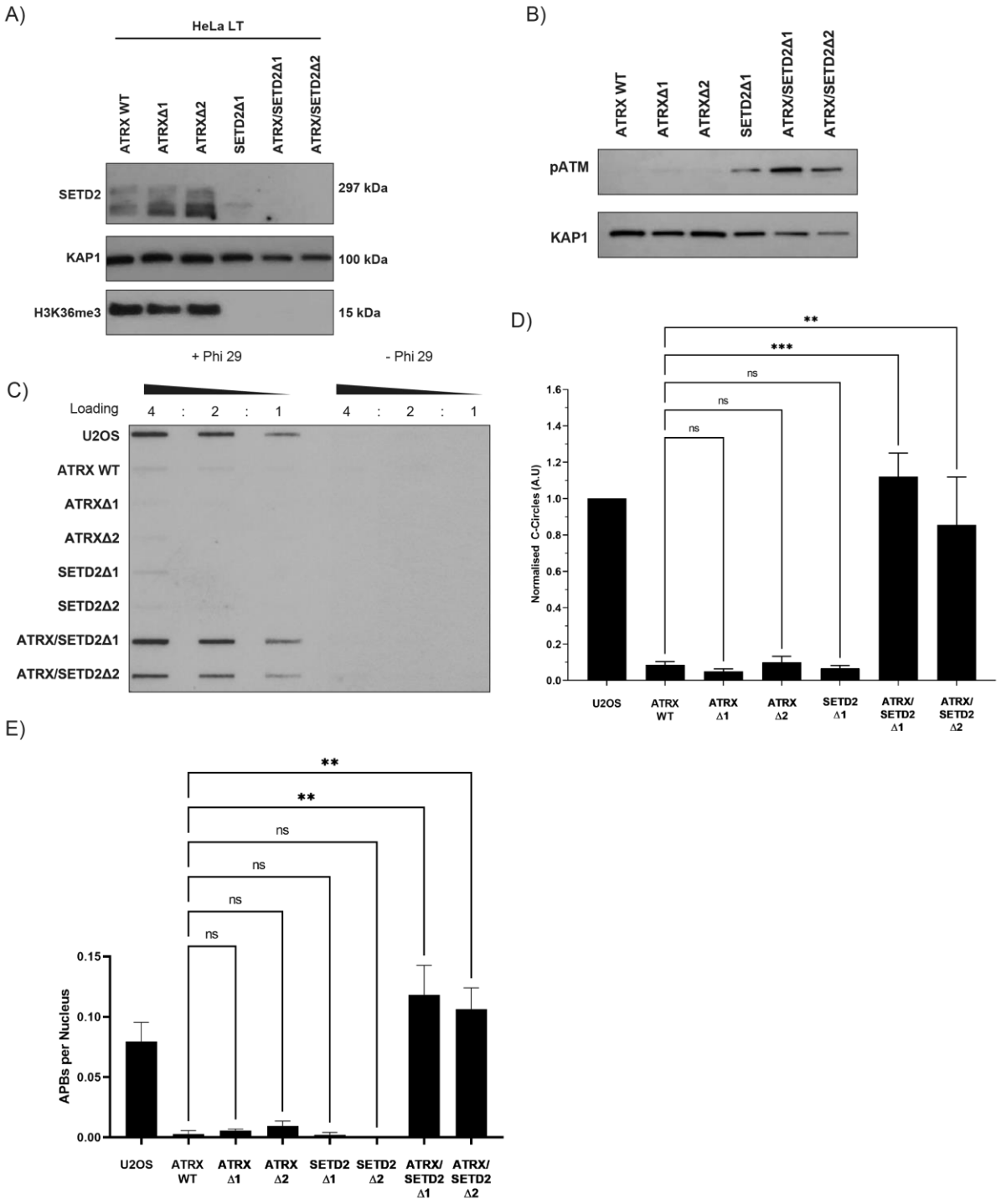

Figure 27: SETD2 loss in combination with ATRX loss induces the ALT phenotype. A) Western of SETD2 knockout clones. B) pATMs1981 assessed by western blotting in SETD2 KO clones. C-D) C-circle assay and quantification. E) Quantification of APBs. N=3, >50 nuclei per repeat for Immuno-FISH experiments. Western blots and C-circles (A-D) performed by Tomas Goncalves, APBs (E) performed by Sam Shepherd.

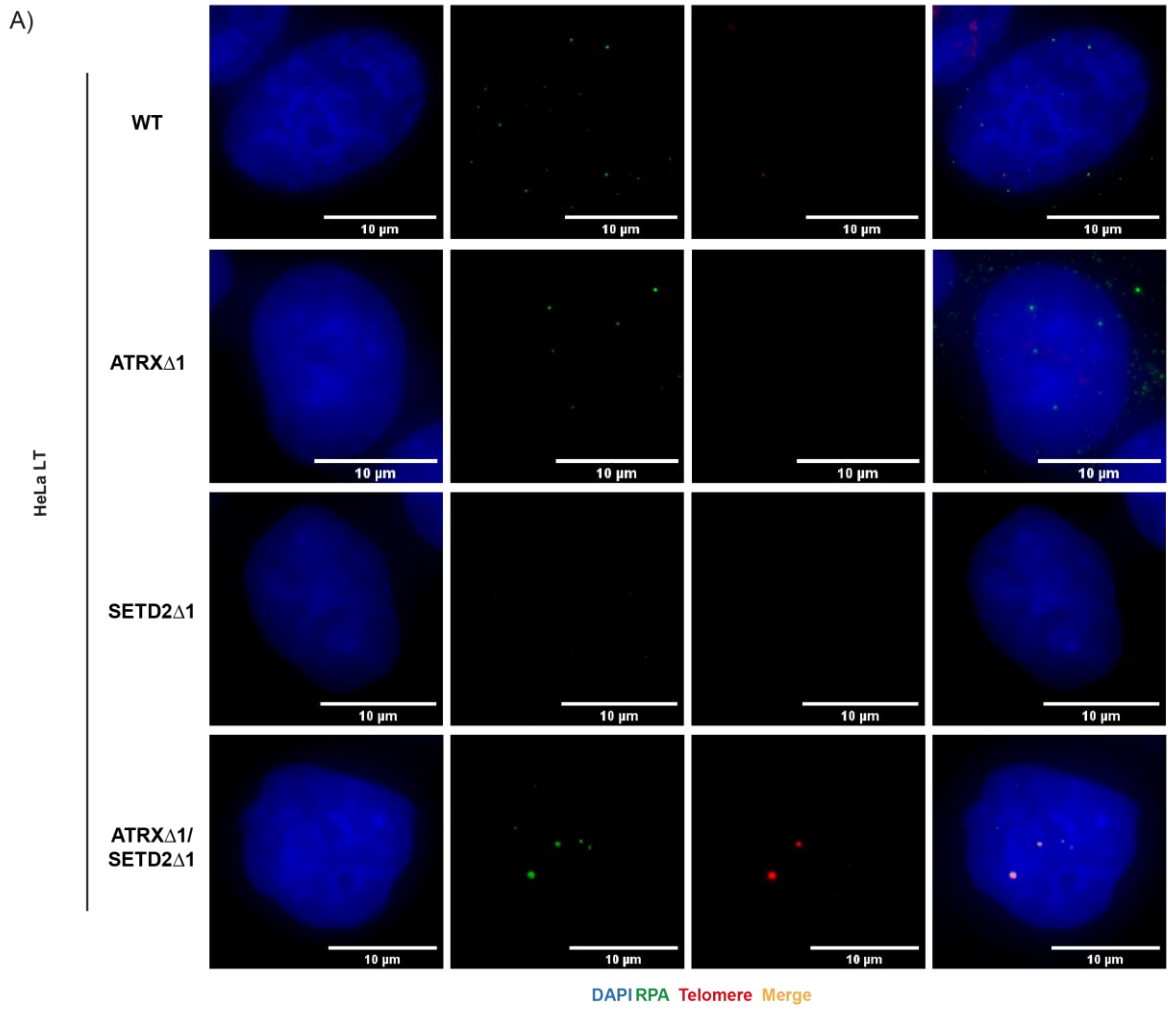

Figure 28: RPA+ssTel assay in SETD2 KO cells. A) Representative images of RPA+ssTel Immuno-FISH in SETD2 KO cells. B) Quantification of A.

To assay the ALT phenotype we assayed C-circles, APBs, and RPA+ssTel (Figure 27~~Figure 27~~ and Figure 28~~Figure 28~~). Loss of SETD2 alone, much like loss of ATRX alone, was insufficient to generate ALT in the HeLa LT model system. Strikingly, however, loss of both ATRX and

SETD2 together induced a measurable ALT phenotype. Both C-circles and RPA+ssTel foci were significantly increased in the ATRX/SETD2 double knockout cells, indicating a de novo ALT response.

Together these data suggest that SETD2 loss, when combined with ATRX loss, generates the environment necessary for ALT induction, whilst removing the suppressive effects of ATRX of the ALT pathway. As previously mentioned, SETD2 loss is not universal among ALT tumours, however, this hypothesis, one of increased replication stress at telomeres combined with loss of ATRX/DAXX, could be applied to other ALT tumours that have yet undiscovered mutations that lead, ultimately, to this ALT-permissive environment.

Results Chapter 3: ATRX loss permits out of register Break Induced Replication

5.1 ATRX loss induces loss of cohesion of telomeres

While the previously shown data explain how replication stress in ATRX deficient cells, due to adducts on the DNA, leads to the generation of DSBs, and ultimately the ALT phenotype, an outstanding question, however, is how the generation of such breaks leads to telomere elongation. Break Induced Replication, the principle method for ALT telomere elongation, ultimately leads to conservative DNA replication. In the case of telomeres, one might expect BIR to, at most, extend a broken sister chromatid to the end of the sister telomere when engaging in intratelomeric BIR, due to the inherent cohesion of sister chromatids during replication.

Whilst it has been shown that, in mice, ALT associated BIR is able to copy telomeric tags onto other telomere ends through intertelomeric recombination, when considering intratelomeric recombination, recent work from the laboratory of Titia De Lange has shown that loss of ATRX results in loss of cohesion of telomere ends (Neumann *et al.*, 2013; Lovejoy *et al.*, 2020). In an ALT model, this loss of cohesion would greatly exacerbate the risk of out of register homology directed repair (HDR) compared to in-register HDR, which in turn would greatly increase the chance of telomere elongation from an invading DSB. In order to verify these results in our own ATRX knockout clones, we assessed telomere cohesion using FISH. Cohesion FISH was performed as described in Section 7.10.7 using commercially available telomere probes designed to detect loss of the DLEU7 gene.

This probe set includes two probes, a chromosome 13q34 subtelomere probe (13qter, green) and a chromosome 13q14.3 probe set that covers the DLEU7 gene (D13S25, red). By performing FISH with these distinct probes it is possible to identify loss of cohesion through the formation of focus doublets.

At cohered telomeres it is expected that HeLa LT, being triploid for chromosome 13, to show 3 distinct green foci. Similarly, 3 distinct red D13S25 foci should be visible. However, in instances where cohesion at telomeres is lost, while the D13S25 foci should remain distinct, green 13q subtelomere foci begin to display doublet formations, indicative of the two daughter strands during replication falling out of register.

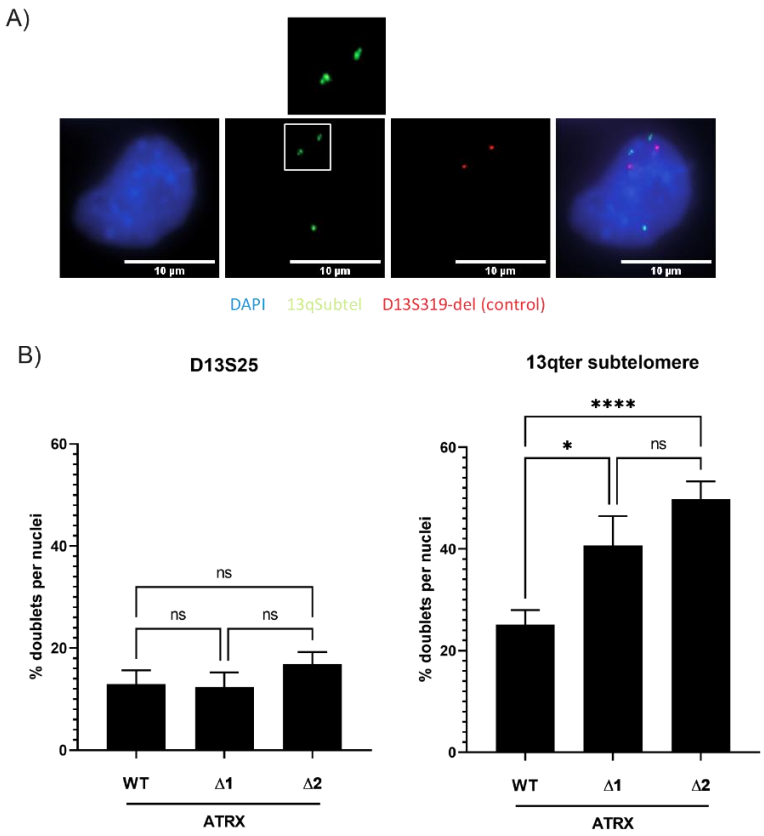

Figure 29: Loss of ATRX induces loss of telomere cohesion in HeLa LT. A) Representative image of doublet formation in HeLa LT ATRX Δ1. B) Quantification of D13S25 control and 13qter cohesion loss through counting the percentage of foci in each nucleus that form doublets. 2 biological replicates, >50 nuclei counted. One Way ANOVA with Welch correction. *, **** P < 0.05, 0.00005. Probing and imaging (A) performed by David Clynes.

Loss of ATRX induced a significant increase in cohesion loss at telomeres, increasing from 25% of telomeres showing loss of cohesion in HeLa LT wild type cells to approximately 45% showing a loss of cohesion in ATRX KO cells. In the control probe, D13S25, however, loss of cohesion was 15% and did not increase with loss of ATRX. These data agree with the data presented in the original findings by the De Lange group in mouse embryonic fibroblasts, where they also showed that loss of ATRX induced approximately 2-fold increase in telomeres showing cohesion loss. These data, and data from the literature, therefore, implicate ATRX loss in the facilitation of ALT through the loss of register during HDR. Loss of cohesion alone, however, is insufficient to generate ALT, as it does not in and of itself induce any kind of damage at telomeres.

Discussion

Despite literature evidence suggesting that 10-15% of all cancers use the Alternative Lengthening of Telomeres as their telomere maintenance mechanism, to date there has been no widespread adoption of testing for ALT status in clinics. This is despite evidence that, in soft tissue cancers such as malignant fibrous histiocytomas, liposarcoma, leiomyosarcoma and uterine sarcomas and carcinosarcomas, as well as in pancreatic neuroendocrine tumours, ALT is associated with decreased survival compared with cancers of these subtypes that utilise telomerase for telomere maintenance (Matsuo *et al.*, 2010; Venturini *et al.*, 2010; Lee, Park and Lee, 2012; Liau *et al.*, 2015; VandenBussche *et al.*, 2017). In contrast, despite breast cancer accounting for a similar 15.2% of cancer diagnoses (30.6% in women), genetic testing for BRCA1/2 mutations, which also have significant effects on prognosis, is becoming routine in the clinic with 25% to 96% of breast cancer patients receiving genetic screening for BRCA1/2 mutations (depending on country and context) (Smittenaar *et al.*, 2016; Thapa *et al.*, 2020). Furthermore, recent work in the field of ALT has significantly increased our understanding of the mechanisms of ALT, and further work in this area could identify druggable targets that markedly improve ALT cancer patient prognosis. Of note, recent work has suggested that certain ALT cancers are sensitive to inhibitors of the DNA damage sensing kinase ataxia telangiectasia and Rad3-related protein (ATR), and other work has shown that ATRX deficient cells display enhanced sensitivity to G-quadruplex stabilising ligands (Flynn *et al.*, 2015; Wang *et al.*, 2019). Additionally, in this thesis we have demonstrated sensitivity of ATRX deficient cells to both UVC and hydrogen peroxide. Whilst further work is required to fully understand ALT cancers and exploit these mechanisms for therapeutic benefit, it is clear that routine identification of ALT in cancer diagnosis could be beneficial.

Many of the markers of ALT are somewhat difficult to assay in clinic, such as the identification of telomere sister chromatid exchanges, or telomere length heterogeneity, both of which require complex and long protocols. Whilst markers such as C-circles and APBs are easier to assay, the identification of novel markers of ALT that are easier still to assay for will only serve to reduce friction of uptake of ALT assays in clinics. The identification of RPA bound to single stranded telomeric sequence could be one such marker. In this thesis we have shown that RPA bound single stranded telomeric sequence is a specific marker of ALT cancers, however, even without RPA immunofluorescence, single stranded telomeric sequence alone is a reproducible and specific marker of ALT cancers. This finding, by our lab and others, raises the possibility of the development of assays to more easily detect this single stranded DNA in clinic from tumour samples.

This work further highlighted the findings of previously published work suggesting that ALT marker generation is not a single process, and that ALT markers are actually generated by distinct cellular processes. When analysing levels of RPA+ssTel across a panel of ALT cells, and comparing these levels to levels of C-circles in the same cell lines, we observed a striking disconnect between the two markers. Although in all cases both markers in ALT cells were significantly higher than in non-ALT cells, ALT cells display variable levels of each marker. These data support previously published literature which shows a similar disconnect between level of APBs and C-circles in ALT cells. In one such publication, levels of APBs and C-circles differ vastly from cell line to cell line, with the ALT positive cell line KPD displaying 2-fold higher than average levels of C-circles, but 2-fold lower than average levels of APBs. Meanwhile, in the same study, U2OS cells displayed lower than the average C-circle level across the panel of ALT cells tested, but higher than average levels of APBs (Goncalves *et al.*,

2020). In our data we see a similar phenomenon, with the cell line Saos-2 displaying 3-fold higher levels of RPA+ssTel than U2OS, but only half the C-circle level.

Together these data help to address one question regarding the RPA+ssTel phenotype: what does it measure? One hypothesis is that the ssTel probe binds G-circles, as these circles have exposed ssDNA portions on them. If this were the case, however, one might expect levels of RPA+ssTel to strongly correlate with G-circle levels, as an increase in G-circles would increase the number of possible sites for RPA+ssTel generation. While we did not directly assay for G-circles, in part due to the difficulties associated with performing such assays, our data suggests that levels of the other T-circle form, C-circles, do not correlate with RPA+ssTel levels. Although it is unclear as to whether C- and G-circle levels are directly correlated, in an environment of increased telomere trimming, one might expect the two forms to increase in ALT. Another hypothesis for the nature of the RPA+ssTel phenotype is that it represents resected ends that occur after DSB formation, and represents an interesting avenue of further study.

Alongside routine detection of ALT cancers in the clinic, it is important that the underlying mechanisms by which ALT arises are understood. It has long been reported that ALT cancers harbour mutations in ATRX, and a number of studies and our own work has demonstrated that ATRX loss alone is insufficient to generate the ALT phenotype. As previously discussed, there have been some instances wherein ATRX loss alone triggered ALT markers, but given the limited number of cell lines used in these studies, it is plausible that some additional factors alongside ATRX loss predisposes these cell lines to ALT induction. In this thesis we have explored mechanisms of ALT induction in two model HeLa cell lines.

Recent work in the field has suggested that the presence of telomeric replicative stress drives the ALT pathway, with the stalling and subsequent collapse of replication forks leading to the generation of one ended DSBs. These DSBs represent the perfect substrate for break induced replication at telomeres, which has been shown to primarily occur in G2 or mitosis (MiDAS). Loss of ATRX has previously been linked to the generation of replicative stress and an increase in telomeric DSBs, however, given the fact that ATRX loss alone is generally insufficient to generate ALT, we reasoned that loss of ATRX/DAXX must be accompanied by additional cellular events. We thus hypothesised that such the presence of lesions at telomeres alone is normally tolerated by cells due to the presence of ATRX/DAXX. When ATRX or DAXX are lost, however, telomeres lose the protective effects of ATRX/DAXX and the cell loses the ability to tolerate such structures, and ultimately leads to the induction of ALT markers.

To address this hypothesis, we presented two model systems of ALT induction, that of induction of ALT in ATRX/DAXX deficient cancers by genotoxic agents, and by the combined effects of ATRX and SETD2 loss.

Specifically, when cells lacking ATRX or DAXX were exposed to genotoxic agents known to cause lesions or structures on the DNA, we observed induction of a number of ALT markers including APBs, C-circles and RPA+ssTel foci. Genotoxic agents shown to induce ALT were the G4 stabilising ligand PDS, the topoisomerase inhibitors CPT and ETO, the DNA polymerase inhibitor Aphidicolin, and the oxidative stress inducing agent H_2O_2. In addition, we showed that treatment with UVC radiation, which is known to generate UV adducts on DNA such as 6-4 photoproducts and pyrimidine dimers, also induced ALT markers.

Previous work has suggested that ATRX deficient cells are sensitive to PDS, possibly implicating ATRX in the response to PDS mediated G4 stabilisation, or the described effects

of TOP2 trapping by PDS (Wang *et al.*, 2019; Olivieri *et al.*, 2020). Similarly, previous work has suggested that even mild doses of CPT and ETO can lead to fork slowing and reversal in the absence of chromosomal breakage, implying that loss of ATRX or DAXX ultimately facilitates fork collapse (Zellweger *et al.*, 2015). This notion is supported by described roles for ATRX in the protection of reversed replication forks from MRE11 mediated degradation (Huh *et al.*, 2016). Additionally, this hypothesis is further supported by the dramatic enrichment of pATMs1981 at telomeres in ATRX deficient cells when treated with PDS and the dependence on MUS81 activity for the generation of ALT markers. Together, these data suggest that ATRX and likely DAXX act to protect telomeres from excessive MUS81-mediated DSB generation at telomeres.

Although we did not confirm sensitivity of ATRX deficient cells to all agents used, we did observe significant sensitivity of ATRX knockout cells to both hydrogen peroxide and UVC. Furthermore, we observed reductions in proliferation of ATRXΔ cells in response to DNA damaging agents. Furthermore, work by others has shown that ATRX deficient cells are sensitive to a number of DNA damaging or lesion inducing agents, including PDS, mitomycin C (MMC), methyl methanesulfonate (MMS) and hydroxyurea (Huh *et al.*, 2012; Clynes *et al.*, 2014; Juhász *et al.*, 2018; Wang *et al.*, 2019). These sensitivities are consistent with our model, wherein ATRX proficient cells are able to tolerate the lesions generated by these drugs, perhaps through protection of replication forks from degradation. In the absence of ATRX, however, cells are unable to tolerate this damage, and as such an increasing level of DSBs are generated. Our observation of increased pATMs1981 levels at telomeres in the absence of ATRX when treating with PDS reflects this increase in DSB formation. The efficiency of DNA repair mechanisms allows cells to tolerate DNA damage to a certain level, as evidenced by the levels of genomic instability within many cancers. However, with all systems, there is a point

wherein, presumably, the system can no longer maintain the genome, ultimately leading to cell death.

In the case of ALT development, low levels of replicative stress and DSB formation are likely essential components of the ALT-permissive environment. Our data suggests that agents capable of generating lesions on the DNA (UVC and hydrogen peroxide), trapping proteins on DNA (ETO, CPT, and to an extent PDS), generating secondary DNA structures (PDS), or generally interfering with replication fork progression (APH) are all capable of generating an ALT phenotype in the absence of ATRX. This data is consistent with previous assertions that replicative stress could be the key to triggering the ALT pathway.

Of these drugs, all induced RPA+ssTel to a certain degree. Importantly, however, we report that low dose aphidicolin was unable to induce both C-circles and APBs, implying that it is not replicative stress *per se* that elicits certain ALT markers in the absence of ATRX/DAXX, but more likely the presence of a lesion or secondary structure on telomeric DNA. In the case of the other agents used, all have predicted mechanisms of lesion/secondary structure formation. For example, PDS has been shown to have G-quadruplex stabilising properties, and G-quadruplexes have been proposed as a barrier to the replisome. One interesting observation, however, is the notion that at telomeres, G-quadruplexes would form on the G-rich lagging strand, and not on the leading strand. It therefore stands to reason that G-quadruplex stabilisation at telomeres would present less of a barrier to replication than at other sites in the genome. Indeed, recent work has shown that blocking lagging strand replication does not arrest fork progression *in vitro*, with Polα/Primase facilitating bypass of these blockages through downstream repriming (Taylor and Yeeles, 2018). In this work, the authors also demonstrate that this process leaves ssDNA gaps on the daughter strand that

are approximately the length of Okazaki fragments (~200nt), which are presumably bound by RPA. We therefore considered that the RPA bound at telomeres may reflect binding to these exposed ssDNA gaps. After further investigation, however, we observed that the RPA+ssTel phenotype was dependent on the endonuclease MUS81, implying that the phenotype represents RPA binding downstream of fork collapse. The persistence of some RPA+ssTel signal after knockdown of MUS81, could reflect ssDNA gaps on daughter telomere strands following Polα/Primase-mediated bypass of PDS induced lesions.

One possible explanation for the ability of PDS to induce ALT markers, despite the formation of quadruplexes on the lagging strand, is that formation of G-quadruplexes may precipitate further inhibition of replication processivity through the co-formation of R-loops at quadruplex sites. Recent work has indeed demonstrated that overexpression of the R-loop depleting nuclease RNaseH1 in cells treated with PDS led to a reduction in DNA damage markers and micronuclei formation, implicating R-loops in the cellular toxicity of PDS (De Magis *et al.*, 2019). Consistent with these findings, overexpression of RNaseH1 in ALT cells has been shown to deplete ALT markers, whereas loss of RNaseH1, or the Fanconi anaemia complex protein FANCM which has also been linked to the prevention of R-loops, instead promotes ALT marker formation (Arora *et al.*, 2014; Lu *et al.*, 2019; Pan *et al.*, 2019; Silva *et al.*, 2019).

Recent large scale screening of DNA damaging agents has revealed that PDS cytotoxicity is dependent on topoisomerase II (TOP2) (Olivieri *et al.*, 2020). In this work we show that treatment of cells with the TOP2 poison etoposide, leads to the generation of ALT markers in ATRX deficient cells. This data supports the notion that, analogous to PDS treatment, inhibition of TOP2 directly precipitates an ALT phenotype in the absence of ATRX. Given the

similar roles of TOP2 and TOP1, we also investigated TOP1 inhibition by camptothecin. Strikingly, camptothecin generated the most significant ALT marker induction as compared with any other agent used. Interestingly, work from yeast in the transcription of ribosomal RNA synthesis has shown that loss of TOP1 promotes the formation of R-loops that then act as persistent transcriptional blockage (El Hage *et al.*, 2010). In mammalian cells, treatment with camptothecin has been shown to directly lead to the formation of R-loops, and subsequently activate DNA damage checkpoints such as pATM (Sordet *et al.*, 2009; Marinello *et al.*, 2013). Together, these data suggest a role for R-loops in the development of ALT, both in the context of PDS treatment and potentially beyond. Indeed, it is likely that in a cell line that lacks ATRX, stabilisation of telomeric quadruplexes, or R-loops directly, leads to R-loop mediated fork progression defects, fork stalling, and eventual collapse. More work is still required to understand the exact significance of R-loops in an ALT development model and is something our lab is actively investigating. Given the increase in R-loop formation in ATRX negative cells, however, it would appear that the R-loop formation as a consequence ATRX loss alone are insufficient to generate ALT (Nguyen *et al.*, 2017).

One explanation for this observation is that ATRX loss does not promote R-loop formation, and instead ATRX promotes replication through, and as such resolution of, R-loops. Therefore, loss of ATRX does not increase the formation of R-loops *per se*, but instead affects persistence of R-loops. One hypothesis for how ATRX loss leads to R-loop persistence can be inferred from recent work regarding FANCD2. FANCD2, a member of the Fanconi anaemia complex, has previously been described to have roles in R-loop resolution, and recent work has shown a functional interaction between FANCD2 and ATRX for the purposes of replication fork recovery (Liang *et al.*, 2019; Okamoto *et al.*, 2019; Raghunandan *et al.*, 2020). It is therefore possible, that the recruitment of ATRX to sites that are likely to form R-loops/quadruplexes,

such as telomeres, allows for transient recruitment of FANCD2 to these sites, ultimately allowing for the depletion of R-loops by FANCD2 and downstream processes.

In contrast to our findings with CPT, ETO and PDS, low dose APH generated a separation of phenotypes. Although low dose APH induced RPA+ssTel to a degree similar to that seen with etoposide, it was unable to induce C-circles or APBs. This separation of phenotypes raises interesting questions as to how low dose APH fundamentally differs from drugs such as CPT, ETO, and PDS, but also how RPA+ssTel relates to APBs and C-circles as a marker of ALT. One possible explanation for the difference in phenotypes is that RPA+ssTel measures something that occurs immediately downstream of replication fork stalling and collapse, whereas C-circles and APBs instead may represent an ALT process that occurs further downstream. Work has shown the need for cell cycle progression in the generation of C-circles (T. Zhang *et al.*, 2019). Considering the reliance on MUS81 activity for RPA+ssTel phenotype induction, we hypothesise that RPA+ssTel represents RPA binding to telomeres soon after fork collapse. C-circles, on the other hand, represent further downstream processing. Furthermore, in PDS treated cells, knockdown of MUS81 was unable to completely ablate RPA+ssTel, raising the possibility that the RPA+ssTel phenotype actually represents two subtly different cellular contexts. The first context is that of a post-cleavage event, wherein, for example, telomeres may be resected, exposing the C-rich or G-rich strand for binding by RPA and subsequent assaying with a DNA probe. As such resection is typically 5’ to 3’, one might expect that a replication fork at telomeres would expose only the C-rich strand following cleavage by MUS81-EME1. *In vitro* evidence, however, suggests that a complex between MUS81 and EME2 are able to cleave 3’ flaps, exposing a DNA end that, when resected, reveals the G-rich strand (Pepe and West, 2014b). Alternatively, RPA+ssTel could bind within the D-loop, following strand invasion by BIR, to the displaced strand. The second context, particularly in

the case of low dose APH, wherein the replicative machinery is inhibited, is the exposure of ssDNA during replication as a consequence of helicase-polymerase uncoupling.

When exposed to inhibitors of replication such as APH, however, polymerase activity is reduced, slowing the replication machinery. The MCM helicase, however, continues to unwind the DNA ahead of the fork. Should this unwinding progress at a speed greater than replication, section of ssDNA are exposed, promoting RPA binding, ATR activation, and CHK1 phosphorylation (Byun *et al.*, 2005).

Therefore, although we observed that ALT marker generation in PDS treated cells depended on MUS81, we did not determine whether RPA+ssTel induced by low dose APH also required MUS81. Thus, we hypothesise that APH induces RPA+ssTel as a consequence of helicase-polymerase uncoupling but fails to induce other ALT markers due to limited DSB formation.

Alongside genotoxic agents like PDS, ETO and CPT, we have sought to understand other potential barriers to replication that could precipitate the ALT phenotype. Our data shows a significant difference in cell survival in response to both UVC and H_2O_2 treatment in ATRXΔ cells when compared to ATRX wild type cells. The striking sensitivity to UVC could be related to H3.3 loss leading to UV sensitivity due to defects in nucleotide excision repair (NER) that have been reported in the literature (Frey *et al.*, 2014). As ATRX/DAXX is the primary histone chaperon complex involved in H3.3 deposition in regions such as the telomeres, loss of this deposition in ATRXΔ cells could have profound effects on UV sensitivity. When assaying ALT markers following exposure to UVC or H_2O_2 we also see induction of ALT markers to some degree. Whilst the level of ALT markers generated in H_2O_2 treated cells is lower than that of other agents, UVC damage generated ALT markers to a level similar to that of camptothecin. Interestingly, previous work has linked hydrogen peroxide treatment to the trapping of TOP1

and the formation of TOP1 cleavage complexes (Daroui *et al.*, 2004). Furthermore, literature evidence suggests that the generation of adducts on DNA by UVC leads to decoupling of RNA polymerase from chromatin, and permits the formation of R-loops (Tresini *et al.*, 2015). Interestingly, one proposed mechanism for the resolution of R-loops excision by the NER nucleases XPF and XPG, and the formation of ssDNA gaps that could ultimately trigger fork collapse in S-phase (Sollier *et al.*, 2014). This finding, combined with our observation of UV sensitivity in ATRX deficient cells and the proposed role of ATRX/DAXX/H3.3 in NER, support the idea that the formation of R-loops could pose a significant problem for ATRX deficient cells.

In order to understand physiologically relevant ALT induction, and what additional factors were required alongside ATRX loss, we analysed large scale datasets and the literature to determine common mutations that arise in ALT cancers alongside ATRX mutations. One of the most frequent mutations to arise alongside ATRX mutations, especially within cancers of the brain such as high grade glioma (HGG), are those in SETD2 or in residues predicted to be bound by SETD2 in histone H3.3 (H3F3A) such as G34 and K36 (Fontebasso *et al.*, 2013). The importance of mutations in H3F3A and SETD2 are twofold. Firstly, SETD2 is responsible for trimethylation of H3.3 at lysine 36 (H3K36me3), and this chromatin mark has been shown to have wide ranging effects on the chromatin landscape. For example, H3K36me3 has been shown to shape chromatin accessibility after transcription through the recruitment of MRG15 (a component of the Rpd3S/Sin3S histone deacetylase complex), PHF1/19 (a component of the polycomb repressive complex 2 (PRC2)) and SPT16 (a component of the FACT complex) (Ballaré *et al.*, 2012; Kumar *et al.*, 2012; Cai *et al.*, 2013; Carvalho *et al.*, 2013). Therefore, it is possible that loss of SETD2, and thus loss of H3K36me3, leads to more a more open chromatin environment, which would be more permissive of the formation of structures such as R-loops

and quadruplexes. Literature evidence supports this hypothesis, with loss of the FACT complex being associated with increases in R-loop formation (Herrera-Moyano *et al.*, 2014).

In addition, H3K36me3 has been shown to recruit the DNA methyltransferase DNMT3b, a methyltransferase involved in CpG methylation, wherein mutations are associated with the immunodeficiency, centromeric instability and facial anomalies syndrome (ICF). Loss of DNMT3b has been shown to induce hypomethylation at subtelomeres and leads to the accumulation of telomeric R-loops in patients with ICF (Sagie *et al.*, 2017).

Whilst SETD2 mutations do co-occur with ATRX mutations, large scale analysis of tumour databases has highlighted that H3F3A mutations in G34 and K36 co-occur with ATRX mutations at significantly higher rates. Interestingly, SETD2 mutations and H3F3A G34/K36 mutations tend to be mutually exclusive, implying that the disruptive properties of G34/K36 mutations are sufficient to phenocopy loss of SETD2 itself (Schwartzentruber *et al.*, 2012; Fontebasso *et al.*, 2013). One caveat of this hypothesis is that, in an ALT model, cells also lack ATRX. As ATRX and DAXX are critical components of the ATRX/DAXX/H3.3 deposition axis, the primary H3.3 deposition mechanism at telomeres, a natural question arises as to how H3.3 is deposited into chromatin at sufficient quantities to impact SETD2 binding due to H3F3A G34/K36 mutations. Recent work, however, has addressed this question, showing that in ATRX/DAXX deficient contexts, the histone H3.3 chaperone HIRA is enriched at telomeres, as an adaptive response to permit continued deposition of H3.3 in telomeric regions (Hoang *et al.*, 2020).

We observed a striking induction of ALT markers in model ATRXΔSETD2Δ cell lines, without the need for exogenous sources of DNA damage through genotoxic agents. This ALT marker induction was not triggered by SETD2Δ alone, suggesting that it is the combined effect of

SETD2 loss and ATRX loss that precipitates this phenotype. In the future, it will be insightful to determine the effects of ATRXΔ and SETD2Δ on R-loop levels in our model systems, and the effects of R-loop depletion on this phenotype. Indeed, our data suggests that treatment of cells on coverslips with RNaseH1 during Immuno-FISH does not deplete the RPA+ssTel phenotype. However, as this treatment occurs post-fixation, it is plausible that the underlying conditions for RPA and DNA probe binding are already present when assaying these coverslips. Instead, cells overexpressing an RNaseH1 construct should be assayed, as under these conditions we would hypothesise that R-loop formation is prevented, and thus the ALT phenotype would not be induced.

Finally, in line with recently published literature on the effects of ATRX loss on telomere sister chromatid cohesion, we demonstrate that loss of ATRX leads to a 2-fold increase in the formation of telomere doublets, indicative of loss of cohesion (Lovejoy *et al.*, 2020). This loss of cohesion in ATRX deficient cells helps to explain the striking frequency of ATRX loss in ALT cancers. Without the loss of ATRX, and the resulting loss of cohesion, one-ended DSBs that form would be significantly more likely to engage in in-register BIR, constraining telomere elongation or shortening to copy that of the sister chromatid. By contrast, following loss of telomere sister cohesion as a result of ATRX loss, it is possible to imagine gross changes in telomere length occur at significantly higher frequency, depending on the position of invasion during the early stages of BIR.

Thus, in our model (Figure 30~~Figure 30~~), we propose that adducts on the DNA form barriers to replication. Adducts include quadruplexes, and associated R-loops, direct protein-DNA adducts (such as trapped TOP1), or direct DNA base modifications, to name a few examples. These adducts, when encountered by an approaching telomeric replication fork , lead to fork

stalling and eventual fork reversal. In line with previously published literature, ATRX works to protect these reversed forks from degradation by the MRN complex (Huh *et al.*, 2016). In the absence of ATRX, therefore, reversed replication forks are degraded, leading to eventual cleavage of forks by the MUS81 endonuclease, and the generation of a one ended DSB. In line with the previously described role for ATRX in the maintenance of telomere sister chromatid cohesion, cells lacking ATRX are unable to perform in-register repair. Thus, when the one-ended DSB is repaired by break induced replication, telomeres can be lengthened or shortened, depending on the point of invasion, resulting in heterogenous telomere lengths as seen in ALT. The increased frequency of break formation leads to DNA damage responses, which ultimately trigger telomere clustering and repair in PML bodies, inducing APB formation. We hypothesise that either resection by one-ended DSBs generated from MUS81-EME2 cleavage, or the elongation of D-loops in BIR expose ssDNA at the telomere that is bound by RPA. Furthermore, consistent with recent work on the origin of C-circles from telomere internal loops, the increase in adducts at telomeres, and their subsequent processing, leads to the formation of C-circles. In line with this notion, work using CRISPR-Cas9 mediated telomeric single strand break formation, which could mimic NER mediated excision of adducts, has been shown to lead to the formation of C-circles (T. Zhang *et al.*, 2019).

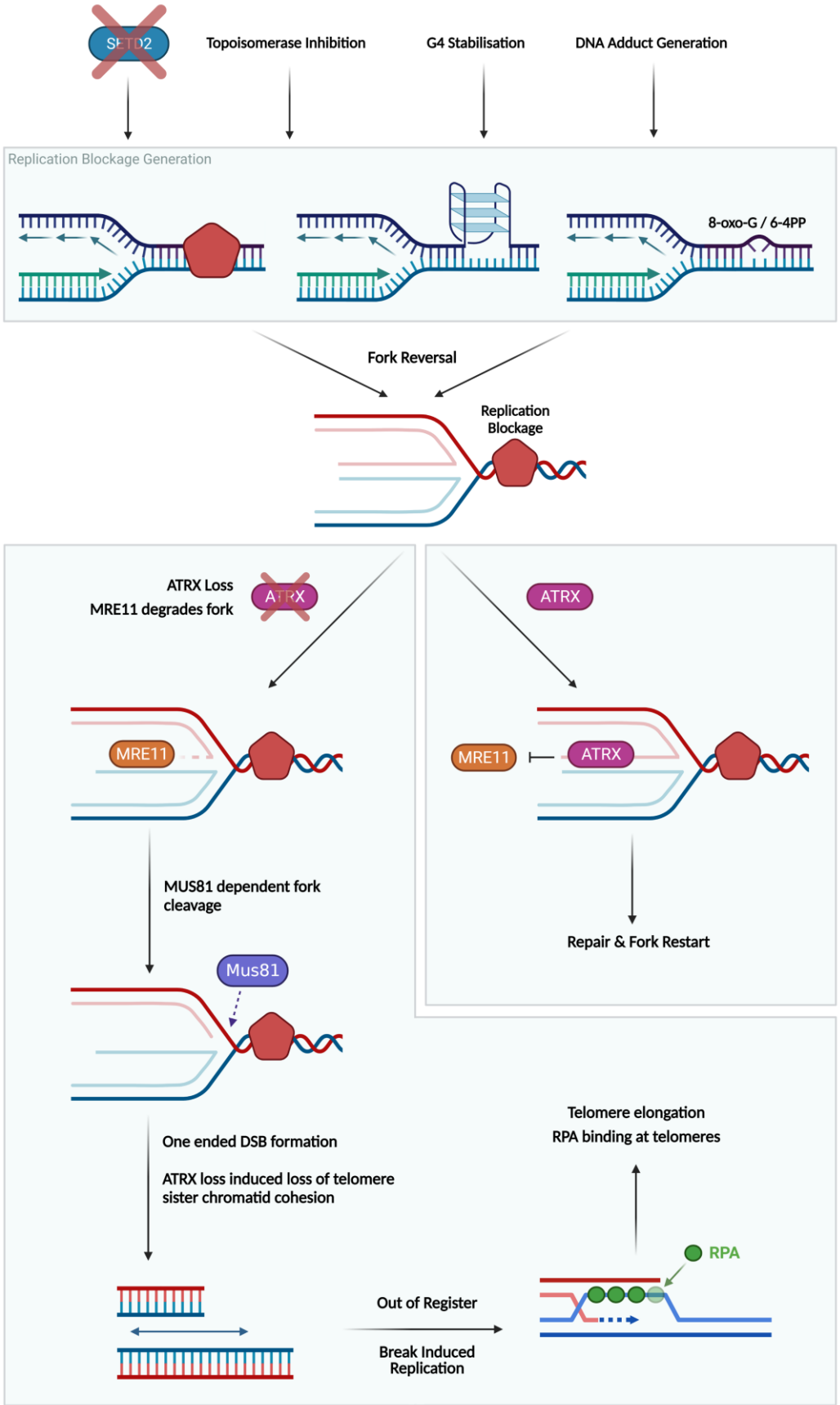

1523

1524 **Figure 30: Model for ALT induction in ATRXΔ cells.**

Methodology

7.1 Antibodies & Reagents

Table 1: Antibodies used for Immuno-FISH experiments

Antibody	Catalogue Number	Dilution
RPA32 (9H8)	Abcam #AB2175	1:500
PML (PG-M3)	Santa Cruz #SC-996	1:500
ATRX	Abcam #AB97508	1:500
pATM s1981 (10H11.E12)	Santa Cruz #SC-47739	1:250

Table 2: siRNA oligos used for knockdown experiments

siRNA	Catalogue Number
siScramble	ON-TARGETplus Non-targeting Control siRNA #1 (Dharmacon, D-001810-01-20)
siMus81	ON-TARGETplus Mus81 siRNA SmartPool (Dharmacon, L-016143-01-0005)

7.2 Cell Lines & Cell Culture

All cell lines were incubated at 37°C with 5% CO2. The SW26, SW39, G292 SaOS2, WI38, HeLa and HeLa LT cell lines were cultured in in Dulbecco's Modified Eagle's Medium (Gibco) with 10% Tet-Approved FBS (Clontech), supplemented with 1X Pen Strep (Thermo Fisher Scientific) and 1% L glutamine (Gibco). U-2 OS^{ATRX} cells were cultured in similar media, but with the further addition of 0.35 mg mL-1 G 418 (Sigma) and 4 µg mL-1 of Puromycin dihydrochloride (Sigma). All cells were cultured to approximately 85% confluency before subculturing with media changes 2-3 times per week.

Subculturing was performed via the use of 1x 0.25% trypsin-EDTA (Life Technologies). Briefly, media was removed, and the plate washed with approximately 5 mL of 1X phosphate buffered saline (PBS) (pH 7.4, Life Technologies). Sufficient trypsin-EDTA (1-2 mL on a 75cm^2 growth area) was added to the growth surface and incubated at 37°C for approximately 5 minutes, or until sufficient cell detachment was achieved. An equal volume or greater of culture media was added to the plate to neutralise the trypsin-EDTA and the resulting suspension was added to a 15 mL tube. Following centrifugation for 5 minutes at 1000 x g, the supernatant was removed and the cell pellet resuspended in an appropriate amount of culture media to allow for a 1:8 subculture ratio.

7.3 Kill Curve Experiments

During the generation of cell lines stably expressing plasmid constructs, cells containing plasmids were held under antibiotic selection to kill untransfected cells. Prior to this, baseline sensitivity to antibiotics of interest were determined using kill curve experiments. In these experiments, 40,000 cells were seeded onto multiple wells of a 6 well plate. Each well was then treated with an increasing concentration of the antibiotic of interest to determine the minimum concentration needed to kill cells with no antibiotic resistance genes. The growth, or death of these cells was compared to a well treated with a vehicle control (typically water or DMSO). After two days, the minimum dosage required to kill >95% of cells was determined, and the next dosage up from this was selected as the appropriate selection concentration.

7.4 UVC Treatment

For UVC treatment, cells were grown in 100mm tissue culture dishes with removeable lids. To treat cells, culture media was removed from dishes to reduce UV absorption. Plates were briefly washed with PBS, and the UVC Stratalinker sterilised using the Auto Crosslink function.

Plates were then placed within the Stratalinker with the lid removed and exposed to the appropriate amount of UVC radiation. Plates were then closed, and fresh culture media add to the cells before returning them to an incubator.

7.5 Whole Cell Extraction

Cells were first harvested from their growth surface as described above, by washing and incubating with 0.25% Trypsin-EDTA, forming a pellet. The pellet was then washed with 5mL of PBS before being further centrifuged at 1000 x g for 5 minutes and was then placed on ice. The supernatant was removed, leaving approximately 20µL. Cells were then resuspended in this volume by gently agitating the tube. The cell suspension transferred to a 1.5 mL Eppendorf, and 200µL of high salt radioimmunoprecipitation assay buffer (RIPA) containing 1M NaCl (Sigma), 1% NP-40 (Thermofisher), 1% Na-Deoxycholate (Sigma), 0.2% SDS (Sigma), and 50 mM Tris-HCl pH 7.4 (Sigma) was added, ensuring the sample remained on ice at all times. The RIPA lysis was performed on ice for 25 minutes with gentle occasional agitation. Following incubation, the sample was slowly passed through a 25-gauge needle attached to a 1 mL syringe 30 times, ensuring that minimal heat was generated. The sample was then centrifuged at 4°C for 10 minutes at 13,000 x g. Finally, the supernatant was transferred to a new 1.5 mL tube and combined with 160µL of 2x loading buffer (New England Biolabs) and 40µL of fresh 1M DTT (Thermofisher), and the entire sample was heated for 5 minutes at 95°C.

7.6 Western Blot

Whole cell extracts prepared in section 7.5 were run, unless otherwise stated, on a 10 or 12 well NuPAGE 4-12% Bis-Tris precast gel (Invitrogen) in a XCell SureLock Mini-cell Electrophoresis System tank (Thermo Fisher Scientific) using 1x NuPAGE® MOPS SDS Running Buffer (Invitrogen). Samples were electrophoretically separated at 120V for around 2 hours,

or until the dye front reached the base of the gel. Samples were run alongside a PageRuler Plus pre-stained 10 to 250 kDa protein ladder (Thermo Fisher Scientific).

Following electrophoretic separation, gel bands were transferred onto Immobilon P PVDF 0.45µM Transfer Membrane (Merck Millipore). Briefly, the transfer stack was constructed by placing the gel and membrane between pieces of Whatman filter paper soaked in transfer buffer containing 1x NuPAGE transfer buffer and 10% methanol. Prior to constructing the stack, the Immobilon membrane was activated by soaking in 100% methanol for 1 minute. The stack was loaded into a transfer tank and transferred for 18 hours at 25 mA.

The transferred membrane was blocked using 5% (w/v) Marvell skimmed milk powder in TBST (0.1% Tween-20 in tris-buffered saline) for 1 hour, henceforth referred to as blocking buffer. Following blocking of the membrane the membrane was cut into distinct fragments, one for each probed protein and a loading control. An appropriate primary antibody was selected and diluted to the appropriate concentration in 2.5% blocking buffer (diluted using TBST) and then primary antibodies were incubated on the membrane at room temperature, with shaking, for 1 hour. The membrane was washed three times with TBST for approximately 5 minutes to remove any unbound antibody. Meanwhile, a HRP-conjugated secondary antibody with reactivity to the species of each primary antibody was prepared using 2.5% blocking buffer. Membranes were incubated for 1 hour with the secondary antibody at room temperature, with shaking, and were again then washed three times in TBST, with the final wash consisting of 15 minutes.

Following final washing, excess TBST was removed from the membrane using absorbent tissue and the full membrane reconstructed in a flat plastic tray to allow for the addition of enhanced chemiluminescent substrate (ECL). SignalFire™ ECL Reagent (Cell Signalling

Technology) was combined into a 1.5 mL tube (750µL of reagent A and B respectively) before being applied to the membrane, ensuring all regions of the membrane were covered. Following a 1 minute incubation excess ECL was drained and the reconstructed membrane was placed in a Hypercassette™ (Amersham Biosciences) inside a polypropylene sleeve. Membranes were then exposed onto Amersham Hyperfilm ECL film (GE Healthcare) for an appropriate amount of time to see clear bands.

7.7 CRISPR-Cas9 Knockout

CRISPR-Cas9 KO of ATRX was performed using a modified pSpCas9(bb)-2A-GFP tagged Cas9 vector containing sgRNAs targeting exon 16 of ATRX (sgRNA sequence - TOP: 5' caccGTCCAATAACAACCA^AGT 3', BOTTOM: 5' aaacACT^TGGTTGTTATTGGAC 3') with an expected cut site at lysine 1536. Cells were sorted on a BD FACSAria Fusion cell sorter 24 hours after transfection into single wells and grown into clones. KO was determined by western blotting. DAXX KOs were performed in the same way, using a commercially available DAXX Cas9 plasmid (Santa Cruz, sc-400686-KO-2) and were selected on GFP positivity. SETD2 Cas9 KO was performed using plasmids obtained from Professor Tim Humphrey, Oxford (Pfister *et al.*, 2015). Transfected cells were selected using 0.4 µg/mL puromycin and then sorted into single wells to obtain clones. Combinatorial KOs were made through sequential KO of genes.

7.8 siRNA Treatment

In instances where siRNA treatment was required, siRNAs were ordered as oligos, and resuspended in MilliQ water to a stock concentration of 20µM. Unless otherwise stated, all siRNA transfections involved a reverse transfection on day 1, followed by a "top up" forward transfection on day 3, and collection on day 5.

7.8.1 Reverse Transfection of siRNA

Reverse transfection on the first day way achieved using HiPerFect transfection reagent, following the manufacturers protocol. Briefly, siRNA was diluted in 50 µL MilliQ water, and spotted to the bottom of the well to give a final concentration of 10nM after the addition of the cells. HiPerFect transfection reagent (50 µL for 60mm dishes, and 120 µL for 100mm dishes) was diluted in an appropriate volume of serum-free DMEM (1600 µL for 60mm dishes and 4380 µL for 100mm dishes). The diluted transfection reagent was then to the bottom of the well and incubated at room temperature for 10 minutes to allow for the creation of transfection complexes.

Freshly trypsinised cells were then seeded directly onto the top of the transfection complexes ($5x10^4$ cells per 60mm dish or $1x10^6$ cells per 100mm dish) and plates were incubated until day 3.

7.8.2 Forward Transfection of siRNA

On day 3, plates were removed from the incubator and the media removed. Cells were briefly washed with room temperature PBS to remove residual transfection complexes. Culture media was then added to the well (to a total volume of 3mL for 60mm dishes or 10mL for 100mm dishes).

Transfection mixes were then prepared by diluting siRNA to a final concentration of 5nM (after addition to the cells above) in serum free media. HiPerFect was then added to this mix (30 µL for 60mm dishes and 75 µL for 100mm dishes) and complexes were allowed to form by incubating at room temperature for 10 minutes. Complexes were then added to the plated cells in a dropwise fashion.

Transfected plates were placed back in a 37°C cell culture incubator with 5% CO2 and were incubated until collection on day 5.

7.8.3 Drug treatment of siRNA transfected cells

In instances where siRNA treated cells were treated with agents such as pyridostatin, the agent was added on the 4th day, the day prior to collection.

7.8.4 Determining knockdown efficiency

On the 5th day, when cells were taken for downstream analysis, or when coverslips were fixed, a portion of the cells (30% of a 60mm dish or 10% of a 100mm dish) were taken for analysis of knockdown efficiency by western blot. This was performed following the instructions in sections 7.5 and 7.6.

7.9 shRNA Generation & Lentiviral Packaging

ATRX shRNA 2 plasmids were generated within the laboratory of Richard Gibbons. Briefly, oligos for the target sequence 5'-GTCGTGTTGGCTGATATT-3' were generated and cloned into a pLKO.1-Puro vector. These vectors were amplified in bacteria and then purified for transfection.

HEK293T cells were used as a viral production host cell owing to the presence of the SV40 large T-antigen, which facilitates efficient episomal replication of transfected plasmids, and the general ease of transfection. A transient 3 plasmid system was used to generate shATRX 2 lentivirus particles, with pCMV-dR8.91 (AddGene) delivering Gag and Pol genes, and a pCMV-VSV-G (AddGene) plasmid delivering the Env gene.

4µg of pCMV-VSV-G, 2µg of pCMV-dR8.91 and 2µg of the pLKO.1-shATRX2 plasmid were transiently transfected into a 10cm dish pre-seeded with 5x10^5 HEK293T cells using

LipoFectamine 2000 reagent following the manufacturers protocol. 4 hours after transfection, media containing transfection complexes was removed and replaced with 10mL of fresh culture media.

After 48 hours, the 10mL of media containing lentiviral particles was collected and filtered using a 0.45µM filter, and aliquoted into 300µL aliquots before being stored at -80°C. For shRNA experiments, 300µL of lentiviral lysate was applied per million cells by directly applying a thawed aliquot to cells growing in culture. Transduced cells were then selected with an appropriate concentration puromycin to kill untransduced cells as determined by kill curve experiments.

7.10 Immunofluorescence and Immuno-FISH

7.10.1 Coverslip Preparation

Cells were grown on 13mm #1.5 thickness (0.16 - 0.19 mm) glass coverslips by placing coverslips into the bottom of 24 well plate wells. A final cell number of $8x10^5$ cells per coverslips was used for each experiment. As such, an appropriate cell number was seeded to 24 well plate wells containing coverslips at least 24 hours prior to fixing. For untreated cells this would be $4x10^5$ cells 24 hours prior to fixing. For longer experiments, an assumed doubling time of 24 hours was used to calculate an appropriate number of cells to seed based upon treatment time.

7.10.2 Pre-permeabilisation and Fixing

Unless otherwise stated, all coverslips used in this project were pre-permeabilised to aid in penetration of antibodies and dyes. Coverslips were first washed with twice with PBS for 5 minutes at room temperature to remove residual culture media, before being pre-permeabilised with 0.5% Triton X-100 on ice for 1 minute. Following a further 5-minute PBS

wash at room temperature, cells on coverslips were fixed for in 5% paraformaldehyde (PFA) in PBS for 20 minutes. Fixed coverslips were then washed 3 times for 5 minutes in PBS at room temperature to removed residual PFA.

7.10.3 Antibody Probing

Fixed coverslips were then permeabilised using 0.5% Triton X-100 for 6 minutes on ice. Coverslips were washed 3 times in PBS for 5 minutes at room temperature. Permeabilised cells were then blocked using blocking buffer (2% Bovine Serum Albumin in PBS) for 1 hour with gentle rocking at room temperature.

Primary antibodies were diluted to appropriate dilutions in blocking solution and applied to coverslips for 1 hour at room temperature with gentle rocking. Following staining, coverslips were washed 3 times in PBS containing 1% Tween (PBS-Tween) for 5 minutes, and then stained with an appropriate fluorophore conjugated secondary antibody, again diluted in blocking solution, for 1 hour at room temperature with gentle rocking. Unbound secondary antibodies were then washed off with 3, 5-minute room temperature, washes in PBS-Tween. Coverslips were then processed according to Sections 7.10.4 or 7.10.5 depending on whether probing of DNA was required (i.e. Immuno-FISH).

7.10.4 Immunofluorescence Mounting

In instances where DNA probing was not required, coverslips were immediately mounted on glass microscope slides using VectaShield mounting media containing DAPI. Coverslips were then secured to glass microscope slides using nail varnish to prevent slipping and subsequent tearing over cells during microscopy.

7.10.5 Immuno-FISH

In instances where DNA probing was required, antibodies were post-fixed in 4% PFA for 10 minutes at room temperature to prevent antibody degradation in subsequent steps. Post-fixed coverslips were again washed 2 times at room temperature in PBS-Tween for 5 minutes, before being rinsed in 2x Saline Sodium Citrate (300mM sodium chloride, 30mM trisodium citrate adjusted to pH 7.0 with HCl) (2x SSC).

If probing of denatured DNA was required, such as in APB experiments, coverslips would then be denatured using 3N HCl at room temperature for 13 minutes. The HCl was immediately washed using ice-cold PBS in 3 1-minute washes. If DNA denaturation was not required, this step was skipped.

To probe coverslips, an appropriate fluorophore-labelled DNA oligo was suspended in Hybridisation Buffer (25% formamide, 2x SSC, 200ng/µL salmon sperm, 5x Denhardt's solution, 50mM Phosphate buffer, 1mM EDTA) to a dilution of 1:50. 5µL of the probe solution was then spotted onto a glass microscope slide, and the coverslip placed faced down into the solution. To prevent evaporation, coverslips were covered in a rubber cement solution ("Fixogum", Maribu) and transferred to a slide box containing wet tissue. This box was then incubated at 37°C overnight to create a humid environment conducive to oligo hybridisation.

The following day, coverslips were returned to 24 well plate wells with cells facing upwards. They were then washed 3 times at 37°C for 10 minutes in 2x SSC, and washed a further 2 times in Tris-Saline-Tween (150 mM NaCl, 50 mM Tris-HCl, pH 7.6 with 0.05% Tween-20) at room temperature for 5 minutes. Residual Tween-20 was then washed out with a 5 minute, room temperature, wash with Tris-Saline and coverslips were mounted on microscope slides as described in Section 7.10.4.

7.10.6 RNase treatment

For RNase controls 1*U* of RNase A or RNase H was added to coverslips prior to hybridisation with telomere probes and incubated at 37°C for 1 hour. Coverslips were washed in PBS for 5 minutes to remove residual RNase before continuing with the protocol.

7.10.7 Cohesion FISH

Cohesion FISH was performed using Cytocell probes designed to detect deletion of DLEU7 on chromosome 13 (Cytocell, Cat. #LPH-043). FISH was performed following the manufacturers protocol on coverslips pre-seeded with HeLa LT ATRX WT or ATRX KO cells.

7.11 Immunofluorescence and Immuno-FISH analysis

7.11.1 Microscopy

Immunofluorescence and Immuno-FISH experiments were imaged on a Deltavision wide-field microscope using a 100x oil-immersion objective with an image size of 1024 pixels by 1024 pixels. In all instances, images were taken using Z-stacking with 30 planes to acquire information across the entire depth of the cell. To achieve this, a z-step distance of 0.2µM was used to give a 6µM total depth.

7.11.2 Image Analysis

Images were analysed in two pieces of software: FIJI and CellProfiler. FIJI Is Just ImageJ, or FIJI, was used to process the Deltavision images by projecting all Z-stacks onto a single image using maximum intensity projection. In this case, the maximum pixel intensity on any z-slice is used as the final pixel intensity.

Following z-projection and output in TIFF format, images were ingested into CellProfiler for quantification.

7.11.2.1 Pipeline outline

A bespoke pipeline was used and analysis settings changed for each set of experimental conditions to allow for differences in feature properties between conditions. In brief, the pipeline first identified nuclei in the DAPI channel (Channel 0) using the *IdentifyPrimaryObjects* module, automatically optimised contrast for foci identification using the *EnhanceOrSuppressFeatures* module, then identified foci in each channel (henceforth referred to as Channel 1 and Channel 2 in a 3 colour experiment) using the *IdentifyPrimaryObjects* module. After identifying objects (nuclei or foci) the foci objects were related back to their parent nuclei using the *RelateObjects* module to allow the script to determine the number of foci in each nucleus. Additionally, a mask was used using the *MaskObjects* module to identify colocalising foci, subtracting any identified pixels in Channel 2 that were not also present in Channel 1. This allowed for the counting of colocalised foci within each nucleus.

7.11.2.2 Thresholding

When identifying nuclei and foci the *IdentifyPrimaryObjects* module was set to use the Otsu thresholding method in a three-class configuration. Briefly, the Otsu thresholding mechanism creates three “classes” for pixels – a foreground class containing foci, a background class containing the image background, and a third middle class of pixels that in this instance is assigned to be background also.

The reason for choosing a three-class configuration is to remove any halo effects caused by out of focus light in wide field images. In this instance it is assumed that foci represent bright pixels relative to background or out of focus pixels.

The Otsu method then automatically determines two threshold points for the bound between the lower and middle class and middle and upper class. When determining a threshold parameter the Otsu method aims to choose threshold values that lead to the minimum intraclass variance in pixel intensity. The end of effect of this is automatic segmentation of images into foreground foci and background pixels.

When applying the Otsu method, a minimum threshold value of 0.075 a.u. (within a range of 0 to 1, where 0 is black and 1 is white) was used as a lower bound cutoff. The reason for this cutoff was to ensure that in images that contained no foci (such as in negative control images) the automatic thresholding by Otsu was not adjusted to be in the bottom 7.5% of possible intensity values, and that any pixel below 7.5% of maximum intensity was assumed to be black. Without this manual cutoff Otsu would attempt to determine 2 threshold values in images with only background signal, leading to false identification of noise as foci.

Additionally, when thresholding, a minimum feature size cutoff was employed. This parameter allowed for the script to discard objects that were too small. This was particularly useful in the removal of instances where single pixels were identified as foci. Care was taken to not discard real foci in images by sampling a number of outputted images manually.

7.12 Telomere Restriction Fragment Assay

The telomere restriction fragment assay was performed by digesting 20µg of genomic DNA with both HinfI-HF (New England Biolabs) and RsaI-HF (New England Biolabs) in a double digest in CutSmart buffer (see Table 3~~Table 3~~). The final volume of this reaction was maintained at 50 µL to allow for the whole volume to be loaded onto a gel for analysis.

Table 3: Genomic DNA digest conditions for telomere restriction fragment assay

Reagent	Volume
DNA	X (20µg)
CutSmart Buffer (10x)	5 µL
HinfI-HF	2 µL
RsaI-HF	2 µL
Total	50 µL

Digests were allowed to continue at 37°C overnight to ensure adequate digestion even with large amounts of high molecular weight DNA. Following digestion, reactions were stopped by adding in the appropriate volume of DNA loading dye (10 µL of 6x loading dye for a 50 µL reaction).

In instances where denatured and native DNA was intended to be visualised simultaneously, half of the final working solution was loaded into a well, with the other half retained for the other half of the gel. In instances where only native or denatured DNA was intended to be visualised the entire volume was loaded. Gels were made and run following the instructions in section 7.13.

7.13 Southern Blot

7.13.1 Southern Gel

For Southern blotting a 1% agarose gel was made using UltraPure Agarose (CATALOGUE) and 0.5x Tris-Borate EDTA (TBE) in a large gel tank. Briefly, agarose was melted in TBE in a microwave until agarose crystals were completely dissolved and allowed to cool until warm to the touch with gentle stirring. Gels were poured without any intercalating DNA dye, such as Ethidium Bromide (EtBr), due to the length of gel running.

Gels were loaded with samples combined with Gel Purple loading dye (New England Biolabs) and a Lambda HindIII DNA ladder (New England Biolabs) for size determination. Samples were run at 50v for 18 hours to allow for large fragment separation. Following running, gels were post-stained with EtBr (at a concentration of 1:10000) for 10 minutes, then destained twice with 10 minute washes in water. EtBr stained gels were visualised under a transilluminator to check for equal well loading.

7.13.1.1 DNA Denaturation

In instances where DNA in all or part of the gel required denaturation, the required gel sections were cut from the remaining gel and denatured in 1M NaOH for 30 minutes. While this section denatured, remaining gel sections were kept in 0.5x TBE to prevent drying of the gel. Following denaturation, the NaOH was neutralised in "Neutralisation Solution" (0.5 M Tris-HCl pH 7.4, 2M NaCl) for 2 hours. Neutralisation solution was changed and the gel neutralised for a further 2 hours.

7.13.2 Blotting

A large sponge was laid in a tray and covered in a large sheet of Whatmann paper. 0.6x SSC was then added to the tray until the sponge was saturated. Gels were reconstructed face-down on the Whatmann paper and covered in cling film to prevent evaporation. With a scalpel the cling film covering the face of the gel was excised leaving a 5mm gap around the edge. Onto this the ZetaProbe membrane (BioRad) was placed covering the entire gel face. Paper towels were then stacked at least 20cm tall on membrane and gel trying to distribute pressure evenly and were secured in place by placing a glass pane on top and adding an empty bottle to apply even pressure to the gel.

DNA was allowed to blot onto the membrane overnight, and the following day the stack was deconstructed. The membrane was UV crosslinked using the "Auto Crosslink" setting on a Stratalinker 2000 (UV A). The membrane was then dried at 80°C for 3 hours for longer term storage, or processed immediately.

7.13.3 DIG-Probing

Membranes were probed using an antibody method that utilises a Digoxigenin (DIG) tagged probe. Briefly, membranes were soaked in 2xSSC for 5 minutes to ensure the membrane was adequately rehydrated. Membranes were then applied to the inside of a glass rolling tube, ensuring that DNA was facing away from the glass and the membrane was not overlapping. To this tube, 20mL of PerfectHyb hybridisation buffer was added, and the membrane allowed to pre-hybridise for 20 minutes at room temperature on a roller.

Meanwhile, a DIG-labelled $[CCCATT]_3$ probe was suspended in 20mL of PerfectHyb hybridisation buffer to a concentration of 40nM. After removing pre-hybridisation buffer, the DIG-labelled probe buffer was added to the tube and allowed to hybridise at 37°C for 2 hours. Following hybridisation, the membrane was removed from the glass rolling tube and laid face-up into a large container. The membrane was then washed 3 times with gentle shaking in "Wash Buffer" (0.1M Maleic acid, 3M NaCl; 0.1% Tween 20 adjusted to pH 7.5) at room temperature for 15 minutes.

Membranes were blocked for 30 minutes using Blocking Buffer (0.1M Maleic acid, 3M NaCl, 0.5% milk, 0.5% BSA). An anti-DIG antibody was suspended to a concentration of 1:1000 in Blocking Buffer and applied to the membrane. The antibody was incubated on the membrane for 30 minutes at room temperature with gentle rocking. The antibody was then washed 3 times for 15 minutes at room temperature in Wash Buffer. Following washing, 2mL of CDP-

Star solution (Sigma) was applied to the membrane and incubated in the dark for 1 minute. Residual CDP-Star was drained from the membrane, and the membrane inserted between two pieces of clear plastic inside a cassette.

Multiple exposures of the membrane were then made onto Amersham Hyperfilm chemiluminescence film (GE Healthcare). Films were scanned at 300DPI using a large flatbed scanner and analysed in FIJI.

7.14 C-circle Assay

7.14.1 Genomic DNA Extraction

Genomic DNA was extracted from approximately $1x10^6$ cells using the PureGene Gentra Core B kit using an adapted protocol. Briefly, cell pellets were completely suspended in 300µL of the included Cell Lysis Buffer. In instances where the pellet was difficult to fully suspend in the lysis buffer the sample was heated at 37°C for 15 minutes. After lysis, samples were incubated with 1.5µL of RNase A solution at 37°C for 5 minutes to remove residual RNA. Proteins in the sample were precipitated with 100µL of the included Protein Precipitation Buffer and centrifuged to allow for extraction of the C-circle containing supernatant. DNA was then precipitated in isopropanol and subsequently washed with 70% ethanol. After allowing the ethanol to evaporate the DNA was resuspended in pH 7.4 20mM Tris buffer, incubated at 65°C for 1 hour and then allowed to fully dissolve overnight at room temperature.

7.14.2 C-circle Amplification

DNA extracted as described in section 7.14.1 was quantified at least 3 times on a Nanodrop to ensure that the DNA was fully dissolved. In this regard, the criteria of consistent readings and a 260/280 ratio of >2 was used. If samples were of insufficient quality the experiment

was repeated. If the readings were inconsistent, the DNA was briefly vortexed and measured again. If the DNA was still inconsistent it was heated at 37°C for 2 hours and remeasured.

After acquiring DNA of sufficient quality, 250ng of genomic DNA was digested with HinfI and RsaI for 3 hours at 37°C (see Table 4~~Table 4~~). High fidelity versions of HinfI and RsaI were used to ensure buffer compatibility. When diluting DNA care was taken to ensure accuracy in the amount of genomic DNA used, as variance could impact the C-circle result. As such, in instances where genomic DNA stocks were high (i.e. >100 ng/µL) serial dilutions of the genomic DNA were performed, with multiple quantifications of genomic DNA concentrations until a concentration of approximately 50 ng/µL was reached.

Table 4: Genomic DNA digestion protocol for the C-circle assay

Reagent	Final Amount
Genomic DNA	250 ng
CutSmart Buffer (10x)	5 µL
HinfI-HF	0.1 µL
RsaI-HF	0.1 µL
10mg/mL BSA	0.5 µL
RNase A	0.5 µL
Water	To 50 µL

150 ng (30 µL) of digested genomic DNA was then amplified using ϕ29 polymerase along with dATP, dGTP and dTTP (see Table 5~~Table 5~~). In order to ensure specificity of amplification of C-circles and not other circular DNA species dCTP was not included in amplification. Thus, only circles with single stranded regions of adenine, guanine and thymine bases could amplify. In the case of C-circles, only the C-rich strand contains single stranded regions.

Table 5: C-circle amplification reaction using ϕ29 polymerase

Reagent	Final Amount
Digested DNA	150 ng
Each of 100mM dATP, dGTP, dCTP	1 µL
20 mg/mL BSA	0.5 µL
1% Tween-20	5 µL
ϕ29 Buffer (10x)	10 µL
Φ29 Polymerase	3.75 µL
Water	To 100 µL

Reactions were incubated at 30°C for 8 hours, followed by incubation at 65°C for 20 minutes to heat inactivate the ϕ29 polymerase.

7.14.3 Slot Blotting

Amplified C-circle samples were slot blotted onto ZetaProbe membrane using a Bio-Dot slot blotting apparatus (BioRad). Briefly, the apparatus was constructed following the manufacturers protocol, ensuring a tight seal with the rubber gasket to allow for adequate vacuum pressure to be obtained. Both the membrane and Whatmann paper spacers beneath within the slot blotter were pre-soaked in 2xSSC.

Samples were diluted in 2xSSC to final volume of 200µL. While running the vacuum three sequential volumes of the sample were loaded into adjacent wells: 100 µL, 50 µL and 25 µL. This was to aid in downstream analysis, and to ensure that a linear range was achieved.

Following blotting, the vacuum was allowed to dry under vacuum pressure for 5 minutes and removed from the blotting apparatus. Blotted DNA was crosslinked to membranes using the "Auto Crosslink" setting on a Stratalinker with a UV A bulb. Membranes were dried until probing following the protocol described in section 7.13.3 with a $[CCCTAA]_3$ DIG-labelled probe.

7.14.4 C-circle Analysis

After exposure to X-ray film, films were scanned at 300 DPI using a flatbed scanner and imported into FIJI for analysis. The gel lane tool was then used to designate each lane of the slot blot wells. The “Plot Lanes” function was then used to generate an intensity profile of the lane, taking an average of the pixel intensity across the width of the lane at each Y position.

Using FIJI’s line tool, a line was then drawn across the graph just above the intensity of background pixels (i.e. the pixels between slow blot wells) to segment the graph into a series of peaks. The area of the peaks was then analysed and plotted in Excel. The areas of each of the three dilutions were compared, reversing the dilution factor by multiplying the value by 1, 2, or 4. Taking an average of these three normalised readings allowed for accurate comparison between conditions.

7.15 Clonogenic Survival Assay (CSA)

For clonogenic survival assays, 500 cells were seeded into a 6 well plate well in 2mL media, with triplicate wells for each condition. Cells were allowed to attach overnight and were treated with an appropriate concentration of an agent on the second day. On the third day, the agent was removed, the well washed with PBS and fresh media replaced. The clonogenic survival plates were then allowed to grow for 10 further days, to allow for the formation of colonies. Multiple, incrementally increasing concentrations of each agent were used, alongside the appropriate vehicle control to determine survival impairment.

To fix the colonies to the wells for counting, the media was removed from the plate, and the wells washed with PBS. Wells were stained for 15 minutes using a fixative and staining solution consisting of 50% methanol, 10% glacial acetic acid, and 0.1% Coomassie Brilliant

Blue R-250 (w/v). Following staining, plates were destained and washed by dipping the plate in three consecutive beakers of water, yielding a destained plate with countable colonies.

Colonies were counted by hand, excluding colonies that were <1mm in width. Colony counts for the three replicate wells for each concentration were averaged and plotted in GraphPad Prism.

7.16 Cell Cycle Quantification

Cell cycle quantification was performed using propidium iodide staining and flow cytometry. Briefly, cells were cultures in their respective conditions for 24 hours prior to cell cycle quantification. Cells were then trypsinised from cell culture plates and washed with PBS, and then resuspended in 150 µL PBS to ensure thorough resuspension and minimal clumping. Cells were then added dropwise from a height of 30 cm into a falcon tube containing cold 70% ethanol while slowly vortexing. This step ensured consistent fixing as well as minimal clumping. Following fixing, cells were fixed for a further 30 minutes in the ethanol in a fridge at 4°C. Cells were gently centrifuged at 500 x g for 5 minutes before washing and centrifuging again in PBS. Cells were then treated for 4 hours at 4°C with a solution containing 50 µg/ml propidium iodide and 500 ng/mL RNase A in PBS. This RNase treatment step is essential to ensure that the propidium iodide stains DNA and not RNA.

Samples were then analysed by flow cytometry on an Attune NxT flow cytometer. Cells were first gated on live cells based on FSC/SSC and then gated to remove doublets. Propidium iodide levels were then plotted on a histogram to show the PI levels for each singlet cell.

Attribution

All work in this thesis was the work on Thomas Kent, with the exception of the following figures.

Figure	Work By	Details
5A	Sam Shepherd	Western blot & Cell culture
6B	Siobhan Cunniffe	Western blot & Cell culture
7	Sam Shepherd, Tomas Goncalves	APB analysis by S.S., C-circle by T.G.
13	Sam Shepherd, Tomas Goncalves	APB analysis by S.S., C-circle by T.G.
14	Tomas Goncalves	Southern blotting and Analysis by T.G.
17	Sam Shepherd	Knockout clone generation and Western blot
18	Sam Shepherd, Tomas Goncalves	APB analysis by S.S., C-circle by T.G.
22	Sam Shepherd, Tomas Goncalves	APB analysis by S.S., C-circle by T.G.
23	Sangwoo Kim	CTG assay by S.K.
27	Sam Shepherd, Tomas Goncalves	Western blots and C-circle by T.G. and APB analysis by S.S.
29	David Clynes	Probing & Imaging by D.C. analysis by T.K.

References

Andersen, P. L. *et al.* (2011) 'Sequential assembly of translesion DNA polymerases at UV-induced DNA damage sites', *Molecular Biology of the Cell*. doi: 10.1091/mbc.E10-12-0938.

Argentaro, A. *et al.* (2007) 'Structural consequences of disease-causing mutations in the ATRX-DNMT3-DNMT3L (ADD) domain of the chromatin-associated protein ATRX', *Proceedings of the National Academy of Sciences of the United States of America*. doi: 10.1073/pnas.0704057104.

Arora, R. *et al.* (2014) 'RNaseH1 regulates TERRA-telomeric DNA hybrids and telomere maintenance in ALT tumour cells', *Nature Communications*. doi: 10.1038/ncomms6220.

Badens, C. *et al.* (2006) 'ATRX syndrome in a girl with a heterozygous mutation in the ATRX Zn finger domain and a totally skewed X-inactivation pattern', *American Journal of Medical Genetics, Part A*. doi: 10.1002/ajmg.a.31400.

Ballaré, C. *et al.* (2012) 'Phf19 links methylated Lys36 of histone H3 to regulation of Polycomb activity', *Nature Structural and Molecular Biology*. doi: 10.1038/nsmb.2434.

Bender, S. *et al.* (2013) 'Reduced H3K27me3 and DNA Hypomethylation Are Major Drivers of Gene Expression in K27M Mutant Pediatric High-Grade Gliomas', *Cancer Cell*. doi: 10.1016/j.ccr.2013.10.006.

Betous, R. *et al.* (2009) 'Role of TLS DNA polymerases eta and kappa in processing naturally occurring structured DNA in human cells', *Molecular Carcinogenesis*. doi: 10.1002/mc.20509.

Bétous, R. *et al.* (2012) 'SMARCAL1 catalyzes fork regression and holliday junction migration to maintain genome stability during DNA replication', *Genes and Development*. doi: 10.1101/gad.178459.111.

1995 Bodnar, A. G. *et al.* (1998) 'Extension of life-span by introduction of telomerase into normal
1996 human cells', *Science*. doi: 10.1126/science.279.5349.349.

1997 Boisvert, F. M., Hendzel, M. J. and Bazett-Jones, D. P. (2000) 'Promyelocytic leukemia (PML)
1998 nuclear bodies are protein structures that do not accumulate RNA', *Journal of Cell Biology*.
1999 doi: 10.1083/jcb.148.2.283.

2000 Brosnan-Cashman, J. A. *et al.* (2018) 'ATRX loss induces multiple hallmarks of the alternative
2001 lengthening of telomeres (ALT) phenotype in human glioma cell lines in a cell line-specific
2002 manner', *PLoS ONE*. doi: 10.1371/journal.pone.0204159.

2003 Bryan, T. M. *et al.* (1995) 'Telomere elongation in immortal human cells without detectable
2004 telomerase activity', *EMBO Journal*. doi: 10.1002/j.1460-2075.1995.tb00098.x.

2005 Bryan, T. M. *et al.* (1997) 'Evidence for an alternative mechanism for maintaining telomere
2006 length in human tumors and tumor-derived cell lines', *Nature Medicine*. doi:
2007 10.1038/nm1197-1271.

2008 Byun, T. S. *et al.* (2005) 'Functional uncoupling of MCM helicase and DNA polymerase
2009 activities activates the ATR-dependent checkpoint', *Genes and Development*. doi:
2010 10.1101/gad.1301205.

2011 Cai, L. *et al.* (2013) 'An H3K36 Methylation-Engaging Tudor Motif of Polycomb-like Proteins
2012 Mediates PRC2 Complex Targeting', *Molecular Cell*. doi: 10.1016/j.molcel.2012.11.026.

2013 Cardoso, C. *et al.* (1998) 'Specific interaction between the XNP/ATR-X gene product and the
2014 SET domain of the human EZH2 protein', *Human Molecular Genetics*. doi:
2015 10.1093/hmg/7.4.679.

2016 Carvalho, S. *et al.* (2013) 'Histone methyltransferase SETD2 coordinates FACT recruitment

2017 with nucleosome dynamics during transcription', *Nucleic Acids Research*. doi:
2018 10.1093/nar/gks1472.

2019 Cerritelli, S. M. and Crouch, R. J. (2009) 'Ribonuclease H: The enzymes in eukaryotes', *FEBS*
2020 *Journal*. doi: 10.1111/j.1742-4658.2009.06908.x.

2021 Cesare, A. J. and Griffith, J. D. (2004) 'Telomeric DNA in ALT Cells Is Characterized by Free
2022 Telomeric Circles and Heterogeneous t-Loops', *Molecular and Cellular Biology*. doi:
2023 10.1128/mcb.24.22.9948-9957.2004.

2024 Cesare, A. J. and Reddel, R. R. (2013) 'Alternative Lengthening of Telomeres in Mammalian
2025 Cells', in *Madame Curie Bioscience Database*. Landes Bioscience;

2026 Chen, Q., Ijpma, A. and Greider, C. W. (2001) 'Two Survivor Pathways That Allow Growth in
2027 the Absence of Telomerase Are Generated by Distinct Telomere Recombination Events',
2028 *Molecular and Cellular Biology*. doi: 10.1128/mcb.21.5.1819-1827.2001.

2029 Cho, N. W. *et al.* (2014) 'Interchromosomal homology searches drive directional ALT telomere
2030 movement and synapsis', *Cell*. doi: 10.1016/j.cell.2014.08.030.

2031 Chu, H. P. *et al.* (2017) 'TERRA RNA Antagonizes ATRX and Protects Telomeres', *Cell*. doi:
2032 10.1016/j.cell.2017.06.017.

2033 Chung, I. *et al.* (2012) 'PML body meets telomere: The beginning of an ALTernate ending?',
2034 *Nucleus (United States)*. doi: 10.4161/nucl.20326.

2035 Clynes, D. *et al.* (2014) 'ATRX dysfunction induces replication defects in primary mouse cells',
2036 *PLoS ONE*. doi: 10.1371/journal.pone.0092915.

2037 Clynes, D. *et al.* (2015) 'Suppression of the alternative lengthening of telomere pathway by

2038 the chromatin remodelling factor ATRX', *Nature Communications*. doi:
2039 10.1038/ncomms8538.

2040 Collins, K. and Mitchell, J. R. (2002) 'Telomerase in the human organism', *Oncogene*. doi:
2041 10.1038/sj/onc/1205083.

2042 Compton, S. A. *et al.* (2007) 'Xrcc3 and Nbs1 are required for the production of
2043 extrachromosomal telomeric circles in human alternative lengthening of telomere cells',
2044 *Cancer Research*. doi: 10.1158/0008-5472.CAN-06-3672.

2045 Cong, Y.-S., Wright, W. E. and Shay, J. W. (2002) 'Human Telomerase and Its Regulation',
2046 *Microbiology and Molecular Biology Reviews*. doi: 10.1128/mmbr.66.3.407-425.2002.

2047 Conte, D. *et al.* (2012) 'Loss of Atrx Sensitizes Cells to DNA Damaging Agents through p53-
2048 Mediated Death Pathways', *PLoS ONE*. doi: 10.1371/journal.pone.0052167.

2049 Cox, K. E., Maréchal, A. and Flynn, R. L. (2016) 'SMARCAL1 Resolves Replication Stress at ALT
2050 Telomeres', *Cell Reports*. doi: 10.1016/j.celrep.2016.01.011.

2051 Daroui, P. *et al.* (2004) 'Hydrogen Peroxide Induces Topoisomerase I-mediated DNA Damage
2052 and Cell Death', *Journal of Biological Chemistry*. doi: 10.1074/jbc.M311370200.

2053 Dhayalan, A. *et al.* (2011) 'The ATRX-ADD domain binds to H3 tail peptides and reads the
2054 combined methylation state of K4 and K9', *Human Molecular Genetics*. doi:
2055 10.1093/hmg/ddr107.

2056 Dilley, R. L. *et al.* (2016) 'Break-induced telomere synthesis underlies alternative telomere
2057 maintenance', *Nature*. doi: 10.1038/nature20099.

2058 Diplas, B. H. *et al.* (2018) 'The genomic landscape of TERT promoter wildtype-IDH wildtype

2059 glioblastoma', *Nature Communications*. doi: 10.1038/s41467-018-04448-6.

2060 Dong Fang, 1 *et al.* (2016) 'The histone H3.3K36M mutation reprograms the epigenome of
2061 chondroblastomas', *Science*.

2062 Drané, P. *et al.* (2010) 'The death-associated protein DAXX is a novel histone chaperone
2063 involved in the replication-independent deposition of H3.3', *Genes and Development*. doi:
2064 10.1101/gad.566910.

2065 Eddy, S. *et al.* (2016) 'Human Translesion Polymerase κ Exhibits Enhanced Activity and
2066 Reduced Fidelity Two Nucleotides from G-Quadruplex DNA', *Biochemistry*. doi:
2067 10.1021/acs.biochem.6b00374.

2068 Eid, R. *et al.* (2015) ' Genetic Inactivation of ATRX Leads to a Decrease in the Amount of
2069 Telomeric Cohesin and Level of Telomere Transcription in Human Glioma Cells ', *Molecular*
2070 *and Cellular Biology*. doi: 10.1128/mcb.01317-14.

2071 Eustermann, S. *et al.* (2011) 'Combinatorial readout of histone H3 modifications specifies
2072 localization of ATRX to heterochromatin', *Nature Structural and Molecular Biology*. doi:
2073 10.1038/nsmb.2070.

2074 Falaschi, A. *et al.* (2007) 'Molecular and structural transactions at human DNA replication
2075 origins', *Cell Cycle*. doi: 10.4161/cc.6.14.4495.

2076 Fang, J. *et al.* (2018) 'Cancer-driving H3G34V/R/D mutations block H3K36 methylation and
2077 H3K36me3-MutSα interaction', *Proceedings of the National Academy of Sciences of the*
2078 *United States of America*. doi: 10.1073/pnas.1806355115.

2079 Feng, J. *et al.* (1995) 'The RNA component of human telomerase', *Science*. doi:
2080 10.1126/science.7544491.

Flynn, R. L. *et al.* (2011) 'TERRA and hnRNPA1 orchestrate an RPA-to-POT1 switch on telomeric single-stranded DNA', *Nature*. doi: 10.1038/nature09772.

Flynn, R. L. *et al.* (2015) 'Alternative lengthening of telomeres renders cancer cells hypersensitive to ATR inhibitors', *Science*. doi: 10.1126/science.1257216.

Fontebasso, A. M. *et al.* (2013) 'Mutations in SETD2 and genes affecting histone H3K36 methylation target hemispheric high-grade gliomas', *Acta Neuropathologica*. doi: 10.1007/s00401-013-1095-8.

Frey, A. *et al.* (2014) 'Histone H3.3 is required to maintain replication fork progression after UV damage', *Current Biology*. doi: 10.1016/j.cub.2014.07.077.

Garcia-Exposito, L. *et al.* (2016) 'Proteomic Profiling Reveals a Specific Role for Translesion DNA Polymerase η in the Alternative Lengthening of Telomeres', *Cell Reports*. doi: 10.1016/j.celrep.2016.10.048.

Gibbons, R. J. *et al.* (1995) 'Mutations in a putative global transcriptional regulator cause X-linked mental retardation with α-thalassemia (ATR-X syndrome)', *Cell*. doi: 10.1016/0092-8674(95)90287-2.

Gibbons, R. J. *et al.* (2003) 'Identification of acquired somatic mutations in the gene encoding chromatin-remodeling factor ATRX in the α-thalassemia myelodysplasia syndrome (ATMDS)', *Nature Genetics*. doi: 10.1038/ng1213.

Gibbons, R. J. *et al.* (2008) 'Mutations in the chromatin-associated protein ATRX', *Human Mutation*. doi: 10.1002/humu.20734.

Goldberg, A. D. *et al.* (2010) 'Distinct Factors Control Histone Variant H3.3 Localization at Specific Genomic Regions', *Cell*. doi: 10.1016/j.cell.2010.01.003.

2103 Goncalves, T. *et al.* (2020) 'Selective Elimination of Osteosarcoma Cell Lines with Short
2104 Telomeres by Ataxia Telangiectasia and Rad3-Related Inhibitors', *ACS Pharmacology and*
2105 *Translational Science*. doi: 10.1021/acsptsci.0c00125.

2106 Graham, M. K. *et al.* (2019) 'Functional loss of ATRX and TERC activates Alternative
2107 Lengthening of Telomeres (ALT) in LAPC4 prostate cancer cells', *Molecular Cancer Research*.
2108 doi: 10.1158/1541-7786.MCR-19-0654.

2109 Grant, J. D. *et al.* (2001) 'Telometric: A tool providing simplified, reproducible measurements
2110 of telomeric DNA from constant field agarose gels', *BioTechniques*. doi: 10.2144/01316bc02.

2111 Greider, C. W. (1993) 'Telomerase and telomere-length regulation: Lessons from small
2112 eukaryotes to mammals', in *Cold Spring Harbor Symposia on Quantitative Biology*. doi:
2113 10.1101/SQB.1993.058.01.079.

2114 Griffith, J. D. *et al.* (1999) 'Mammalian telomeres end in a large duplex loop', *Cell*. doi:
2115 10.1016/S0092-8674(00)80760-6.

2116 Grobelny, J. V., Godwin, A. K. and Broccoli, D. (2000) 'ALT-associated PML bodies are present
2117 in viable cells and are enriched in cells in the G2/M phase of the cell cycle', *Journal of Cell*
2118 *Science*.

2119 El Hage, A. *et al.* (2010) 'Loss of Topoisomerase I leads to R-loop-mediated transcriptional
2120 blocks during ribosomal RNA synthesis', *Genes and Development*. doi: 10.1101/gad.573310.

2121 Ten Hagen, K. G. *et al.* (1990) 'Replication timing of DNA sequences associated with human
2122 centromeres and telomeres.', *Molecular and Cellular Biology*. doi: 10.1128/mcb.10.12.6348.

2123 Hanahan, D. and Weinberg, R. A. (2011) 'Hallmarks of cancer: The next generation', *Cell*. doi:
2124 10.1016/j.cell.2011.02.013.

Heaphy, C. M., De Wilde, R. F., *et al.* (2011) 'Altered telomeres in tumors with ATRX and DAXX mutations', *Science*. doi: 10.1126/science.1207313.

Heaphy, C. M., Subhawong, A. P., *et al.* (2011) 'Prevalence of the alternative lengthening of telomeres telomere maintenance mechanism in human cancer subtypes', *American Journal of Pathology*. doi: 10.1016/j.ajpath.2011.06.018.

Henson, J. D. *et al.* (2009) 'DNA C-circles are specific and quantifiable markers of alternative-lengthening-of-telomeres activity', *Nature Biotechnology*. doi: 10.1038/nbt.1587.

Henson, J. D. and Reddel, R. R. (2010) 'Assaying and investigating Alternative Lengthening of Telomeres activity in human cells and cancers', *FEBS Letters*. doi: 10.1016/j.febslet.2010.06.009.

Herrera-Moyano, E. *et al.* (2014) 'The yeast and human FACT chromatinreorganizing complexes solve R-loopmediated transcription-replication conflicts', *Genes and Development*. doi: 10.1101/gad.234070.113.

Higa, M., Fujita, M. and Yoshida, K. (2017) 'DNA replication origins and fork progression at mammalian telomeres', *Genes*. doi: 10.3390/genes8040112.

Hoang, S. M. *et al.* (2020) 'Regulation of ALT-associated homology-directed repair by polyADP-ribosylation', *Nature Structural and Molecular Biology*. doi: 10.1038/s41594-020-0512-7.

Huh, M. S. *et al.* (2012) 'Compromised genomic integrity impedes muscle growth after Atrx inactivation', *Journal of Clinical Investigation*. doi: 10.1172/JCI63765.

Huh, M. S. *et al.* (2016) 'Stalled replication forks within heterochromatin require ATRX for protection', *Cell Death and Disease*. doi: 10.1038/cddis.2016.121.

Iwase, S. *et al.* (2011) 'ATRX ADD domain links an atypical histone methylation recognition mechanism to human mental-retardation syndrome', *Nature Structural and Molecular Biology*. doi: 10.1038/nsmb.2062.

Ji, J. *et al.* (2017) 'Inherited germline ATRX mutation in two brothers with ATR-X syndrome and osteosarcoma', *American Journal of Medical Genetics, Part A*. doi: 10.1002/ajmg.a.38184.

Jiao, Y. *et al.* (2011) 'DAXX/ATRX, MEN1, and mTOR pathway genes are frequently altered in pancreatic neuroendocrine tumors', *Science*. doi: 10.1126/science.1200609.

Juhász, S. *et al.* (2018) 'ATRX Promotes DNA Repair Synthesis and Sister Chromatid Exchange during Homologous Recombination', *Molecular Cell*. doi: 10.1016/j.molcel.2018.05.014.

Keszthelyi, A., Minchell, N. E. and Baxter, J. (2016) 'The causes and consequences of topological stress during DNA replication', *Genes*. doi: 10.3390/genes7120134.

Kim, J. *et al.* (2018) 'Replication Stress Shapes a Protective Chromatin Environment across Fragile Genomic Regions', *Molecular Cell*. doi: 10.1016/j.molcel.2017.11.021.

Kim, J. *et al.* (2019) 'The macroH2A1.2 histone variant links ATRX loss to alternative telomere lengthening', *Nature Structural and Molecular Biology*. doi: 10.1038/s41594-019-0192-3.

Kockler, Z. W., Comeron, J. M. and Malkova, A. (2021) 'A unified alternative telomere-lengthening pathway in yeast survivor cells', *Molecular Cell*. doi: https://doi.org/10.1016/j.molcel.2021.02.004.

Koschmann, C. *et al.* (2016) 'ATRX loss promotes tumor growth and impairs nonhomologous end joining DNA repair in glioma', *Science Translational Medicine*. doi: 10.1126/scitranslmed.aac8228.

Krogh, B. O. and Symington, L. S. (2004) 'Recombination proteins in yeast', *Annual Review of Genetics*. doi: 10.1146/annurev.genet.38.072902.091500.

Kumar, G. S. *et al.* (2012) 'Sequence requirements for combinatorial recognition of histone H3 by the MRG15 and Pf1 subunits of the Rpd3S/Sin3S corepressor complex', *Journal of Molecular Biology*. doi: 10.1016/j.jmb.2012.06.013.

Lallemand-Breitenbach, V. and de Thé, H. (2010) 'PML nuclear bodies.', *Cold Spring Harbor perspectives in biology*. doi: 10.1101/cshperspect.a000661.

Lang, M. *et al.* (2010) 'Three-dimensional organization of promyelocytic leukemia nuclear bodies', *Journal of Cell Science*. doi: 10.1242/jcs.053496.

De Lange, T. (2005) 'Shelterin: The protein complex that shapes and safeguards human telomeres', *Genes and Development*. doi: 10.1101/gad.1346005.

De Lange, T. (2009) 'How telomeres solve the end-protection problem', *Science*. doi: 10.1126/science.1170633.

Law, M. J. *et al.* (2010) 'ATR-X syndrome protein targets tandem repeats and influences allele-specific expression in a size-dependent manner', *Cell*. doi: 10.1016/j.cell.2010.09.023.

Le, S. *et al.* (1999) 'RAD50 and RAD51 define two pathways that collaborate to maintain telomeres in the absence of telomerase', *Genetics*.

Lechner, M. S. *et al.* (2005) 'The mammalian heterochromatin protein 1 binds diverse nuclear proteins through a common motif that targets the chromoshadow domain', *Biochemical and Biophysical Research Communications*. doi: 10.1016/j.bbrc.2005.04.016.

Lee, Y. K., Park, N. H. and Lee, H. (2012) 'Prognostic value of alternative lengthening of

telomeres-associated biomarkers in uterine sarcoma and uterine carcinosarcoma', *International Journal of Gynecological Cancer*. doi: 10.1097/IGC.0b013e31823ca017.

Leung, J. W. C. *et al.* (2013) 'Alpha thalassemia/mental retardation syndrome X-linked gene product ATRX is required for proper replication restart and cellular resistance to replication stress', *Journal of Biological Chemistry*. doi: 10.1074/jbc.M112.411603.

Lewis, P. W. *et al.* (2010) 'Daxx is an H3.3-specific histone chaperone and cooperates with ATRX in replication-independent chromatin assembly at telomeres', *Proceedings of the National Academy of Sciences of the United States of America*. doi: 10.1073/pnas.1008850107.

Lewis, P. W. *et al.* (2013) 'Inhibition of PRC2 activity by a gain-of-function H3 mutation found in pediatric glioblastoma', *Science*. doi: 10.1126/science.1232245.

Liang, Z. *et al.* (2019) 'Binding of FANCI-FANCD2 Complex to RNA and R-Loops Stimulates Robust FANCD2 Monoubiquitination', *Cell Reports*. doi: 10.1016/j.celrep.2018.12.084.

Liau, J. Y. *et al.* (2015) 'Leiomyosarcoma with alternative lengthening of telomeres is associated with aggressive histologic features, loss of ATRX expression, and poor clinical outcome', *American Journal of Surgical Pathology*. doi: 10.1097/PAS.0000000000000324.

Loe, T. K. *et al.* (2020) 'Telomere length heterogeneity in ALT cells is maintained by PML-dependent localization of the BTR complex to telomeres', *Genes and Development*. doi: 10.1101/gad.333963.119.

Lovejoy, C. A. *et al.* (2012) 'Loss of ATRX, genome instability, and an altered DNA damage response are hallmarks of the alternative lengthening of Telomeres pathway', *PLoS Genetics*. doi: 10.1371/journal.pgen.1002772.

Lovejoy, C. A. *et al.* (2020) 'ATRX affects the repair of telomeric DSBs by promoting cohesion and a DAXX-dependent activity', *PLoS biology*. doi: 10.1371/journal.pbio.3000594.

Lu, C. *et al.* (2016) 'Cancer: Histone H3K36 mutations promote sarcomagenesis through altered histone methylation landscape', *Science*. doi: 10.1126/science.aac7272.

Lu, R. *et al.* (2019) 'The FANCM-BLM-TOP3A-RMI complex suppresses alternative lengthening of telomeres (ALT)', *Nature Communications*. doi: 10.1038/s41467-019-10180-6.

Lundblad, V. and Blackburn, E. H. (1993) 'An alternative pathway for yeast telomere maintenance rescues est1- senescence', *Cell*. doi: 10.1016/0092-8674(93)90234-H.

De Magis, A. *et al.* (2019) 'DNA damage and genome instability by G-quadruplex ligands are mediated by R loops in human cancer cells', *Proceedings of the National Academy of Sciences of the United States of America*. doi: 10.1073/pnas.1810409116.

Marinello, J. *et al.* (2013) 'Antisense transcripts enhanced by camptothecin at divergent CpG-island promoters associated with bursts of topoisomerase I-DNA cleavage complex and R-loop formation', *Nucleic Acids Research*. doi: 10.1093/nar/gkt778.

Mason-Osann, E. *et al.* (2018) 'Identification of a novel gene fusion in ALT positive osteosarcoma', *Oncotarget*. doi: 10.18632/oncotarget.26029.

Matsuo, T. *et al.* (2010) 'Alternative lengthening of telomeres as a prognostic factor in malignant fibrous histiocytomas of bone', *Anticancer Research*.

Mazzucco, G. *et al.* (2020) 'Telomere damage induces internal loops that generate telomeric circles', *Nature Communications*. doi: 10.1038/s41467-020-19139-4.

McCarroll, R. M. and Fangman, W. L. (1988) 'Time of replication of yeast centromeres and

2231 telomeres', *Cell*. doi: 10.1016/0092-8674(88)90072-4.

2232 McEachern, M. J. and Haber, J. E. (2006) 'Break-induced replication and recombinational
2233 telomere elongation in yeast', *Annual Review of Biochemistry*. doi:
2234 10.1146/annurev.biochem.74.082803.133234.

2235 McGee, J. S. *et al.* (2010) 'Reduced Rif2 and lack of Mec1 target short telomeres for elongation
2236 rather than double-strand break repair', *Nature Structural and Molecular Biology*. doi:
2237 10.1038/nsmb.1947.

2238 Min, J. and Shay, J. W. (2019) 'Telomere clustering drives ALT', *Aging*. doi:
2239 10.18632/aging.102369.

2240 Min, J., Wright, W. E. and Shay, J. W. (2017a) 'Alternative lengthening of telomeres can be
2241 maintained by preferential elongation of lagging strands', *Nucleic Acids Research*. doi:
2242 10.1093/nar/gkw1295.

2243 Min, J., Wright, W. E. and Shay, J. W. (2017b) 'Alternative Lengthening of Telomeres Mediated
2244 by Mitotic DNA Synthesis Engages Break-Induced Replication Processes', *Molecular and*
2245 *Cellular Biology*. doi: 10.1128/mcb.00226-17.

2246 Min, J., Wright, W. E. and Shay, J. W. (2019) 'Clustered telomeres in phase-separated nuclear
2247 condensates engage mitotic DNA synthesis through BLM and RAD52', *Genes and*
2248 *Development*. doi: 10.1101/gad.324905.119.

2249 Mitson, M. *et al.* (2011) 'Functional significance of mutations in the Snf2 domain of ATRX',
2250 *Human Molecular Genetics*. doi: 10.1093/hmg/ddr163.

2251 Mortensen, U. H. *et al.* (1996) 'DNA strand annealing is promoted by the yeast RaD52 protein',
2252 *Proceedings of the National Academy of Sciences of the United States of America*. doi:

10.1073/pnas.93.20.10729.

Moser, B. A. *et al.* (2009) 'Differential arrival of leading and lagging strand DNA polymerases at fission yeast telomeres', *EMBO Journal*. doi: 10.1038/emboj.2009.31.

Nabetani, A. and Ishikawa, F. (2009) 'Unusual Telomeric DNAs in Human Telomerase-Negative Immortalized Cells', *Molecular and Cellular Biology*. doi: 10.1128/mcb.00603-08.

Napier, C. E. *et al.* (2015) 'ATRX represses alternative lengthening of telomeres', *Oncotarget*. doi: 10.18632/oncotarget.3846.

Neumann, A. A. *et al.* (2013) 'Alternative lengthening of telomeres in normal mammalian somatic cells', *Genes and Development*. doi: 10.1101/gad.205062.112.

New, J. H. *et al.* (1998) 'Rad52 protein stimulates DNA strand exchange by Rad51 and replication protein A', *Nature*. doi: 10.1038/34950.

Nguyen, D. T. *et al.* (2017) ' The chromatin remodelling factor ATRX suppresses R-loops in transcribed telomeric repeats ', *EMBO reports*. doi: 10.15252/embr.201643078.

O'Sullivan, R. J. *et al.* (2014) 'Rapid induction of alternative lengthening of telomeres by depletion of the histone chaperone ASF1', *Nature Structural and Molecular Biology*. doi: 10.1038/nsmb.2754.

Ogi, T. and Lehmann, A. R. (2006) 'The Y-family DNA polymerase κ (pol κ) functions in mammalian nucleotide-excision repair', *Nature Cell Biology*. doi: 10.1038/ncb1417.

Okamoto, Y. *et al.* (2019) 'FANCD2 protects genome stability by recruiting RNA processing enzymes to resolve R-loops during mild replication stress', *FEBS Journal*. doi: 10.1111/febs.14700.

Olivieri, M. *et al.* (2020) 'A Genetic Map of the Response to DNA Damage in Human Cells', *Cell*. doi: 10.1016/j.cell.2020.05.040.

Olovnikov, A. M. (1973) 'A theory of marginotomy. The incomplete copying of template margin in enzymic synthesis of polynucleotides and biological significance of the phenomenon', *Journal of Theoretical Biology*. doi: 10.1016/0022-5193(73)90198-7.

Pan, X. *et al.* (2017) 'FANCM, BRCA1, and BLM cooperatively resolve the replication stress at the ALT telomeres', *Proceedings of the National Academy of Sciences of the United States of America*. doi: 10.1073/pnas.1708065114.

Pan, X. *et al.* (2019) 'FANCM suppresses DNA replication stress at ALT telomeres by disrupting TERRA R-loops', *Scientific Reports*. doi: 10.1038/s41598-019-55537-5.

Panier, S. *et al.* (2019) 'SLX4IP Antagonizes Promiscuous BLM Activity during ALT Maintenance', *Molecular Cell*. doi: 10.1016/j.molcel.2019.07.010.

Pathak, P. *et al.* (2015) 'Altered global histone-trimethylation code and H3F3A-ATRX mutation in pediatric GBM', *Journal of Neuro-Oncology*. doi: 10.1007/s11060-014-1675-z.

Pepe, A. and West, S. C. (2014a) 'MUS81-EME2 promotes replication fork restart', *Cell Reports*. doi: 10.1016/j.celrep.2014.04.007.

Pepe, A. and West, S. C. (2014b) 'Substrate specificity of the MUS81-EME2 structure selective endonuclease', *Nucleic Acids Research*. doi: 10.1093/nar/gkt1333.

Pfister, S. X. *et al.* (2015) 'Inhibiting WEE1 Selectively Kills Histone H3K36me3-Deficient Cancers by dNTP Starvation', *Cancer Cell*. doi: 10.1016/j.ccell.2015.09.015.

Pladevall-Morera, D. *et al.* (2019) 'Proteomic characterization of chromosomal common

fragile site (CFS)-associated proteins uncovers ATRX as a regulator of CFS stability', *Nucleic Acids Research*. doi: 10.1093/nar/gkz510.

Poole, L. A. *et al.* (2015) 'SMARCAL1 maintains telomere integrity during DNA replication', *Proceedings of the National Academy of Sciences of the United States of America*. doi: 10.1073/pnas.1510750112.

Potts, P. R. and Yu, H. (2007) 'The SMC5/6 complex maintains telomere length in ALT cancer cells through SUMOylation of telomere-binding proteins', *Nature Structural and Molecular Biology*. doi: 10.1038/nsmb1259.

Quinet, A. *et al.* (2016) 'Translesion synthesis mechanisms depend on the nature of DNA damage in UV-irradiated human cells', *Nucleic Acids Research*. doi: 10.1093/nar/gkw280.

Raghunandan, M. *et al.* (2020) 'Functional cross talk between the Fanconi anemia and ATRX/DAXX histone chaperone pathways promotes replication fork recovery', *Human molecular genetics*. doi: 10.1093/hmg/ddz250.

Ramamoorthy, M. and Smith, S. (2015) 'Loss of ATRX Suppresses Resolution of Telomere Cohesion to Control Recombination in ALT Cancer Cells', *Cancer Cell*. doi: 10.1016/j.ccell.2015.08.003.

Ratnakumar, K. *et al.* (2012) 'ATRX-mediated chromatin association of histone variant macroH2A1 regulates α-globin expression', *Genes and Development*. doi: 10.1101/gad.179416.111.

Rodriguez, R. *et al.* (2012) 'Small-molecule-induced DNA damage identifies alternative DNA structures in human genes', *Nature Chemical Biology*. doi: 10.1038/nchembio.780.

Root, H. *et al.* (2016) 'FANCD2 limits BLM-dependent telomere instability in the alternative

2317 lengthening of telomeres pathway', *Human Molecular Genetics*. doi: 10.1093/hmg/ddw175.

2318 Sagie, S. *et al.* (2017) 'Telomeres in ICF syndrome cells are vulnerable to DNA damage due to
2319 elevated DNA:RNA hybrids', *Nature Communications*. doi: 10.1038/ncomms14015.

2320 Schwartzentruber, J. *et al.* (2012) 'Driver mutations in histone H3.3 and chromatin
2321 remodelling genes in paediatric glioblastoma', *Nature*. doi: 10.1038/nature10833.

2322 Sertic, S. *et al.* (2018) 'Coordinated Activity of Y Family TLS Polymerases and EXO1 Protects
2323 Non-S Phase Cells from UV-Induced Cytotoxic Lesions', *Molecular Cell*. doi:
2324 10.1016/j.molcel.2018.02.017.

2325 Sfeir, A. *et al.* (2009) 'Mammalian Telomeres Resemble Fragile Sites and Require TRF1 for
2326 Efficient Replication', *Cell*. doi: 10.1016/j.cell.2009.06.021.

2327 Silva, B. *et al.* (2019) 'FANCM limits ALT activity by restricting telomeric replication stress
2328 induced by deregulated BLM and R-loops', *Nature Communications*. doi: 10.1038/s41467-
2329 019-10179-z.

2330 Smittenaar, C. R. *et al.* (2016) 'Cancer incidence and mortality projections in the UK until
2331 2035', *British Journal of Cancer*. doi: 10.1038/bjc.2016.304.

2332 Sobinoff, A. P. *et al.* (2017) 'BLM and SLX4 play opposing roles in recombination-dependent
2333 replication at human telomeres', *The EMBO Journal*. doi: 10.15252/embj.201796889.

2334 Sollier, J. *et al.* (2014) 'Transcription-Coupled Nucleotide Excision Repair Factors Promote R-
2335 Loop-Induced Genome Instability', *Molecular Cell*. doi: 10.1016/j.molcel.2014.10.020.

2336 Solomon, D. A. *et al.* (2016) 'Diffuse Midline Gliomas with Histone H3-K27M Mutation: A
2337 Series of 47 Cases Assessing the Spectrum of Morphologic Variation and Associated Genetic

2338 Alterations', *Brain Pathology*. doi: 10.1111/bpa.12336.

2339 Sordet, O. *et al.* (2009) 'Ataxia telangiectasia mutated activation by transcription- and
2340 topoisomerase I-induced DNA double-strand breaks', *EMBO Reports*. doi:
2341 10.1038/embor.2009.97.

2342 Spivak, G. (2015) 'Nucleotide excision repair in humans', *DNA Repair*. doi:
2343 10.1016/j.dnarep.2015.09.003.

2344 Stansel, R. M., De Lange, T. and Griffith, J. D. (2001) 'T-loop assembly in vitro involves binding
2345 of TRF2 near the 3' telomeric overhang', *EMBO Journal*. doi: 10.1093/emboj/20.19.5532.

2346 Stavropoulos, D. J. *et al.* (2002) 'The bloom syndrome helicase BLM interacts with TRF2 in ALT
2347 cells and promotes telomeric DNA synthesis', *Human Molecular Genetics*. doi:
2348 10.1093/hmg/11.25.3135.

2349 Stevenson, R. E. (2020) 'Alpha-thalassemia-X-linked intellectual disability syndrome', in
2350 *Definitions*. doi: 10.32388/zjyi82.

2351 Taylor, M. R. G. and Yeeles, J. T. P. (2018) 'The Initial Response of a Eukaryotic Replisome to
2352 DNA Damage', *Molecular Cell*. doi: 10.1016/j.molcel.2018.04.022.

2353 Teng, S.-C. and Zakian, V. A. (1999) 'Telomere-Telomere Recombination Is an Efficient Bypass
2354 Pathway for Telomere Maintenance in Saccharomyces cerevisiae', *Molecular and Cellular*
2355 *Biology*. doi: 10.1128/mcb.19.12.8083.

2356 Teng, S. C. *et al.* (2000) 'Telomerase-independent lengthening of yeast telomeres occurs by
2357 an abrupt Rad50p-dependent, Rif-inhibited recombinational process', *Molecular Cell*. doi:
2358 10.1016/S1097-2765(05)00094-8.

Thapa, S. *et al.* (2020) 'Implementation of interventions targeting the uptake of genetic testing services for breast cancer risk: protocol for a systematic review', *BMJ open*. doi: 10.1136/bmjopen-2019-031727.

Tresini, M. *et al.* (2015) 'The core spliceosome as target and effector of non-canonical ATM signalling', *Nature*. doi: 10.1038/nature14512.

VandenBussche, C. J. *et al.* (2017) 'Alternative lengthening of telomeres and ATRX/DAXX loss can be reliably detected in FNAs of pancreatic neuroendocrine tumors', *Cancer Cytopathology*. doi: 10.1002/cncy.21857.

Venneti, S. *et al.* (2013) 'Evaluation of histone 3 lysine 27 trimethylation (H3K27me3) and enhancer of zest 2 (EZH2) in pediatric glial and glioneuronal tumors shows decreased H3K27me3 in H3F3A K27M mutant glioblastomas', *Brain Pathology*. doi: 10.1111/bpa.12042.

Venturini, L. *et al.* (2010) 'Prognostic relevance of ALT-associated markers in liposarcoma: A comparative analysis', *BMC Cancer*. doi: 10.1186/1471-2407-10-254.

Verdun, R. E. and Karlseder, J. (2006) 'The DNA Damage Machinery and Homologous Recombination Pathway Act Consecutively to Protect Human Telomeres', *Cell*. doi: 10.1016/j.cell.2006.09.034.

Wang, R. C., Smogorzewska, A. and De Lange, T. (2004) 'Homologous recombination generates t-loop-sized deletions at human telomeres', *Cell*. doi: 10.1016/j.cell.2004.10.011.

Wang, Y. *et al.* (2019) 'G-quadruplex DNA drives genomic instability and represents a targetable molecular abnormality in ATRX-deficient malignant glioma', *Nature Communications*. doi: 10.1038/s41467-019-08905-8.

Weatherall, D. J. *et al.* (1981) 'Hemoglobin H Disease and Mental Retardation: A New

2381 Syndrome or a Remarkable Coincidence?', *The New England journal of medicine*. doi:
2382 10.1056/NEJM198109103051103.

2383 Wong, L. H. *et al.* (2009) 'Histone H3.3 incorporation provides a unique and functionally
2384 essential telomeric chromatin in embryonic stem cells', *Genome Research*. doi:
2385 10.1101/gr.084947.108.

2386 Wong, L. H. (2010) 'Epigenetic regulation of telomere chromatin integrity in pluripotent
2387 embryonic stem cells', *Epigenomics*. doi: 10.2217/epi.10.49.

2388 Wright, W. E. *et al.* (1999) 'Normal human telomeres are not late replicating', *Experimental
2389 Cell Research*. doi: 10.1006/excr.1999.4602.

2390 Wu, G. *et al.* (2003) 'Assembly of functional ALT-associated promyelocytic leukemia bodies
2391 requires nijmegen breakage syndrome 1', *Cancer Research*.

2392 Wu, G., Lee, W. H. and Chen, P. L. (2000) 'NBS1 and TRF1 colocalize at promyelocytic leukemia
2393 bodies during late S/G2 phases in immortalized telomerase-negative cells. Implication of
2394 NBS1 in alternative lengthening of telomeres', *Journal of Biological Chemistry*. doi:
2395 10.1074/jbc.C000390200.

2396 Xue, Y. *et al.* (2003) 'The ATRX syndrome protein forms a chromatin-remodeling complex with
2397 Daxx and localizes in promyelocytic leukemia nuclear bodies', *Proceedings of the National
2398 Academy of Sciences of the United States of America*. doi: 10.1073/pnas.1937626100.

2399 Yang, X. *et al.* (1997) 'Daxx, a novel fas-binding protein that activates JNK and apoptosis', *Cell*.
2400 doi: 10.1016/S0092-8674(00)80294-9.

2401 Yang, Y. *et al.* (2018) 'Diverse roles of RAD18 and Y-family DNA polymerases in tumorigenesis',
2402 *Cell Cycle*. doi: 10.1080/15384101.2018.1456296.

Yeager, T. R. *et al.* (1999) 'Telomerase-negative immortalized human cells contain a novel type of promyelocytic leukemia (PML) body', *Cancer Research*.

Zellweger, R. *et al.* (2015) 'Rad51-mediated replication fork reversal is a global response to genotoxic treatments in human cells', *Journal of Cell Biology*. doi: 10.1083/jcb.201406099.

Zeng, S. *et al.* (2009) 'Telomere recombination requires the MUS81 endonuclease', *Nature Cell Biology*. doi: 10.1038/ncb1867.

Zhang, H. *et al.* (2020) 'Nuclear body phase separation drives telomere clustering in ALT cancer cells', *Molecular Biology of the Cell*. doi: 10.1091/mbc.E19-10-0589.

Zhang, J. M. *et al.* (2019) 'Alternative Lengthening of Telomeres through Two Distinct Break-Induced Replication Pathways', *Cell Reports*. doi: 10.1016/j.celrep.2018.12.102.

Zhang, J. M. *et al.* (2021) 'Alternative lengthening of telomeres is a self-perpetuating process in ALT-associated PML bodies', *Molecular Cell*. doi: 10.1016/j.molcel.2020.12.030.

Zhang, T. *et al.* (2019) 'Strand break-induced replication fork collapse leads to C-circles, C-overhangs and telomeric recombination', *PLoS Genetics*. doi: 10.1371/journal.pgen.1007925.